Effect of Geometry and Anisotropy on the Magnetic Moment of Type II Superconductors

by

Jinglei Meng

Thesis submitted to the University of Ottawa

in partial fulfilment of the requirements

for the degree of Master of Science in Physics

Department of Physics

University of Ottawa, Ottawa, Canada

May, 1994

ISBN 0-612-00485-6

UNIVERSITÉ D'OTTAWA
UNIVERSITY OF OTTAWA

ACKNOWLEDGEMENTS

I am deeply and sincerely grateful to my research supervisor, Professor Marcel Leblanc who guided me in the development of the formulae describing the effects of geometry and anisotropy which are presented in my thesis. I have found great help from the extensive notes of his graduate course on Superconductivity and on internal seminars in writing the introduction to my thesis. Also I thank him for his patience and care in revising the successive drafts of this thesis. It is to recognize his contribution that the subject we (not the "royal" we) replaces the subject I throughout the text of the thesis.

I would like to express my thanks to my parents who brought me up, gave me the chance for an education and made my dream to study in Canada and get the degree come true. I would like to thank also my grandma and wish her a good health. I should not forget my sister and brother-in-law for their care when I was attending Tongji University in Shanghai. Finally, I would like to dedicate this thesis to my wife, Rona for her direct help in this project, as well as the love, encouragement and moral support throughout our lives together.

ABSTRACT

Formulae for the magnetic moment $\vec{\mu}$ of anisotropic platelets of high T_c superconductors developed by Gyorgy et al and Peterson are frequently exploited by these and other researchers to estimate, j_c^c and j_c^{ab}, the critical current densities along the c axis and in the ab plane taken to be independent of the magnetic flux density B. These formulae were derived using the basic definition, $< \vec{M} >= (< B > -\mu_0 H_a)/\mu_0$ and ignoring end effects, (i.e. any demagnetizing fields), hence implied that the aspect ratio along the magnetizing field H_a is large. This approximation is inappropriate for platelets penetrated by H_a.

We develop these formulae using the alternative basic definition of a magnetic moment, $\vec{\mu} = 1/2 \int (\vec{R} \times \vec{j}) dV$. Now however, for the approach to be valid, $\vec{j} = j_c^c$ or $\vec{j} = j_c^{ab}$ must be independent of B (Bean approximation) and fill the entire volume of the specimen (i.e. a saturated critical state must be established). We show that these formulae are correct under these restrictions regardless of the configuration of $\vec{B}(x, y, z)$ and the neglect of end effects and attendant demagnetizing fields.

Pursuing this framework and the latter definition we develop formulae for $\vec{\mu}$ for isotropic parallelepipeds of various aspect ratios as a function of their inclination θ with respect to

the magnetizing field $\vec{H}_a$. We maintain throughout the critical assumption that the induced persistent currents circulate transverse to $\vec{H}_a$. The graphs of computations with these formulae are useful in identifying the role of geometry on the magnitude of $\vec{\mu}$.

Next we envisage two simple but basic regimes of anisotropy of the critical current densities. The formulae are amended to incorporate these concepts. Families of computed curves display the resulting behaviour and their comparison with the first set enables us to separately assess the effect of various degrees of anisotropy on $\vec{\mu}$.

The catalogue of model predictions we have compiled should prove useful in the selection of optimum experimental arrangements to identify the effects of geometry and anisotropy on magnetic phenomena in type II superconductors.

Contents

Chapter 1

INTRODUCTION

1-1 General

The ability of type II superconductors to support a lossless stationary current in intense static magnetic fields is perhaps their most important property for technological applications. The critical current density j_c, the threshold value for the onset of resistivity in these materials, depends on the temperature $T < T_c$, where T_c is the critical temperature, and $H < H_{c2}$, the upper critical field for the suppression of the bulk superconducting state. Since the transport properties of single crystals of high T_c superconductors are highly anisotropic, j_c in these materials also depends dramatically on the direction of the current flow with respect to the crystalline axes. Generally in the ceramic oxide high T_c superconductors, $\vec{j}_c$ directed along the C axis is very small compared with $\vec{j}_c$ directed in

the basal (ab) plane. Also some differences have been observed between $\vec{j_c}$ directed along the $\vec{a}$ and $\vec{b}$ axes. The latter difference is generally not appreciable and is usually neglected in a " first approximation " analysis of the behaviour of these materials.

Two different approaches have been exploited to determine I_c hence j_c. They are denoted the ' four probe' technique and the 'magnetic' method. We now outline both of these schemes.

1-2 Four Probe Technique

The 'four probe' technique is conceptually simple although not always straightforward in implementation. Current leads are attached to the ends of the specimen and connected to a current source. Voltage leads are secured to the specimen at two positions located between the current connections and some distance from the latter. It is important that the cross section S of the specimen between the voltage leads be uniform and accurately known. The onset of a voltage detected by a sensitive voltmeter between these leads as I is impressed determines I_c . Thus the spatial average, $< j_c >= I_c/S$ is readily obtained vs H_a and T. Since the sensitivity of voltmeters is limited, the accuracy of these measurements diminishes as the length of the specimen is diminished and the cross section is enlarged. The main problem with this technique arises from the fact that a contact resistance R_c inevitably exists between the current leads and the superconducting specimen. Joule

(i.e. I^2R_c) heating at the two interfaces causes the temperature of the superconducting material in their vicinity to rise, thereby severely disturbing the superconducting state and its lossless current carrying capacity. Much effort and skill have been devoted to minimizing R_c and to diminishing its effects. The magnitudes of the critical current and current densities coming into play in the most technologically promising materials are so large however, particularly in the range of low and weak fields, that the best contacts continue to present a major obstacle in these circumstances.

Another major problem with the four probe technique is that the magnitudes of j_c for the technologically interesting type II superconductors are considerable. Current densities exceeding 10^6 Amperes per cm^2 have been reported in thin films and single crystals of high-T_c superconductors even at 77K. Further j_c increases rapidly from these impressive values as T is diminished from 77K. Consequently, the critical currents, $I_c =< j_c > S$ are quite large even for specimens of modest cross section S. Thus precautions must be taken and sensitive protective circuits introduced in the measuring system to avoid irreversible damage of the specimen when I attains and exceeds I_c.

1-3 Magnetic Method

To circumvent the contact 'bottleneck' and specimen destruction, and also to obtain complementary data, a variety of 'magnetic' schemes have been devised and explored. The

essential features of these various methods are also straightforward.

By Faraday's law of induction, a change $\Delta\Phi$, of the magnetic flux threading a specimen generates an emf ε, hence an electric field E is related to ε by the definition $\varepsilon = \oint \vec{E} \cdot d\vec{l}$. The electric field E(t) accelerates the superelectrons (i.e. Cooper pairs of density n^* and charge e^*) giving rise to a current density,

$$j = n^* e^* v \tag{1.1}$$

which grows until a critical value j_c is attained where the dissipation of the kinetic energy begins to take place by various processes. Hence an effective resistivity appears in the superconducting state until j decays infinitesimally below the critical value. After the increment (or decrement) ΔH_a of the applied field has taken place, a steady state ensues where a pattern of circulating induced current density is established at the threshold (critical) value over part or all of the volume of the specimen.

We recall that an element of current,

$$\Delta I = \vec{j} \cdot \Delta\vec{S} \tag{1.2}$$

flowing around the periphery of an area A constitutes an elementary magnetic moment or magnetic dipole,

$$\Delta\vec{\mu} = (\Delta I)\vec{A} = (\vec{j} \cdot \Delta\vec{S})\vec{A} \tag{1.3}$$

Thus, the persistent circulating currents induced by the change of H_a cause the specimen to develop a magnetic moment,

$$\vec{\mu} = \int d\vec{\mu} = \int (\vec{j} \cdot \Delta\vec{S})\vec{A} = \frac{1}{2}\int \vec{R} \times \vec{j} dV \tag{1.4}$$

which can be measured by a variety of schemes and instruments (eg. pickup coils feeding an amplifier-integrator, vibrating sample magnetometer, SQUID magnetometer). Here $\vec{R}$ is the position vector. The magnetic moment or the magnetization,

$$< \vec{M} >= \frac{\vec{\mu}}{V} \tag{1.5}$$

where V is the volume of the specimen,and $< \vec{M} >$ is the spatial average of $\vec{\mu}$, yield information on j_c vs H_a.

A basic requisite for this method to yield valid data is that the entire sample be occupied by persistent circulating current at the final value of H_a. The situation where persistent currents fill the entire volume of the specimen is often referred to as the saturated critical state. To achieve such a saturated critical state configuration, ΔH_a the change or sweep or swing of H_a from some initial value to the final value must be sufficiently great in magnitude so as to induce persistent currents around and over the entire cross section of the specimen. This magnitude can be estimated and illustrated by taking,

$$\Delta B_a = \mu_0 \Delta H_a \approx \mu_0 < j_c > W \tag{1.6}$$

Thus a platelet of half width W=0.1 mm, which can support a critical current density of spatial average $< j_c >= 10^6 A/cm^2$, will require an increment (or decrement), $\Delta B_a \approx 1$ Tesla in order that a saturated critical state be established throughout the dimension penetrated by the magnetizing field ΔH_a.

Further we note that the magnetic flux density which threads the specimen will not correspond to the final applied field H_a, but will vary over a range ΔB_a. Thus measurements of the saturated magnetic moment only provide data on the spatial average of the critical current density j_c for some average of H_a lying between the final H_a and $H_a \pm \Delta H_a$. Consequently careful analysis of data on saturated magnetic moments over a broad range of the final values of H_a is needed to extract information on the dependence of j_c on the magnetic flux density B, when j_c varies rapidly as a function of B.

The complications noted above can of course be minimized by using small samples, thereby causing ΔH_a needed for saturation to be diminished even if j_c is large. The accurate measurement of the magnetic moment of small samples, however requires access to sophisticated, sensitive and therefore expensive equipment such as vibrating sample and SQUID magnetometers. Fortunately, the critical current density of strong pinning single crystals of high T_c superconductors is not very sensitive to the magnitude of B. Hence for these materials the problems we have just outlined are not significant. Consequently most workers, in a first approximation, regard j_c at a fixed temperature to be independent of B over the

dimensions of their specimen. This approximation is often referred to as the Bean Model or Bean approximation (3,6,17,24). This is the perspective we will exploit in this thesis.

1-4 Saturated Critical State

To ensure that a saturated critical state is generated by the change of H_a, the experimental worker can proceed as follows. First, the specimen is cooled from T_c to the chosen temperature T in a static magnetic field H_i. This procedure is denoted field cooling and abbreviated to F.C. in the literature. Then the applied magnetic field is either increased or decreased by a convenient amount ΔH_{a1}, to a final value H_f. Let μ_1 devote the magnetic moment thereby induced in the specimen. To determine whether ΔH was sufficiently large to induce a saturated magnetic moment the worker then repeats the procedure but now uses a larger ΔH_a denoted ΔH_{a2}, but keeps H_f the same. Let μ_2 denote the magnetic moment induced by ΔH_{a2}. The augmentation of ΔH_{an} is continued until the corresponding induced μ_n for the chosen final $H_a = H_f$ ceases to increase. This saturation of the magnetic moment provides assurance that a saturated critical state is generated by using the corresponding threshold value for ΔH_a or a slightly greater ΔH_a. Unfortunately this straightforward procedure has been ignored by some workers, thus casting a shadow of doubt on the reliability of the related observations.

1-5 Size Dependence of the Magnetization

1-5-1 Uniformly Magnetized Superconductors

The magnetic moment of uniformly magnetized materials of course increases linearly with the volume. This is the situation which prevails in Type I superconductors and ideal (i.e. reversible or pinning free) type II superconductors of dimensions large compared with the penetration depth λ. In the case of type I superconductors, the magnetization arises entirely from I_M, the Meissner shielding current flowing in the penetration depth at the surface of the specimen and perfectly screening its volume from the externally applied magnetic field H_a. Thus here, B, the magnetic flux density in the body of the specimen is zero and $< M >= -H_a < H_c$, where H_c is the thermodynamic critical field. In ideal type II superconductors, when $0 < H_a < H_{C1}$, the situation is identical to that encountered in type I materials.

Alternatively and equivalently we can view the magnetic moment μ in the perspective of a total surface current $I_{total} = I_M Z$, (where Z is the "height" of the specimen along H_a), flowing around hence embracing A, the area or cross section of the specimen ($A = \pi R^2$ *or* XY). Thus,

$$\mu = \mu_M = -I_{total} A = -I_M ZXY = I_M Z(\pi R^2) = -I_M V = - < M > V \qquad (1.7)$$

Hence,

$$I_M = < M > = -H_a \tag{1.8}$$

in type I superconductors and ideal type II superconductors when $H_a \leq H_{C1}$.

The situation in ideal type II superconductors is somewhat more complicated in the range $H_{C1} < H_a < H_{C2}$. Persistent currents circulating around the axis or core of each quantized vortex generate localized magnetic moments, μ_v, inside the specimen. In pinning free, hence ideal and reversible type II materials, n, the density of quantized vortices or flux lines is uniform and exists in equilibrium with the externally applied field. This equilibrium is governed by the mutual repulsion of the vortices and their interaction with the magnetic field in the penetration depth at the surface of the specimen. Since the density of the flux lines is uniform, no net macroscopic persistent currents flow in the body of the specimen. A "diamagnetic", i.e. field opposing Meissner current flows in the penetration depth at the surface of the specimen. The sum, $N\mu_v$, the quasi-macroscopic magnetic moments generated by N, the total number of individual vortex currents combined with, μ_M, the large diamagnetic moment created by the Meissner current embracing the surface of the specimen leads to the well known Abrikosov $< M >$ vs H curve for ideal type II superconductors which is sketched below.

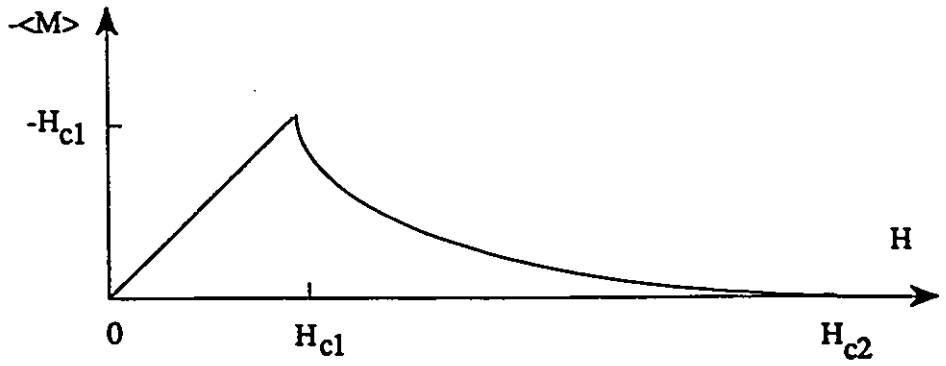

The Magnetic moment μ_v of each vortex is proportional to its length Z. Also N, the number of vortices in a fixed H_a increases in proportion to the cross section A of the specimen threaded by the flux lines. Thus, $N\mu_v$, the total magnetic moment associated with the vortices scales linearly with the volume of the specimen in a chosen H, since $N\mu_v = (nA)Z\mu_v^1 = nV\mu_v^1$. Here μ_v^1 is the magnetic moment per unit length of a vortex. As indicated above, the magnetic moment, μ_M generated by the Meissner surface current is also proportional to the volume of the specimen. In this perspective it is easy to see that the magnetization of bulk ideal type II superconductors is size independent and can be written,

$$< M >= \frac{\mu_{total}}{V} = \frac{N\mu_v - \mu_M}{V} = \frac{n\mu_v^1(AZ) - I_M(AZ)}{V} = n\mu_v^1 - I_M \qquad (1.9)$$

It is often convenient, instructive and useful to write,

$$< M >= -I_A = n\mu_v^1 - I_M \qquad (1.10)$$

where I_A is regarded as a <u>net</u> diamagnetic surface current per unit length Z along H_a. Here the subscript "A" refers to Abrikosov who first developed the framework we have just outlined (1).

For completeness, we now express the picture above in the classical and familiar context.

$$< B >= \mu_0 H_a + \mu_0 < M > \tag{1.11}$$

where $\mu_0 = 4\pi(10^{-7})$ Tesla-meter/ampere.

The vortex currents circulate in a paramagnetic sense, i.e. they create a local magnetic field configuration along the direction of the applied magnetic field. Let $< B >_v$ denote the spatial average of this vortex magnetic flux density. The Meissner current I_M flowing in a diamagnetic (i.e. field opposing) sense generates a magnetic field H_M, hence a magnetic flux density,

$$B_M = \mu_0 M = \mu_0 I_M \tag{1.12}$$

which "overwhelms" the magnetic flux density sustained by the vortex currents. The resultant magnetic flux density can then be written,

$$< B >=< B >_v - B_M + \mu_0 H_a =< B >_v - \mu_0 I_M + \mu_0 H_a = \mu_0 H_a + \mu_0 < M > \tag{1.13}$$

Hence,

$$< M >= \frac{< B >_v}{\mu_0} - I_M \tag{1.14}$$

and is diamagnetic since $I_M >< B >_v / \mu_0$.

Since each vortex contains a unit of magnetic flux,

$$\Phi_0 = \frac{h}{2e} \tag{1.15}$$

then,

$$< B >_v = n\Phi_0 \tag{1.16}$$

and, introducing eqn 1.16 into 1.14 and comparing with eqn 1.9 we see that,

$$\mu_v^1 = \frac{\Phi_0}{\mu_0} \tag{1.17}$$

In closing this section we stress that $I_A = I_M = H_a$ when $H_a < H_{C1}$. However I_A is smaller than H_{C1} when $H_a > H_{C1}$ consequently , I_A is a "small" current since H_{c1} is $<< H_c << H_{c2}$ in high T_c superconductors.

1-5-2 Inhomogeneously Magnetized Type II Superconductors

The saturated critical state magnetic moment of hysteretic (i.e. pinning permeated, hence themodynamically irreversible) type II superconductors is however <u>not</u> linearly proportional to the volume but increases as some power of the volume. In other words, the saturated magnetization $< M >= \mu/V$ of these materials is size dependent. This size effect was first discovered by Bean in 1962 (3) and provided clear evidence that net macroscopic persistent transport currents penetrated and occupied the interior of type II superconductors. Further, this observation set the background for the critical state model, now generally referred to as the Bean Model.(6, 24)

Although the maximum critical current density $j_c \approx 10^{12} A/m^2$ attained in the bulk

or volume of strong pinning type II superconductors is lower than the current density $j_M = I_M/\lambda \approx 10^{13} A/m^2$ of the Meissner current, the critical current I_c in these massive materials dominates I_M and therefore dominates $I_A << I_M$. Consequently in examining the situation in these specimens we will ignore thermodynamically reversible surface currents I_A and I_M and focus only on j_c and I_c.

Hysteretic type II superconductors, also called "hard" superconductors, can sustain large persistent transport currents because the flux lines or vortices can be firmly pinned by imperfections in the specimen such as microscopic voids, dislocations, grain boundaries, concentrations of impurities, etc. Consequently, steep gradients of flux line densities can be established in the material. By Maxwell's equation, $\nabla \times \vec{B} = \mu_0 \vec{j}$, a macroscopic persistent current density $\vec{j}$ corresponds to these static spatial variations of $\vec{B}$. When the net mutual repulsion of the inhomogeneous configuration of flux lines becomes excessive and sufficiently strong to overcome the pinning force density and unpin the flux lines, their distribution adjusts to a new stable arrangement, thus the corresponding transport current transforms from a temporarily supercritical to a critical current density pattern. To illustrate that volume persistent currents lead to a size dependent magnetization, it is convenient to consider j_c to be uniform, hence independent of B. This useful simplification is denoted the Bean approximation.(3, 6, 17,24)

We examine a segment Y of a long rectangular slab of length L along the y axis, width W

along x and height h along the z axis. We consider $L >> Y$, W and h. The slab is in a saturated critical state hence the persistent current density j_{cy} occupies the entire width, height and length of the slab. The persistent currents have been induced to circulate along the length L by ΔH_a applied along the height h, hence $j_c = -j_{cy}$ and $j_c = +j_{cy}$ in the halves of the slab situated in the space $0 < x \leq W/2$ and $-W/2 \leq x < 0$ respectively, as sketched below.

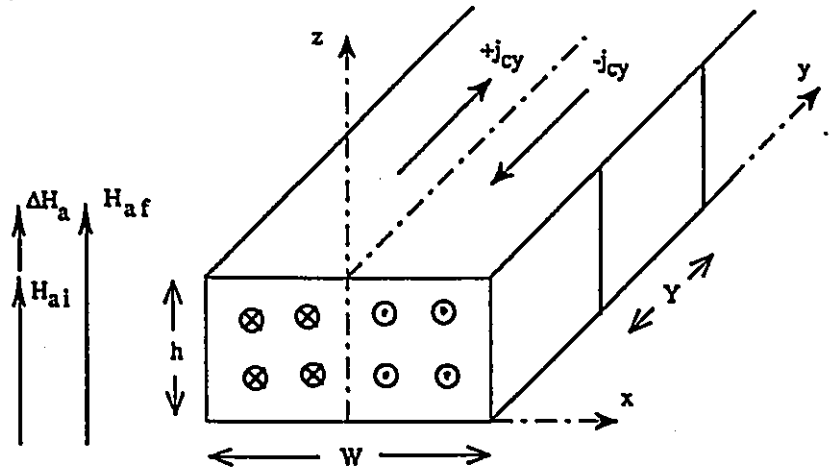

The "return" loops or U-turns of the pattern of the circulating currents are at the "ends" of the length L and do not play a significant geometric role here, since $L >> Y$. Later in this chapter and in this thesis we will examine many situations where these portions of the circulating current configuration will be important. Here,

$$\Delta\mu = (\Delta I)A = (j_{cy}\Delta x \Delta z)(Y 2x) \tag{1.18}$$

since $\Delta I = \vec{j} \cdot \vec{\Delta S} = j_{cy} \Delta x \Delta z$ and the area embraced by a "symmetric" current loop can be written A=Y2x (we ignore the sign of μ and focus only on its magnitude). Thus,

$$\mu = \int d\mu = 2 j_{cy} Y \int_0^{W/2} x dx \int_0^h dz = j_{cy} Y (\frac{W}{2})^2 h = j_{cy} V \frac{W}{4} \tag{1.19}$$

where V=WYh.

It is clear from the right hand side of eqn 1.19 that μ increases as the product of the volume and the dimension W transverse to $\vec{H}_a$, the magnetizing field direction. Thus the magnetization,

$$< M >= \frac{\mu}{V} = j_{cy} \frac{W}{4} \tag{1.20}$$

is proportional to the width W of the slab.

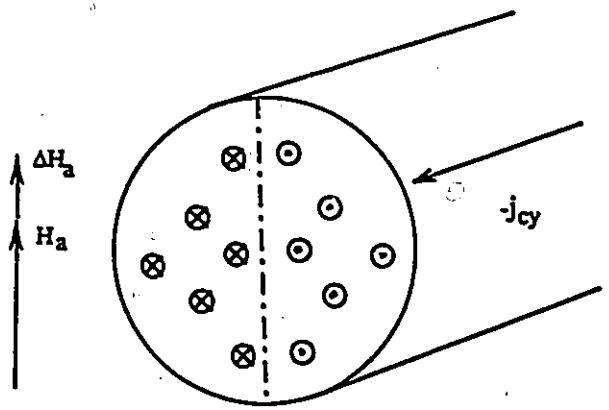

For a cylindrical rod whose length $L >> R$, is oriented transverse to the magnetizing field H_a, the element of current,

$$\Delta I = j_{cy} r \Delta\theta \Delta r \tag{1.21}$$

embraces an area,

$$A = (2rsin\theta)Y \tag{1.22}$$

hence,

$$\mu_{\perp} = 2Yj_{cy}r^2\Delta rsin\theta\Delta\theta \tag{1.23}$$

and,

$$\mu_{\perp} = 2Yj_{cy}\int_0^R r^2dr\int_0^{\pi} sin\theta d\theta = \frac{4}{3}j_{cy}YR^3 = \frac{4}{3\pi}j_{cy}VR \tag{1.24}$$

where, $V = (\pi R^2 Y)$, hence,

$$< M >_{\perp} = \frac{4}{3\pi}j_{cy}R \tag{1.25}$$

scales with the radius R.

1-6 Orientation Dependence of the Magnetization

A feature intimately related to the size dependence of the magnetization of hysteretic type II superconductors is the dependence of $< M >$ on the orientation of a specimen of fixed dimensions with respect to the magnetizing field H_a which induces the saturated critical state.

If the cylindrical rod is oriented with its length along the magnetizing field, which we take to be directed along the z axis, the induced persistent currents circulate azimuthally. Now,

the element of current,

$$\Delta I = \vec{j_c} \cdot \Delta \vec{S} = j_{c\phi} \Delta r \Delta z \tag{1.26}$$

embraces an area,

$$A = \pi r^2 \tag{1.27}$$

Thus,

$$\mu_{//} = j_{c\phi} \pi \int_0^R r^2 dr \int_0^L dz = j_{c\phi} \pi \frac{R^3}{3} L = j_{c\phi} \frac{VR}{3} \tag{1.28}$$

where $V = (\pi R^2)L$. Hence,

$$< M >_{//} = j_{c\phi} \frac{R}{3} \tag{1.29}$$

agains scales linearly with the radius. We note that, keeping R fixed and $j_c = j_{c\phi} = j_{cy}$ the change of orientation of a cylindrical specimen, with respect to the magnetizing field, has caused a small change in the numerical coefficient of $< M >_{\perp}$ and $< M >_{//}$ from $4/3\pi$ to $1/3$.

Rotation by 90° of a long rectangular slab (dimensions W and h fixed) in the x-z plane so that $W >> h$ is now the dimension // to the magnetizing field will lead to a diminution of $< M >$ by a factor h/W since by eqn 1.19, $< M >$ will change from, $j_{cy}W/4$ to, $j_{cy}h/4$. Natural single crystals of high T_c superconductors are generally platelets whose thickness or height h is very small compared with their width W and length L. Vibrating sample magnetometer and SQUID magnetometer measurements of these small platelets revealed that $\mu_1 << \mu_2$. Here μ_1 and μ_2 denote the magnetic moments with the magnetizing field

directed along a large dimension and along the small dimension h, respectively. In these single crystal platelets, the C axis is directed along the small dimension h and the ab plane is parallel to the "large" LW plane. Initially the dramatic difference between μ_1 and μ_2 was entirely attributed to anisotropy of the critical current densities j_c^c and j_c^{ab}. Here j_c^c and j_c^{ab} denote the critical current densities along the C axis and in the ab plane respectively. Later, however, analysis along the lines we have outlined, showed that platelets whose j_c is isotropic will exhibit dramatic variations of μ arising from the "aspect ratio", i.e. the orientation of the specimen with respect to the magnetizing field.

1-7 Objective of the Thesis

In this thesis we attempt to model and identify the effects of the aspect ratio, orientation, geometry and anisotropy of j_c on the saturation magnetic moment of parallelepipeds. For instance, it is clear from our introductory analysis that a long square rod where $W = h << L$, and where j_c is isotropic will exhibit no change in μ whether H_a is directed along W or h. We expect however that μ will exhibit some variation at intermediate orientations of H_a in the hW plane from its value with H_a // to h or W. In particular, we mention here, the "simple" case where H_a is directed along a diagonal in the hW plane of a square specimen. The magnetizing field now "sees" a diamond shaped object. The symmetry of this situation is of special interest and simplifies the analysis in this case.

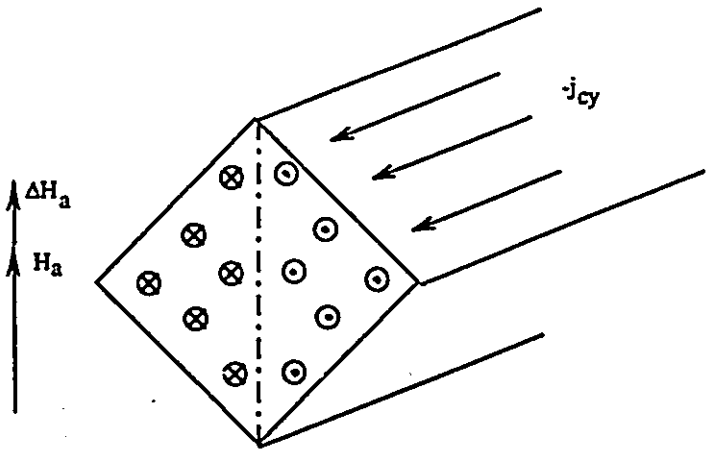

Further we have up to now in this introduction ignored the region where the circulating induced persistent currents turn around. For a realistic examination of real samples, that is samples finite along all three dimensions this region must be taken into account. We will therefore also pursue this feature in some detail in our investigation. Indeed we note that the pattern of circulation of the persistent currents in a square rod whose axis or length is directed along the magnetizing field consists entirely of U turns as illustrated in sketch (a) below. It is also important that the anisotropy of the critical current density be taken into account.

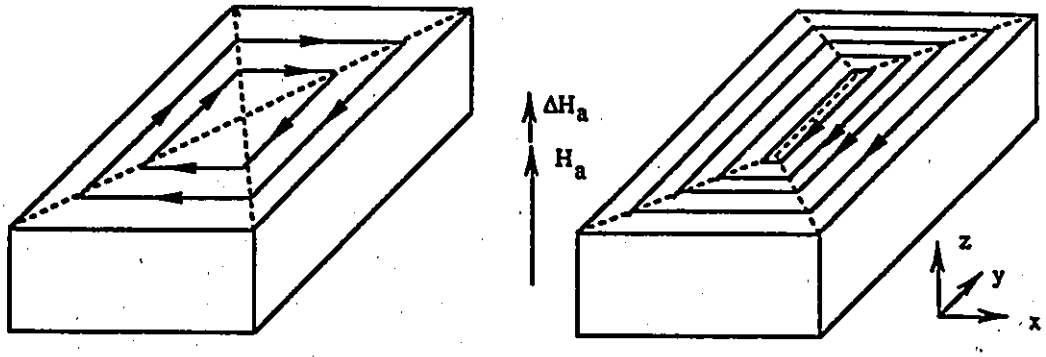

(a) (b)

Sketch (b) displays the pattern of induced persistent currents in the xy plane of a block of identical size and shape as that shown in (a). In sketch (b) howevev, j_{cx}, the critical current density along the x direction is smaller than j_{cy}, the critical current density along the y axis.

The simple situations we have described above are illustrative examples of the spectrum of saturated configurations of circulating critical persistent currents which we examine in this thesis.We develop closed form expressions for the resulting magnetic moments and magnetizations and our analysis includes configurations where j_c is anisotropic . Throughout our analysis we regard j_c to be independent of B, hence exploit the Bean approximation.

Chapter 2

THE BASIC FRAMEWORK and FORMULAE (Part I)

Part I

2-1 Introduction

In this Chapter we describe the basic framework and develop the key formulae which will then be applied to a variety of situations in the subsequent chapter.

The basic formulae which we exploit in our work were derived by Gyorgy et al (14) and Peterson (20) and independently by us. These workers addressed this problem in the

framework of the constitutive equation,

$$< B >= \mu_0 H_a + \mu_0 < M > \tag{2.1}$$

It is instructive to present and comment on this approach.

2-2 Framework of $< B >$

These workers consider a specimen of uniform rectangular cross section in the xy plane and of infinite length along the z axis. The magnetizing field H_a is directed along the z axis and $\triangle H_a$ is sufficiently large so as tc induce persistent currents to circulate throughout the volume of the specimen and establish concomitant critical gradients of flux line density extending from the centre to the surface of the specimen.

The spatial configuration of magnetic flux density in cartesian coordinates,

$$\vec{B}(x,y,z,) = \hat{x}B_x(x,y,z) + \hat{y}B_y(x,y,z) + \hat{z}B_z(x,y,z) \tag{2.2}$$

can be simplified to read,

$$\vec{B}(x,y,z) = \hat{z}B_z(x,y,z) \tag{2.3}$$

if the specimen is regarded as infinite, isotropic and of uniform cross section along the z direction. Introducing eqn 2.3 into Maxwell's equation, $\nabla \times \vec{B} = \mu_0 \vec{j}$, leads to,

$$\hat{y}\frac{\partial B_z(x,y)}{\partial x} = -\hat{y}\mu_0 j_{cy}(x,y)$$

$$\hat{x}\frac{\partial B_z(x,y)}{\partial y} = \hat{x}\mu_0 j_{cx}(x,y) \tag{2.4}$$

where the current densities are taken to exist at critical levels. The critical current density along the x axis is viewed as invariant along that direction and similarly, the critical current density along the y axis is viewed as uniform along the y direction. Consequently eqn 2.4 reads,

$$\frac{\partial B_z}{\partial x} = -\mu_0 j_{cy}(x)$$

$$\frac{\partial B_z}{\partial y} = \mu_0 j_{cx}(y) \tag{2.5}$$

which apply along the appropriate slopes of the $B_z(x,y)$ profiles. Anisotropy in the xy plane is taken into account by considering, $j_{cx}(y) \neq j_{cy}(x)$.

In this framework it is possible to consider the general situation where j_{cx} and j_{cy} may not only depend on B_z but also depend on B_z in different ways. These authors however and other workers have restricted their analysis to the special case where j_{cx} and j_{cy} are independent of B, i.e., to the Bean approximation. Under these circumstances, the $B_z(x,y)$ profiles are linear and given by,

$$B_{z2}(x) = \mu_0 H_a - \mu_0 j_{cy}(X - x)$$

$$B_{z1}(y) = \mu_0 H_a - \mu_0 j_{cx}(Y - y) \tag{2.6}$$

which follow from integration of eqn. 2.5 and apply over the corresponding regions. The boundaries of the segments or regions B_{z1} and B_{z2} are determined by the requirement that

B_z must be continuous. Hence, along the contact surface, $B_{z1}(y) = B_{z2}(x)$ gives,

$$j_{cx}(Y - y) = j_{cy}(X - x) \tag{2.7}$$

which we shall derive below from conservation of current (i.e. the equation of current continuity).

Now eqn 2.6 is introduced into the definition,

$$< B_z >= \frac{1}{XY} \int \int B_{z1}(y) dx dy + \frac{1}{XY} \int \int B_{z2}(y) dx dy \tag{2.8}$$

where the integrations are carried out over the corresponding cross sections (see sketch below).

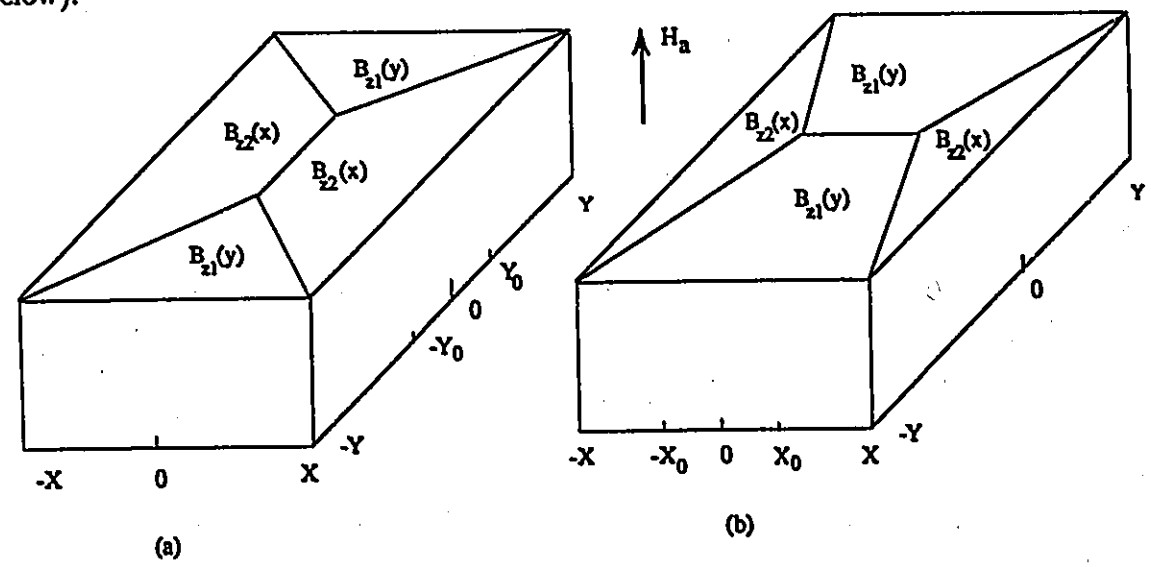

Two situations need to be investigated as sketched above. If the minima of the $B_{z1}(y)$ and $B_{z2}(x)$ profiles meet along the surface x=0, $-Y_0 \leq y \leq Y_0$, as in sketch (a), then the continuity of $B_z(x, y)$ reads,

$$B_{z1}(Y_0) = B_{z2}(0) \tag{2.9}$$

and eqn 2.7 yields,

$$j_{cx}(Y - Y_0) = j_{cy}X \tag{2.10}$$

If the minima of the $B_{z1}(y)$ and $B_{z2}(x)$ profiles meet along the surface y=0, $-X_0 \leq x \leq X_0$, as in sketch (b), then the continuity of $B_z(x,y)$ reads,

$$B_{z1}(0) = B_{z2}(X_0) \tag{2.11}$$

and eqn 2.7 yields,

$$j_{cx}Y = j_{cy}(X - X_0) \tag{2.12}$$

If the profiles meet at the axis of the infinitely long rectangular slab, then $X_0 = Y_0 = 0$, hence,

$$j_{cx}Y = j_{cy}X \tag{2.13}$$

and eqns 2.10 and 2.12 become identical.

Noting that eqn 2.7 expresses y as a function of x (or alternatively x as a function of y) at the boundary between the different zones of the $B_z(x,y)$ profiles and carrying out the straightforward but tedious double integrations of eqn 2.8, leads to,

$$< M >= J_{cy}X\{1 - \frac{1}{3}(\frac{j_{cy}}{j_{cx}})\frac{X}{Y}\} \tag{2.14}$$

$$< M >= J_{cx}Y\{1 - \frac{1}{3}(\frac{j_{cx}}{j_{cy}})\frac{Y}{X}\} \tag{2.15}$$

where we have made use of eqn 2.1 (i.e. $< M >= (< B > -\mu_0 H_a)/\mu_0$).

Equation 2.14 applies if the B_z profiles meet at x=0 and eqn 2.15 when they meet at y=0

(sketches(a) and (b) respectively).

The framework exploited by Gyorgy et al (13) and Peterson (20) has the virtue that it is applicable to situations where J_{cx} varies with y and/or j_{cy} varies with x. Such variations will be encountered when j_{cx} and j_{cy} depend on B. Further the dependence of j_{cx} and j_{cy} on B need not to be the same. This generality however comes at a price. The procedure followed by these authors in their derivation of eqn 2.14, is only valid if, as stated above, (i) the cross section of the specimen and (ii) j_{cx} and j_{cy} are uniform along the length of the rectangular specimen. Further the specimen must be, (iii) infinitely long and, (iv) have its axis parallel to H_a. These authors, however, either chose to neglect constraint (iii) or are not aware of this condition for the validity of their derivation and proceeded to apply these results to rectangular platelets where H_a is directed along the small dimension. We shall demonstrate below that eqns 2.14 and 2.15 are however fortuitously correct and valid regardless of the length of the sample.

We wish to stress in closing this section that for a specimen of finite length none of the expressions for the $B_z(x,y)$ profiles derived above are valid even if requirements (i) (ii) and (iv) enumerated above are satisfied. The reason for this is due to the fact that eqn 2.2 cannot be correctly reduced to eqn 2.3 for a finite sample. Of course when the demagnetization factor is small, it is acceptable to introduce the approximation that, $\vec{B}(x,y,z) = \hat{z}B_z(x,y)$. This however is certainly not the situation which prevails when the

length of the slab is comparable to or smaller than its "lateral" dimensions.

In the next section we derive the basic formulae (eqns 2.14 and 2.15) in a consistent and correct manner.

Chapter 3

THE BASIC FRAMEWORK AND FORMULAE

Part II

3-1 Introduction

Recently, Gyorgy et al (13) and Peterson (20) have developed expressions for the critical state magnetization of parallelepipeds of anisotropic type II superconductors. The formulae they have derived are very useful for extracting information on the anisotropic critical current densities j_c^c and j_c^{ab} along the c axis and in the ab plane of platelets of high temperatures superconductors.

These workers, however, derived these expressions in a framework which requires that the dimension of the specimen along the homogeneous magnetizing field, $\vec{H} = \hat{z}\ H_a$, be infinite and that the XY cross section be uniform, since they implicitly or explicitly stipulate that the spatial configuration of the magnetic flux density $\vec{B}$ (x,y,z) which in its general cartesian form reads,

$$\vec{B}(x,y,z) = \hat{x}\ B_x(x,y,z) + \hat{y}\ B_y(x,y,z) + \hat{z}\ B_z(x,y,z) \qquad (1)$$

can be simplified to read,

$$\vec{B}\ (x,y,z) = \hat{z}\ B_z\ (x,y) \qquad (2)$$

hence $\vec{B}$ is translationally invariant in the z direction.

As a consequence, the approach these authors have exploited is, in a strict sense, valid only when the demagnetizing factor is negligible so that "end" effects can be ignored. This caveat is certainly not satisfied when the magnetizing field is made to pierce the broad surfaces of the platelets (5,8,9,12,15)

In this thesis we exploit an alternative framework to calculate the magnetic moment of isotropic and anisotropic parallelepipeds. Our approach circumvents the constraint of idealized infinite geometry. Consequently this method enables us to investigate the variation of the magnetic moment of isotropic and anisotropic specimens of finite geometry as a function of their orientation with respect to the magnetizing field. Our approach however is applicable only to situations where the critical current densities are independent of the magnitude of the magnetic flux density (the well known Bean-London approximation (3,17)) and fill the entire volume of the specimen.

3-2 Development of our Framework

For algebraic simplicity, Gyorgy et al (13) and Peterson (20), confined their analysis to the case where j_c^c and j_c^{ab} are

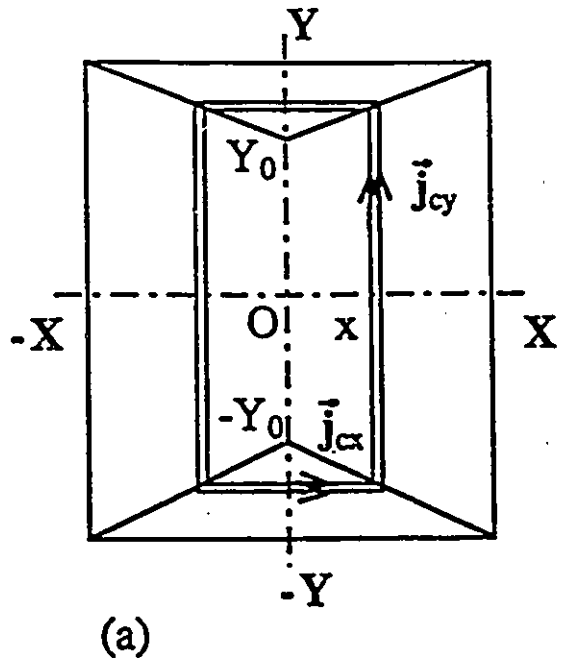

(a)

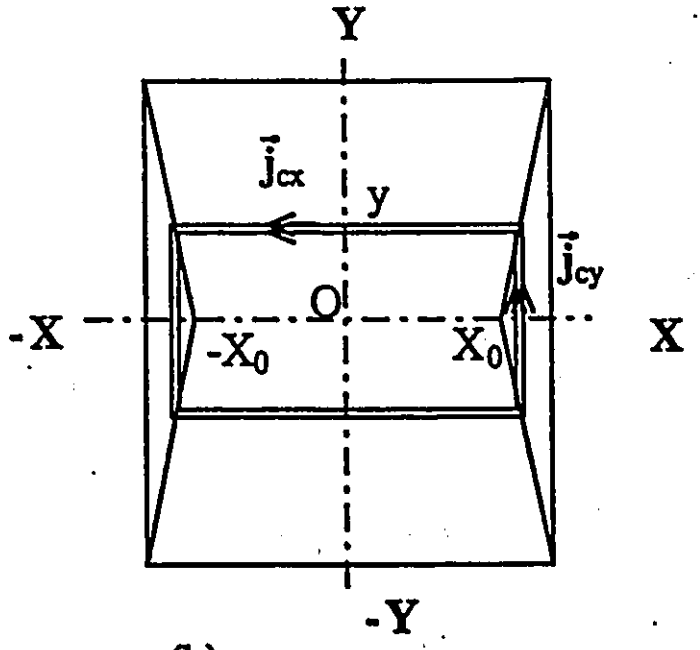

(b)

Fig. 1. Schematically displays the two situations which can occur when elementary rectangular circuits of persistent currents of critical density $j_{cx} > j_{cy}$, fill a specimen of arbitrary width and length, in accord with the principle of conservation (continuity) of the current. In (a), $j_{cy}X = j_{cx}(Y - Y_o)$. In (b) $j_{cy}(X - X_o) = j_{cx}Y$

independent of B. This stipulation is an essential element in our approach since, in our framework, the configuration of the magnetic flux density $\vec{B}(x,y,z)$ in the specimen plays no role.

The starting point for our development is a basic and standard definition of an elementary magnetic moment, namely,

$$\Delta\vec{\mu} = \vec{A}\Delta I \tag{3}$$

where,

$$\Delta I = \vec{j}\cdot\Delta\vec{S} \tag{4}$$

is an element of current of density $\vec{j}$ flowing through a cross section $\Delta\vec{S}$ at the periphery of an area $\vec{A}$. In this thesis we focus on parallelepiped geometry, hence $\vec{A}$ can be written,

$$\vec{A} = \hat{z}\ 4xy \tag{5}$$

where x and y are not independent variables but are linked by the principle of conservation of current (see Fig. 1).

For our choice of geometry, the conservation of current, hence the equation of continuity, $\nabla\cdot\vec{j} = 0$, reads,

$$\Delta I = j_{cy}\ \Delta x\Delta z = j_{cx}\ \Delta y\Delta z \tag{6}$$

where the critical current densities j_{cx} and j_{cy} along the x and y axes respectively will be assumed to depend only on their direction with respect to the axes of the parallelepiped.

By conservation of current, eqn. 6 leads to,

$$\int_{x}^{X} j_{cy}\, dx = j_{cy}\,(X - x) = \int_{y}^{Y} j_{cx}\, dy = j_{cx}\,(Y - y) \qquad (7)$$

where we have stipulated that j_{cx} and j_{cy} do not depend on the coordinate z. The upper limits of integration, X and Y, denote the boundaries of a rectangle whose center is located at x = 0, y = 0. Eqns. 5 and 6 also imply that the persistent currents circulate only in the xy planes regardless of the orientation of the specimen with respect to the magnetizing field $\vec{H} = \hat{z}\, H_o$.

After rearrangement, eqn. 7 reads,

$$y = Y\left\{1 - \left(\frac{j_{cy}}{j_{cx}}\right)\frac{X}{Y}\right\} + \left(\frac{j_{cy}}{j_{cx}}\right)x \qquad (8a)$$

$$x = X\left\{1 - \left(\frac{j_{cx}}{j_{cy}}\right)\frac{Y}{X}\right\} + \left(\frac{j_{cx}}{j_{cy}}\right)Y \qquad (8b)$$

We visualize that the persistent critical circulating currents fill the entire cross sections of the specimen. This is often denoted the fully penetrated critical state or the saturated critical state. Under these circumstances eqn. 8(a) should be used if $y \neq 0$ when $x = 0$ and eqn. 8(b) should be used if $x \neq 0$ when $y = 0$ (see Fig. 1).

Introducing eqns. 5, 6 and 8(a) or 8(b) into eqn. 3 and integrating over the volume of the sample leads to,

$$\vec{\mu} = \hat{z}\, 4j_{cy} \int_{z_i}^{z_f} dz \int_{o}^{X} x \left[Y\left\{1 - \left(\frac{j_{cy}}{j_{cx}}\right) \frac{X}{Y}\right\} + \left(\frac{j_{cy}}{j_{cx}}\right) x \right] dx \qquad (9a)$$

$$\vec{\mu} = \hat{z}\, 4j_{cx} \int_{z_i}^{z_f} dz \int_{o}^{Y} y \left[X\left\{1 - \left(\frac{j_{cx}}{j_{cy}}\right) \frac{Y}{X}\right\} + \left(\frac{j_{cx}}{j_{cy}}\right) y \right] dy \qquad (9b)$$

where Z_f and Z_i denote the extremities of the parallelepiped along the z axis regardless of its orientation with respect to that axis. The X and Y boundaries of the parallelepiped will be seen to depend on its orientation with respect to $\vec{H} = \hat{z}\, H_o$ and also on the coordinate z.

Integrating eqn. 9(a) with respect to x yields,

$$\vec{\mu} = \hat{z}\, 2j_{cy} \int_{z_i}^{z_f} dz\, X^2 Y \left\{1 - \frac{1}{3}\left(\frac{j_{cy}}{j_{cx}}\right) \frac{X}{Y}\right\} \qquad (10a)$$

and integrating eqn. 9(b) with respect to y yields,

$$\vec{\mu} = \hat{z}\, 2j_{cx} \int_{z_i}^{z_f} dz\, XY^2 \left\{1 - \frac{1}{3}\left(\frac{j_{cx}}{j_{cy}}\right) \frac{Y}{X}\right\} \qquad (10b)$$

We wish to emphasize that eqns. 10(a) and 10(b) can be applied to calculate $\vec{\mu}$ for a large variety of symmetric objects (such as prisms, pyramids, ziggurats etc.) where $\vec{H}$ is directed along the axis or plane of symmetry. The essential ingredient is

the knowledge of the X and Y dimensions of the object as a function of z. In this thesis we confine our application of these equations to prisms of uniform length Y and "tilted" parallelepipeds.

The spatial average of the non uniform magnetization $\langle\vec{M}\rangle$ is obtained from

$$\langle\vec{M}\rangle = \frac{\vec{\mu}}{V} \tag{11}$$

where V is the volume of the parallelepiped.

Eqn. 10(a) applies when the total current circulating in an elementary slab of height Δz, reads,

$$\frac{I}{\Delta z} = j_{cy}\, X = j_{cx}\, (Y - Y_o) \tag{12a}$$

and eqn. 10(b) applies in the case where,

$$\frac{I}{\Delta z} = j_{cy}\, (X - X_o) = j_{cx}\, Y \tag{12b}$$

See Figs. 1(a) and 1(b).

A special limiting case is encountered when $j_{cy} X = j_{cx} Y$, hence $Y_o = X_o = 0$ because $x = 0$ when $y = 0$ in eqn. 8.

Gyorgy et al (13) and Peterson (20) have focused on orthorhombic geometry. For this geometry eqns. 10(a) and 10(b) lead to,

$$\vec{\mu} = \hat{z}\ 4\ j_{cy}\ X^2YZ \left\{1 - \frac{1}{3}\left(\frac{j_{cy}}{j_{cx}}\right)\frac{X}{Y}\right\} \qquad (13a)$$

$$\vec{\mu} = \hat{z}\ 4\ j_{cx}\ XY^2Z \left\{1 - \frac{1}{3}\left(\frac{j_{cx}}{j_{cy}}\right)\frac{Y}{X}\right\} \qquad (13b)$$

taking $Z_i = 0$ and $Z_f = 2Z$. These formulae are identical to that obtained by Gyorgy et al (13) and Peterson (20) in a different framework and also reported by Aguillon et al. (2). Our development demonstrates that these expressions are valid for orthorhombic samples of finite dimension along the magnetizing field, hence for platelets whose broad surfaces are pierced by $\vec{H}$.

Chapter 4

$\vec{\mu}$ vs. θ WITH ISOTROPIC $\vec{j}_c$

4-1 Introduction

In the preceding chapter we developed formulae for anisotropic parallelepipeds where, however, the magnetizing field was always directed along a plane of symmetry. We now confine our study to parallelepipeds which are isotropic, i.e. $j_{cx} = j_{cy} = j_o$. In this chapter we examine the dependence of the magnetic moment of an isotropic parallelepiped as a function of the orientation of its faces with respect to the magnetizing field $\vec{H} = \hat{z}\, H_a$.

4-2 Description of the Framework

Let $\vec{A}$, $\vec{L}$ and $\vec{W}$ denote the magnitude and direction of the edges of the parallelepiped. Let θ denote the angle subtended by $\vec{H}$ and the edge vector $\vec{A}$, and take the edge vector $\vec{L}$ to be directed along the y axis which is the axis of rotation (see Fig. 2). We visualize that the persistent currents circulate perpendicularly to $\vec{H}$, hence in xy planes, and fill the entire volume of the specimen.

Fig. 2. (a) Displays a parallellepiped of height A, length L and width W along the z, y and x axes respectively. The y axis is the axis of rotation. (b) The parallelepiped is inclined (rotated) an angle $\theta < \theta_c$ with respect to the z axis. Its volume is decomposed into two prisms of base $W/\cos\theta$ and height Z'_{Δ} and a parallelogram of height $Z'_{//}$. (c) $\theta = \theta_c$ when the diagonal is along the x axis and the base of the prisms $D = W/\cos\theta_c = A/\sin\theta_c$ (d) $\theta_c < \theta < \pi/2$. The base and height of the two prisms are now $A/\sin\theta$ and Z''_{Δ}. The height of the parallelogram is $Z''_{//}$.

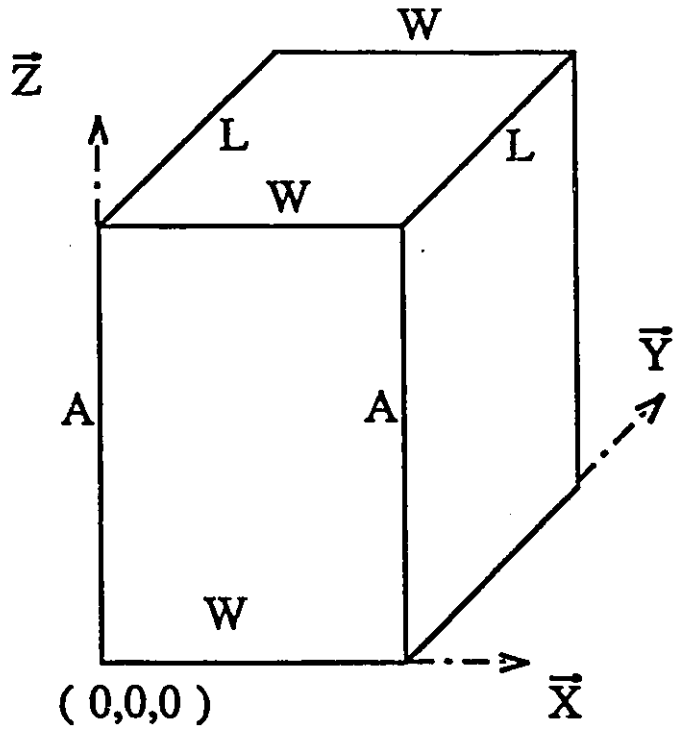
W
$\vec{Z}$
L
L
W
$\vec{Y}$
A
A
W
$\vec{X}$
(0,0,0)

(a)

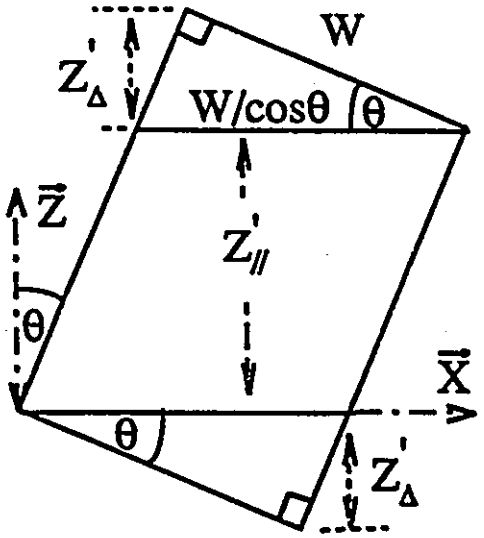
W
Z'_Δ
W/cosθ
θ
$\vec{Z}$
$Z'_{//}$
θ
$\vec{X}$
θ
Z'_Δ

(b)

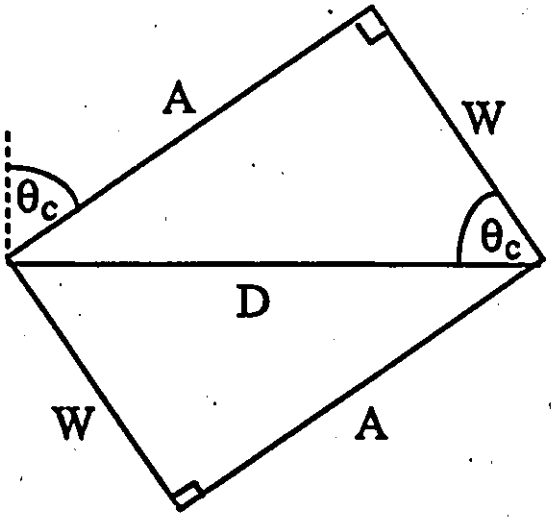
A
W
θ_c
θ_c
D
W
A

(c)

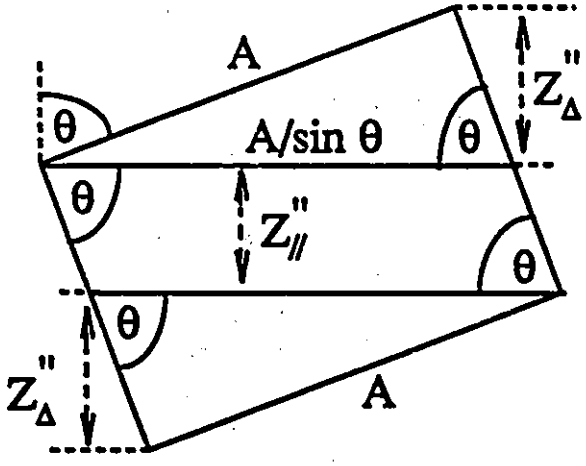
A
Z''_Δ
θ
A/sin θ
θ
θ
$Z''_{//}$
θ
θ
Z''_Δ
A

(d)

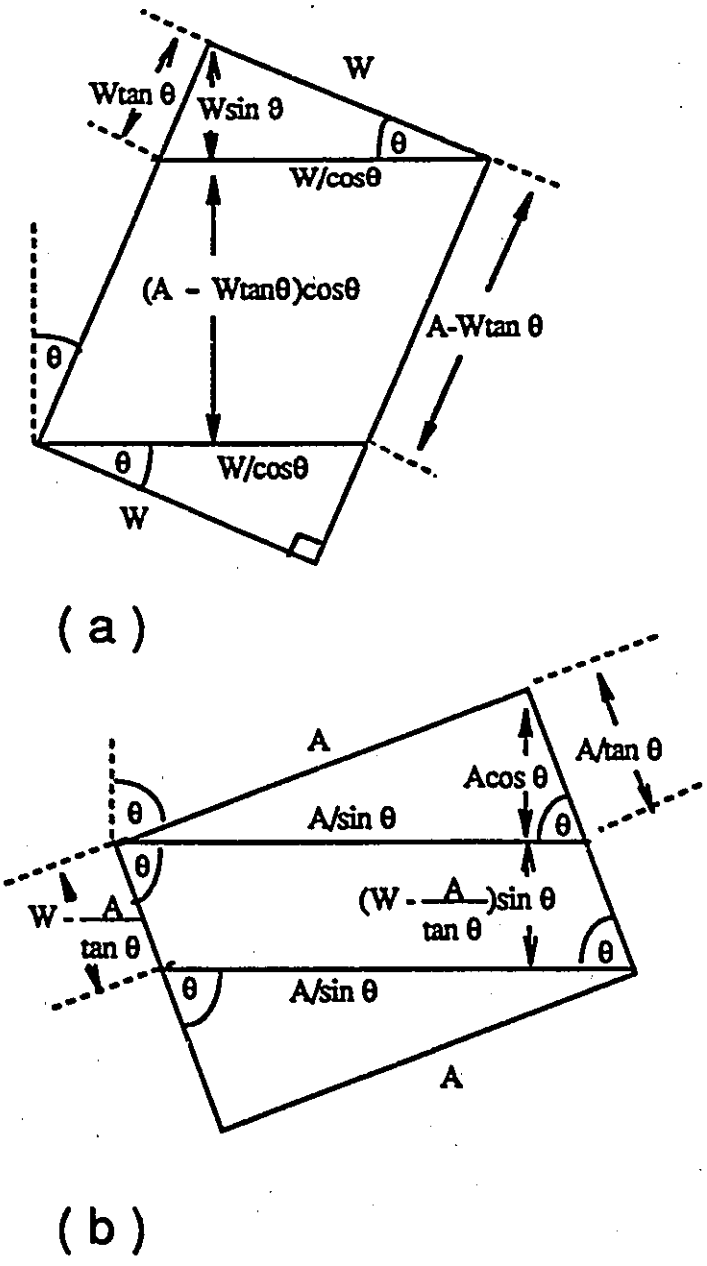

Fig. 3: Complements Fig. 2 by illustrating the expressions for, (a) Z'_{Δ}, $Z'_{//}$ and related dimensions when $0 < \theta < \theta_c$ and (b) Z''_{Δ}, $Z''_{//}$ and related dimensions when $\theta_c < \theta < \pi/2$.

Fig. 2 illustrates the geometric feature that a cross section of the parallelepiped in a xz plane can be decomposed into two triangles and a central parallelogram. The shape of these geometric objects varies as a function of θ. The length L of the two prisms and the central parallelepiped remain constant, with L = 2Y, always along the axis of rotation. However, the width of the prisms along the x axis varies as a function of z and θ and the width of the parallelogram depends on θ. Further, the height of these geometric components varies with θ. Thus to exploit eqns. 10(a) and 10(b), the boundaries $X(z,\theta)$, $Z_f(\theta)$ and $Z_i(\theta)$ must first be specified for the triangles and parallelogram.

We note that the central parallelogram vanishes when the bases of the triangles (prisms) coincide with the diagonal $D = \sqrt{A^2 + W^2}$ of the large rectangle whose edges are $\vec{A}$ and $\vec{W}$. Let θ_c denote the corresponding angle θ. Since $D = A/\sin\theta_c = W/\cos\theta_c$, then,

$$\theta_c = \tan^{-1}\left(\frac{A}{W}\right) \qquad (14)$$

In the range $0 \leq \theta < \theta_c$ it is the width W which "governs" the relevant dimensions whereas in the range $\theta_c < \theta < \pi/2$ it is the height A which enters into the pertinent expressions for $X(z,0)$, $Z_f(\theta)$ and $Z_i(\theta)$. Although A is chosen larger than W in Figs 2 and 3, the formulae developed below apply both when A > W and A < W.

Let the subscripts // and Δ denote the central parallelogram and the triangles (prisms) respectively. We use $Z_{//}$ (Z_Δ) to denote the height of the parallelogram (triangles) along

the z axis and $X_{//}(X_{\Delta})$ to denote their half width along the x axis. From Fig. 2(b) and 3(a) we see that,

$$Z'_{//} = A \cos \theta - W \sin \theta \tag{15}$$

$$Z'_{\Delta} = W \sin \theta \tag{16}$$

$$2 X'_{//} = \frac{W}{\cos \theta} \tag{17}$$

$$2 X'_{\Delta}(z) = \frac{W}{\cos \theta} - \frac{z}{\sin \theta \cos \theta} \tag{18}$$

where the single prime on Z and X denotes that the expressions correspond to the range $0 \leq \theta \leq \theta_c$.

From Fig. 2(d) and 3(b) we see that,

$$Z''_{//} = W \sin \theta - A \cos \theta \tag{19}$$

$$Z''_{\Delta} = A \cos \theta \tag{20}$$

$$2X''_{//} = \frac{A}{\sin \theta} \tag{21}$$

$$2 X''_{\Delta}(z) = \frac{A}{\sin \theta} - \frac{z}{\sin \theta \cos \theta} \tag{22}$$

where the double prime on Z and X denotes that the expressions correspond to the range $\theta_c \leq \theta \leq \pi/2$.

Since the width $2X_{\Delta}$ of the triangles varies along the

coordinate z, situations must be envisaged where $2X_\Delta(z)$ is greater than L near the base of the triangle but will then become smaller than L near the vertex. This kind of situation is encountered when $W/\cos\theta > L$ or when $A/\sin\theta > L$. In these circumstances eqn. 10(a) will apply over one range of integration over z and eqn. 10(b) over the remaining range of z spanning the height of the prisms. Let $Z_{1\Delta}$ denote the value of z when the X dimension,

$$2X_\Delta(z) = L = 2Y \tag{23}$$

Introducing this condition into eqns. 18 and 22 leads to,

$$Z'_{1\Delta} = (W - L\cos\theta)\sin\theta \tag{24}$$

$$Z''_{1\Delta} = (A - L\sin\theta)\cos\theta \tag{25}$$

Eqn. 24 applies when $W/\cos\theta > L$ and $0 \le \theta \le \theta_c$. Eqn. 25 applies when $A/\sin\theta > L$ and $\theta_c \le \theta \le \pi/2$. The single and double primes continue to indicate the ranges of θ.

4-3 Development of the Formulae

We now proceed to develop explicit expressions for the magnitude of the magnetic moment of the central parallelepiped ($\mu_{//}$) and each prism (μ_Δ) as a function of θ. It is convenient to consider these quantities for θ in the ranges $0 \le \theta \le \theta_c$ and

$\theta_c \leq \theta \leq \pi/2$ separately. Also for each range of θ we must envisage two possibilities, namely whether $2\,X(z = 0) \gtrless L$.

The expressions for the total magnetic moments will not be tabulated since they can readily be obtained by introducing the formulae, which are presented below, into the definition,

$$\mu_{total} = \mu_{//} + 2\,\mu_{\Delta} \tag{26}$$

A. $0 \leq \theta \leq \theta_c$

Two situations need to be envisaged in exploiting eqns. 10(a) and 10(b).

a) $W/\cos\theta \leq L$

Introducing eqn. 17 into eqn. 10(a) and integrating from 0 to $Z'_{//} = A\cos\theta - W\sin\theta$, (eqn. 15), leads to,

$$\mu_{//} = \frac{j_o}{4}\,\frac{ALW^2}{\cos\theta}\,(1 - \frac{W}{A}\tan\theta)(1 - \frac{1}{3}\,(\frac{W}{L})\,\frac{1}{\cos\theta}) \tag{27}$$

Introducing eqn. 18 into eqn. 10(a) and integrating from 0 to $Z'_{\Delta} = W\sin\theta$, (eqn. 16), leads to,

$$\mu_{\Delta} = \frac{j_o}{12}\,LW^3\,\frac{\sin\theta}{\cos^2\theta}\,(1 - \frac{1}{4}\,(\frac{W}{L})\,\frac{1}{\cos\theta}) \tag{28}$$

b) $W/\cos\theta \geq L$

Introducing eqn. 17 into eqn. 10(b) and integrating from 0 to $Z'_{//} = A\cos\theta - W\sin\theta$, (eqn. 15), leads to,

$$\mu_{//} = \frac{j_o}{4}(1 - \frac{W}{A}\tan\theta)\{1 - \frac{1}{3}(\frac{L}{W})\cos\theta\} \qquad (29)$$

Two regions of the prisms must be considered separately. For the volume adjacent to the base eqn. 18 is introduced into eqn. 10(b) and integration from 0 to $Z'_{1\Delta} = (W - L\cos\theta)\sin\theta$, (eqn. 24), leads to,

$$\mu_{\Delta 1} = \frac{j_o}{8} L^2W^2 \tan\theta \{1 - \frac{2}{3}(\frac{L}{W})\cos\theta - \frac{1}{3}(\frac{L}{W})^2\cos^2\theta\} \qquad (30)$$

For the volume near the vertex, eqn. 18 is introduced into eqn. 10(a) and integration from $Z'_{1\Delta}$ to $Z'_{\Delta} = W\sin\theta$ leads to,

$$\mu_{\Delta 2} = \frac{j_o}{16} L^4 \sin\theta\cos\theta \qquad (31)$$

Combining eqns. 30 and 31 we obtain for each prism,

$$\mu_{\Delta} = \frac{j_o}{8} L^2W^2 \tan\theta\{1 - \frac{2}{3}(\frac{L}{W})\cos\theta + \frac{1}{6}(\frac{L}{W})^2\cos^2\theta\} \qquad (32)$$

B. $\theta_c \leq \theta \leq \pi/2$

Again, two situations need to be envisaged in applying eqns. 10(a) and 10(b).

a) $A/\sin \leq L$

Introducing eqn. 21 into eqn. 10(a) and integrating over the height of the parallelogram from 0 to $Z''_{//} = W \sin\theta - A \cos\theta$, (eqn. 19), leads to,

$$\mu_{//} = \frac{j_o}{4} \frac{A^2 LW}{\sin\theta} \left(1 - \frac{A}{W \tan\theta}\right)\left\{1 - \frac{1}{3}\left(\frac{A}{L}\right) \frac{1}{\sin\theta}\right\} \qquad (33)$$

Introducing eqn. 22 into eqn 10(a) and integrating over the height of the prism from 0 to $Z''_{\Delta} = A \cos\theta$, (eqn. 20), leads to,

$$\mu_{\Delta} = \frac{j_o}{12} A^3 L \frac{\cos\theta}{\sin^2\theta} \left\{1 - \frac{1}{4}\left(\frac{A}{L}\right) \frac{1}{\sin\theta}\right\} \qquad (34)$$

b) $A/\sin\theta \geq L$

Introducing eqn. 21 into eqn. 10(b) and integrating over the height of the parallelogram from 0 to $Z''_{//} = W \sin\theta - A \cos\theta$ (eqn. 19), leads to,

$$\mu_{//} = \frac{j_o}{4} AL^2 W \left(1 - \frac{A}{W} \frac{1}{\tan\theta}\right)\left\{1 - \frac{1}{3}\left(\frac{L}{A}\right) \sin\theta\right\} \qquad (35)$$

Again two regions of the prisms must be considered separately. For the volume adjacent to the base, eqn. 22 is introduced into eqn. 10(b) and integrating from 0 to $Z''_{1\Delta} = (A - L \sin\theta) \cos\theta$, (eqn. 25), leads to,

$$\mu_{\Delta 1} = \frac{j_o}{8} A^2 L^2 \frac{1}{\tan\theta}\left\{1 - \frac{2}{3}\left(\frac{L}{A}\right) \sin\theta - \frac{1}{3}\left(\frac{L}{A}\right)^2 \sin^2\theta\right\} \qquad (36)$$

For the volume adjacent to the vertex, eqn. 22 is introduced into eqn. 10(a) and integrating from $Z''_{1\Delta}$ to $Z''_{\Delta} = A \cos\theta$ leads to,

$$\mu_{\Delta 2} = \frac{j_o}{16} L^4 \sin\theta \cos\theta \qquad (37)$$

Combining eqns. 36 and 37 leads to,

$$\mu_{\Delta} = \frac{j_o}{8} A^2 L^2 \frac{1}{\tan\theta} \left\{1 - \frac{2}{3}\left(\frac{L}{A}\right) \sin\theta + \frac{1}{6}\left(\frac{L}{A}\right)^2 \sin^2\theta\right\} \qquad (38)$$

for each prism.

4-4 Application of the Formulae

The solid curves in Figs. A-1 through A-12 and B-1 through B-25 display $\mu_N(\theta)$, the magnetic moment normalized to the maximum value for each case, hence,

$$\mu_N(\theta) = \frac{\mu(\theta)}{\mu_{max}(\theta)} = \frac{\mu_{//}(\theta)+2\mu_{\Delta}(\theta)}{\{\mu_{//}(\theta)+2\mu_{\Delta}(\theta)\}_{max}} \qquad (39)$$

versus θ for isotropic parallelepipeds of various height/width/thickness ratios. These curves illustrate the effect of the "geometry" of the parallelepiped on the magnetization. In the next chapter we explore the effect of current anisotropy on this behavior.

Chapter 5

$\vec{\mu}$ vs. θ WITH ANISOTROPIC $\vec{j}_c$

5-1 Introduction

We pursue two simple regimes of anisotropy. In the first case, the critical current density along the AW planes is considered to be isotropic, hence $j_c^A = j_c^W = j_{cx}$ but differs from $j_{cy} = j_c^L$, the critical current density along the dimension L, where $\vec{L}$ is along $\vec{y}$, the axis of rotation. Here, the vector $\vec{L} = \vec{A} \times \vec{W}$, identifying the isotropic planes remains fixed as θ varies. In the second case, also with $\vec{L}$ along $\vec{y}$ (the axis of rotation always) the vector identifying the isotropic planes (either $\vec{W} = \vec{L} \times \vec{A}$ or $\vec{A} = \vec{W} \times \vec{L}$) rotates in unison with θ. Consequently now the isotropic planes change their orientation with respect to the magnetizing field as θ is varied. In the calculations we will introduce a simple expression for the dependence of j_{cx} on θ. In all the situations we assume that the persistent currents circulate perpendicularly to the magnetizing field $\vec{H}$ and fill the specimen. Recent experiments however indicate that the direction of current flow may not be orthogonal to the magnetizing field $\vec{H}$ but dictated by the anisotropy of the specimen (10,11,16,22,23).

5-2 Anisotropy Parameter Independent of θ

5-2-1 Development of the Formulae

This scenario is akin to that encountered when a single crystal of a high T_c material is oriented with its c axis directed along the axis of rotation (y axis), hence its ab plane coincides with our choice for the x-z plane. Under these circumstances,

$$j_{cy} = j_c^c, \quad j_{cx} = j_c^{ab} \tag{40}$$

where j_c^c is the critical current density along the c axis of the crystal and j_c^{ab}, the critical current density in the ab plane. j_c^{ab} is assumed isotropic in the ab plane. Consequently, we regard both j_{cx} and j_{cy} as constant regardless of the orientation of the $\vec{A}$ and $\vec{W}$ edges of the parallelepiped with respect to $\vec{H}$.

For the isotropic parallelepiped, the simple geometric ratio $X(z,\theta)/Y$ determined whether eqn. 10(a) or 10(b) was utilised for the calculation of the contributions to the total magnetic moment by the central parallelepiped and prisms. With the introduction of anisotropy of $\vec{j}_c$, it is now the ratio, $j_{cx}Y/j_{cy}X(z,\theta)$ which governs this choice. It is then convenient to define an anisotropy parameter,

$$\beta = \frac{j_{cx}}{j_{cy}} \tag{41}$$

It is also useful to rewrite eqns. 10(a) and 10(b) with this term appearing explicitly. Thus,

$$\frac{\vec{\mu}}{j_{cy}} = \hat{z}2 \int_{z_i}^{z_f} dz\ X^2 Y \left\{1 - \frac{1}{3\beta}\left(\frac{X}{Y}\right)\right\} \tag{42a}$$

$$\frac{\vec{\mu}}{j_{cy}} = \hat{z}\ 2\beta \int_{z_i}^{z_f} dz\ XY^2 \left\{1 - \frac{1}{3}\ \beta\ \left(\frac{Y}{X}\right)\right\} \tag{42b}$$

where we have "normalized" μ with respect to j_{cy} directed along the axis of rotation.

It is straightforward to develop expressions for $\mu_{//}$ and μ_{Δ} versus θ for the ranges $0 \leq \theta \leq \theta_c$ and $\theta_c \leq \theta \leq \pi/2$ separately as in section III. We note that the geometric relations (eqns. 15 through 22) continue to apply unchanged in this exercise. The anisotropy, besides appearing as a coefficient in eqns. 42(a) and 42(b) enters into the picture in dictating which of these two equations is pertinent. This choice is now determined by the condition,

$$\frac{W}{\cos\theta} \gtrless \beta L \tag{43}$$

in the range $0 \leq \theta \leq \theta_c$ and the condition,

$$\frac{A}{\sin\theta} \gtrless \beta L \tag{44}$$

in the range $\theta_c \leq \theta \leq \pi/2$.

The anisotropy parameter also plays an important role in prescribing the plane $Z_{1\Delta}$ inside the prisms where a switch has to be made from eqn. 42(a) to 42(b). The expression for this dividing plane now reads,

$$Z'_{1\Delta} = (W - \beta L \cos\theta) \sin\theta \tag{45}$$

for the range, $0 \leq \theta \leq \theta_c$, and,

$$Z''_{1\Delta} = (A - \beta L \sin\theta) \cos\theta \tag{46}$$

for the range, $\theta_c \leq \theta \leq \pi/2$.

Bearing these features in mind and proceeding as in chapter 3 we obtain,

A. $0 \leq \theta \leq \theta_c$

a) $W/\cos\theta \leq \beta L$

$$\mu_{//} = \frac{j_{cy}}{4} \frac{ALW^2}{\cos\theta} \left(1 - \frac{W}{A} \tan\theta\right)\left\{1 - \frac{1}{3}\left(\frac{W}{\beta L}\right) \frac{1}{\cos\theta}\right\} \tag{47}$$

$$\mu_{\Delta} = \frac{j_{cy}}{12} LW^3 \frac{\sin\theta}{\cos^2\theta} \left\{1 - \frac{1}{4}\left(\frac{W}{\beta L}\right) \frac{1}{\cos\theta}\right\} \tag{48}$$

b) $W/\cos\theta \geq \beta L$

$$\mu_{//} = \frac{j_{cy}}{4}\beta A L^2 W \cos\theta\left(1 - \frac{W}{A}\tan\theta\right)\left\{1 - \frac{1}{3}\left(\frac{\beta L}{W}\right)\cos\theta\right\} \quad (49)$$

$$\mu_{\Delta 1} = \frac{j_{cy}}{8}\beta L^2 W^2 \tan\theta\left\{1 - \frac{2}{3}\left(\frac{\beta L}{W}\right)\cos\theta - \frac{1}{3}\left(\frac{\beta L}{W}\right)^2\cos^2\theta\right\} \quad (50)$$

$$\mu_{\Delta 2} = \frac{j_{cy}}{16}\beta^3 L^4 \sin\theta\cos\theta \quad (51)$$

$$\mu_{\Delta} = \frac{j_{cy}}{8}\beta L^2 W^2 \tan\theta\left\{1 - \frac{2}{3}\left(\frac{\beta L}{W}\right)\cos\theta + \frac{1}{6}\left(\frac{\beta L}{W}\right)^2\cos^2\theta\right\} \quad (52)$$

B. $\theta_c \leq \theta \leq \pi/2$

a) $A/\sin\theta \leq \beta L$

$$\mu_{//} = \frac{j_{cy}}{4}\frac{A^2 L W}{\sin\theta}\left(1 - \frac{A}{W\tan\theta}\right)\left\{1 - \frac{1}{3}\left(\frac{A}{\beta L}\right)\frac{1}{\sin\theta}\right\} \quad (53)$$

$$\mu_{\Delta} = \frac{j_{cy}}{12}A^3 L\frac{\cos\theta}{\sin^2\theta}\left\{1 - \frac{1}{4}\left(\frac{A}{\beta L}\right)\frac{1}{\sin\theta}\right\} \quad (54)$$

b) $A/\sin\theta \geq \beta L$

$$\mu_{//} = \frac{j_{cy}}{4}\beta A L^2 W\left(1 - \frac{A}{W\tan\theta}\right)\left\{1 - \frac{1}{3}\left(\frac{\beta L}{A}\right)\sin\theta\right\} \quad (55)$$

$$\mu_{\Delta 1} = \frac{j_{cy}}{8}\frac{\beta A^2 L^2}{\tan\theta}\left\{1 - \frac{2}{3}\left(\frac{\beta L}{A}\right)\sin\theta - \frac{1}{3}\left(\frac{\beta L}{A}\right)^2\sin^2\theta\right\} \quad (56)$$

$$\mu_{\Delta 2} = \frac{j_{cy}}{16} \beta^3 L^4 \sin\theta \cos\theta \qquad (57)$$

$$\mu_{\Delta} = \frac{j_{cy}}{8} \frac{\beta A^2 L^2}{\tan\theta} \left\{1 - \frac{2}{3}\left(\frac{\beta L}{A}\right) \sin\theta + \frac{1}{6}\left(\frac{\beta L}{A}\right)^2 \sin^2\theta\right\} \qquad (58)$$

5-2-2 Application of the Formulae

We note that equations 47 through 58 reduce to the corresponding formulae in chapter 3 in the isotropic limit where $j_{cy} = j_{cx} = j_o$ hence $\beta = 1.0$. The reader may also verify that the corresponding formulae for μ_Δ reduce to identical expressions in the limit where $\theta = \theta_c$ and that $\mu_{//}$ vanishes, as required, in that limit. Further, we note that as required, (i) μ_Δ of eqns 50, 51 and 52 reduces to zero when $\theta = 0$, (ii) μ_Δ of eqns 54, 56, 57 and 58 reduces to zero when $\theta = \pi/2$, (iii) $\mu_{//}$ of eqns 47 and 49 reduces to the correct limit when $\theta = 0$, and (iv) $\mu_{//}$ of eqns 53 and 55 reduces to the correct limit when $\theta = \pi/2$.

The non-solid lines in Figs. A-1 through A-12 illustrate the variation of the "normalized" magnetization $\mu_N(\theta)$ versus θ for several values of the anisotropy parameter β and for parallelepipeds of a variety of height/length/width ratios. For completeness we consider situations where $\beta \gtrless 1.0$, hence $j_c^{ab} \gtrless j_c^c$.

5-3 Anisotropy Parameter β Varying With θ

5-3-1 Development of the Formulae

We now examine a scenario where the anisotropy parameter β varies with the orientation of the parallelepiped with respect to the magnetizing field $\vec{H}$.

Situations where the isotropic "ab plane" of anisotropic high T_c materials and other anisotropic type II superconductors is penetrated by the magnetizing field should also be addressed. It has been envisaged that, under these circumstances, the induced persistent currents may be completely confined to circulate in the ab planes (22) when the ab planes are tilted with respect to $\vec{H}$ although the matrix between these planes (the c axis material) can also sustain persistent currents where $j_c^c << j_c^{ab}$. It is of interest however to explore the alternative picture that the local resultant persistent current density, j_x, is a superposition or combination of the "strong" j_c^{ab} and "weak" j_c^c components.

Consequently we write,

$$j_x = j_c^W f_1(\theta) + j_c^A f_2(\theta) \qquad (59)$$

where $f_1(\theta)$ and $f_2(\theta)$ are functions of θ, the angle subtended by the $\vec{A}$ edges of the parallelepiped and $\vec{H}$. j_c^W and j_c^A are the critical current densities parallel to the $\vec{W}$ and $\vec{A}$ edges of the parallelepiped. To fix ideas, we artitrarily identify j_c^W with j_c^c

and j_c^A with j_c^{ab}. Thus the isotropic ab planes are chosen to correspond to the AL planes of Fig. 2(a). Therefore, here, $j_c^L = j_c^A = j_c^{ab}$. We note that, alternatively, the isotropic ab planes could be chosen to correspond to the WL planes in Fig. 2(a). We assume, for reasons of simplicity as well as physical validity, that $f_1(\theta) = \cos^2\theta$ and $f_2(\theta) = \sin^2\theta$.

The critical current density j_{cx} then obeys the prescription,

$$j_{cx} = j_c^c \cos^2\theta + j_c^{ab} \sin^2\theta \tag{60}$$

and,

$$j_{cy} = j_c^{ab} \tag{61}$$

Consequently the anisotropy parameter $\beta = j_{cx}/j_{cy}$ will now depend on θ, hence read,

$$\beta = \frac{j_{cx}}{j_{cy}} = \frac{\cos^2\theta}{j_c^{ab}/j_c^c} + \sin^2\theta = \frac{\cos^2\theta}{R} + \sin^2\theta \tag{62}$$

where

$$R = j_c^{ab}/j_c^c \tag{63}$$

5-3-2 Application of the Formulae

We continue to visualize that the persistent currents circulate perpendicularly to $\vec{H} = \vec{z}\, H_a$, hence in the xy planes, regardless of the orientation of the parallelepiped with respect to $\vec{H}$. Since β is not a function of x, y and z, the expressions

developed in section 5.2.1 continue to apply. Eqn. 62 or alternative forms of eqn 59 must, however, be taken into account in the computation and in the selection of the appropriate formulae among those enumerated in that section.

The scenario pursued here may correspond to that encountered in high T_c single crystals where the c axis of the platelet specimen coincides with the $\vec{W}$ edges of the parallelepiped of our exercise. Consequently the ab planes of the specimen are associated with the AL planes of the model parallelepiped. Here the ab planes are considered to be isotropic.

The non-solid curves in Figs. B-1 through B-25 display the "normalized" magnetization $\mu_N(\theta)$ versus θ for various choices of $R \gtrless 1$ for parallelepipeds of different height/length/width ratios. The isotropic case ($R = 1$, hence $\beta(\theta) = 1$) continues to be presented by the solid curves and is included for completeness and comparison. Now thirteen physically distinct situations have to be considered. These are displayed in Fig. 4 with the cube left to the imagination of the reader. Although for currently known high T_c superconductors $j_c^{ab} > j_c^c$, hence $R > 1$, for generality and completeness we have computed the behavior when $R < 1$, hence $j_c^{ab} < j_c^c$.

Chapter 6

SUMMARY AND CONCLUSION

We have developed expressions for the magnetic moment of isotropic and anisotropic parallelepipeds of various aspect ratios as a function of their orientation with respect to the magnetizing field. The induced persistent currents, whether isotropic or anisotropic are assumed to,

(i) fill the entire volume of the specimen (i.e. correspond to a saturated critical state),

(ii) possess critical current densities which are independent of the magnetic flux density, (i.e. satisfy the Bean approximation) and,

(iii) circulate perpendicularly to $\vec{H}$ in all circumstances.

It is useful to comment on each of these assumptions or requirements.

A procedure which should be implemented in order to ensure that a saturated critical state

has been established has been described in chapter 1, section 1.4. Although this procedure is straightforward, it is quite tedious and time consuming. Perhaps that is the reason why many workers unfortunately do not carry it out and thereby fail to ascertain that their measurements are based on the existence of a saturated critical state.

Further, the configuration of the flux lines in the specimen, hence the pattern of induced persistent currents must not be " tampered " with in the process of carrying out the measurement of the saturated critical state. This means that the orientation of the specimen must first be set at the chosen θ. Then the saturation magnetization procedure should be carried out with θ maintained fixed. In practice this generally requires that the specimen be field cooled from T_c to a chosen T in a predetermined H_a initial. Next H_a is increased (decreased) to the predetermined H_a final with the change $\Delta H_a = H_{af} - H_{ai}$ sufficiently large to ensure the generation of a saturated critical state. Again the procedure is straightforward but tedious and time consuming. The reason for following the procedure we have just described is that rotation of hysteretic type II superconductors in a static $\vec{H}$ causes flux line cutting and thereby drastically modifies the configuration of the magnetic flux density and the attendant pattern of circulating persistent currents (4, 7, 18, 19, 25). Again, perhaps because the procedure we have described is burdensome, most researchers have elected to rotate their initially magnetized specimen in a stationary field (10, 11, 16, 22, 23). Consequently these data cannot be compared with the predictions of our model.

A few laboratories have recently been very successful in growing relatively large single crystals of high T_c superconductors. Measurements of j_c in these specimens by the magnetic method and also by the four probe technique show that j_c is anisotropic and insensitive to B in the " intermediate " range of $\mu_0 H_a$. These new specimens present an opportunity to "test" some of the "predictions" contained in our catalogue or compilation of calculated curves displayed in appendices A and B of this thesis.

Finally of special interest will be the determination of the validity of our third assumption, namely, that the persistent currents are induced to circulate perpendicularly to the magnetizing field regardless of the geometry and anisotropy. Measurements (22, 23) indicate that in highly anisotropic specimens, the induced persistent currents circulate in the plane of large critical current density only (i.e. the ab plane). However, in the isotropic limit and for symmetric geometry with respect to the axis or plane along $\vec{H}_a$, we expect that the direction of the magnetizing field will dictate the plane of circulation of the persistent critical currents. The question then arises whether there exists a threshold anisotropy where only the current in the strong direction (ab plane) survives and the current in the weak direction (c axis) is suppressed.

Also we note that many of our calculation curves address "fictional" scenarios in the sense that no specimens are presently known to exist with the properties we have postulated. For instance, we have visualized the existence of platelets where $j_c^c > j_c^{ab}$ although no

such type of platelets have been found among any high T_c superconductors. Nevertheless we consider it interesting to include these mythical materials in our computational and graphical survey.

Appendices A and B of this thesis are regarded by us as a useful reference library and guide for future experimental investigations. They should enable us to judicially select the more promising series of measurements for the elucidation of the effects of geometry and anisotropy on the magnetic moment of type II superconductors.

Finally we note that eqns 9(a) and 9(b) can serve as "launching pads" for calculating the magnetic moment of a variety of geometric objects (e.g. rectangular pyramids, truncated pyramids, ziggurats), in the framework of assumptions (i), (ii) and (iii). The formulae we have developed (eqns 47 through 58) can also accommodate, without modification, any scenario where β is assumed to vary with θ only.

Equation 13(a) and 13(b) are frequently applied by workers in the field to estimate j_c^c and j_c^{ab} in platelets of high T_c superconductors. These formulae first published by Gyorgy et al (13) and Peterson (20) were derived using, $< B >= \mu_0 H_a + \mu_0 < M >$ but relied on an unacceptable simplification. We have shown that these equations are nevertheless exact and correct using the definition, $\mu = 1/2 \int \vec{R} \times \vec{j}_c dV$ and the Bean approximation that j_c^c and j_c^{ab} are independent of B.

References

[1]. A. A. Abrikosov, Soviet Physics JETP, 5, 1174 (1957), J. Phys. Chem. Solids 2, 199 (1957)

[2]. C. Aguillon, D.G. McCartney, P. Regnier, S. Senoussi and G.J. Tatlock, J. Appl. Phys. 69, 8261 (1991).

[3]. C.P. Bean, Rev. Mod. Phys. 36, 31 (1964).

[4]. R. Boyer, G. Fillion and M.A.R. LeBlanc, J. Appl. Phys. 51, 1692 (1980).

[5]. E. H. Brandt and M. Indenlom, Phys. Rev. *B*48, 12893 (1993).

[6]. A. M. Campbell and J. E. Evetts, " Critical Currents in Superconductors " (Taylor and Francis, London, 1972), Advances in Physics, 21 199 (1972).

[7]. J.R. Cave and M.A.R. LeBlanc, J. Appl. Phys. 53 1631 (1982).

[8]. L.W. Conner and A.P. Malozemoff, Phys. Rev. *B*43, 402 (1991).

[9]. M. Daümling and D.C. Larbalestier, Phys. Rev. *B*40, 9350 (1989).

[10]. I. Felner, U. Yaron, Y. Yeshurun, G.V. Chandrashekhar and F. Holtzberg, Phys. Rev. *B*40, 5239 (1989).

[11]. I. Felner, U. Yaron and Y. Yeshurun, Phys. Rev. *B*43, 13681(1991).

[12]. D.J. Frankel, J. Appl. Phys. 50, 5402 (1979).

[13]. E.M. Gyorgy, R.B. van Dover, K.A. Jackson, L.F. Schneemeyer and J.V. Waszczak, Appl. Phys. Lett. 55, 283 (1989).

[14]. E.M. Gyorgy, R.B. van Dover, L.F. Schneemeyer, A.E. White, H.M. O'Bryan, R.J. Felder, J.V. Waszczak, W.W. Rhodes and F. Hellman, Appl. Phys. Lett. 56, 2465 (1990).

[15]. H. Hemmes, A.R. Kuper and L.J.M. van de Klundert, IEEE Trans. Magn. 27, 1069 (1991).

[16]. S. Kolesnik, T. Skoskiewicz and J.Igalson, Phys. Rev.*B*43, 13679 (1991).

[17]. H. London, Phys. Lett. 6, 162 (1963).

[18]. Liwen Liu, J.S. Kouvel and T.O. Brun, J. Appl. Phys. 67, 4527 (1990).

[19]. Liwen Liu, J.S. Kouvel and T.O. Brun, Phys. Rev. *B*38, 11799 (1988).

[20]. R.L. Peterson, J. Appl. Phys. 67, 6930 (1990).

[21]. R. A. Richardson, O. Pla and F. Nori, Phys. Rev. Lett. 72, 1268 (1994).

[22]. H. Teshima, A. Oishi, H. Izumi, K. Ohata, T. Morishita and S. Tanaka, Appl. Phys. Lett. 58, 2833 (1991).

[23]. M. Tuominen, A.M. Goldman, Y.Z. Chang and P.Z. Jiang, Phys. Rev. *B*42, 412 (1990).

[24]. H. Ullmaier, " Irreversible Properties of Type II Superconductors ", Springer-Verlag, Berlin (1975).

[25]. Y. Wolfus, Y. Yeshurun and I. Felner, Phys. Rev. *B*37, 3667 (1988).

APPENDIX A

This appendix is a "travel guide" through the display, as a function of θ, of $\mu_N(\theta)$, the magnetic moment (or magnetization) normalized to the maximum value for each curve. Curves where the anisotropy parameter $\beta = j_{cx}/j_{cy} = j_c^{ab}/j_c^c = 10, 5, 2, 1, 1/2, 1/5$ and $1/10$ are presented. (The curves where $j_c^{ab} < j_c^c$, although perhaps hypothetical, are included for completeness). Here j_c^c is along the axis of rotation and the isotropic ab planes are "vertical", hence coincide with the xz planes. The solid lines always exhibit the isotropic case, $\beta = 1$. The symbol or character chosen to depict the curves for a given value of β remains the same throughout the series of figures. The values of β are indicated alongside the curves when necessary and space permits.

The relative dimensions are listed at the top left of each figure. The cube is taken to have a size of 10 x 10 x 10. A denotes the height, initially along the Z axis, and L denotes the length, along the axis of rotation (the y axis). The sketches over each family of curves are intended to assist in visualizing the dimensions of the particular parallelepiped relative to the cube and are not drawn to scale. These schematics represent the parallelepiped when $\theta = 0$. The families of curves for $\pi/2 \leq \theta \leq 2\pi$ "repeat" those displayed.

Eight families of curves, hence eight figures, are necessary in order to present the eight geometrically and physically different situations encountered in this exercise.

Fig. 4. The x axis is horizontal and the z axis vertical in these sketches. The y axis is the axis of rotation. The twelve figures plus the cube represent the thirteen distinct situations which need to be considered when the anisotropy parameter β is a function of θ. When β = constant $\gtrless 1$, the 13 distinct situations reduce to 8 physically different cases since now (a) is equivalent to (i), (b) is equivalent to (l), (f) is equivalent to (h) and (d) is equivalent to (j) after rotation through 90°.

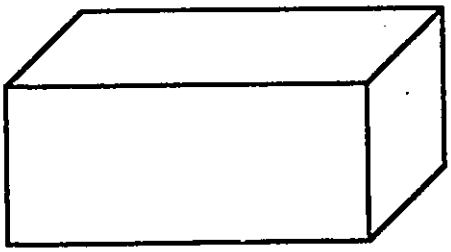

a)

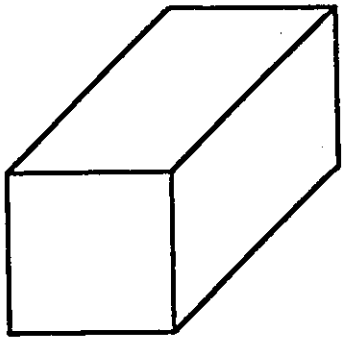

e)

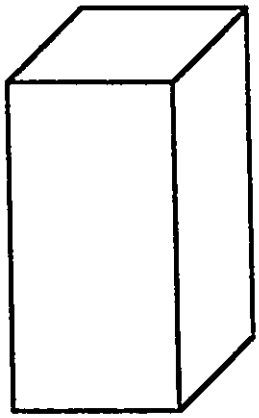

i)

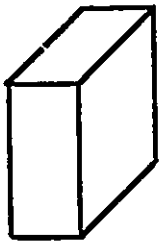

b)

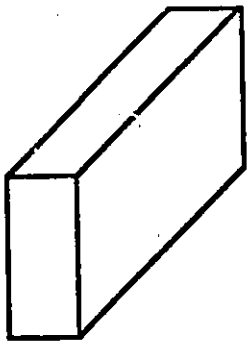

f)

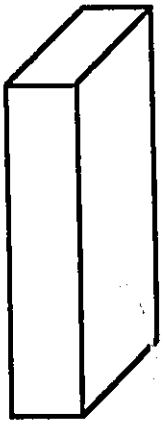

j)

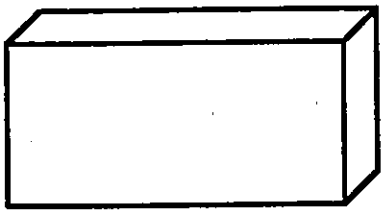

c)

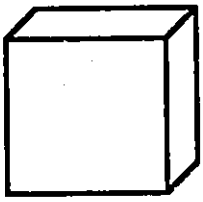

g)

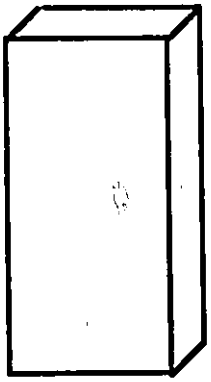

k)

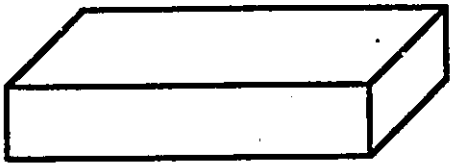

d)

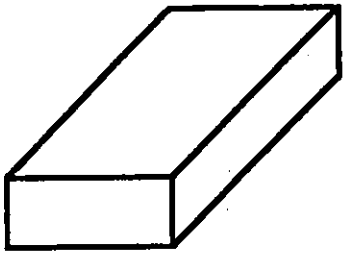

h)

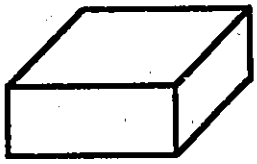

l)

Here, the twelve parallelepipeds displayed in Fig. 4 contain some redundancy, since after rotation through 90°, (a) is equivalent to (i), (b) is equivalent to (l), (f) is equivalent to (h) and, (d) is equivalent to (j). Figs. A-2, A-4, A-6 and A-10 have been included to assist in following more clearly the evolution of the families of curves as the dimensions are modified // and ⊥ to the axis of rotation.

Interesting "sequences" to scan in the series of figures are the following:

(i) A-1 through A-5 illustrate the effect of elongation along the axis of rotation. Note the change in shape and relative position of the various curves which ensues.

(ii) A-5 through A-7, effect of "thinning" a block ⊥ to the axis of rotation.

(iii) A-7 and A-8, effect of change of length of a slab along the axis of rotation.

(iv) A-8 and A-9, effect of change of dimension of a slab ⊥ to the axis of rotation.

(v) A-8, A-10, A-3 then A-11, effect of expansion ⊥ to the axis of rotation.

(vi) A-1 and A-12, effect of stretching of a slab ⊥ to the axis of rotation.

(vii) A-11 and A-12, effect of thinning a block // to the axis of rotation.

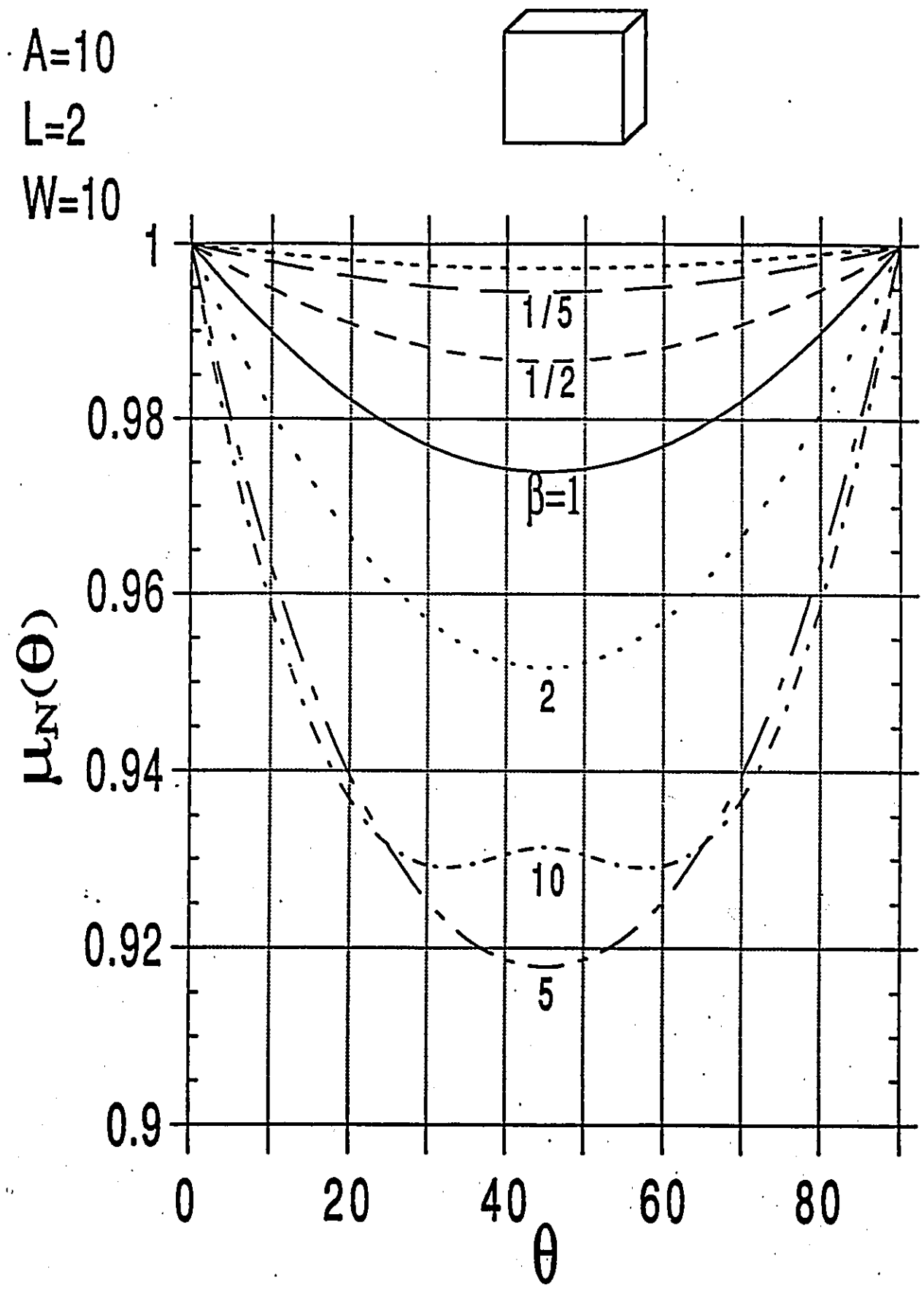
A=10
L=2
W=10
1
0.98
0.96
0.94
0.92
0.9
$\mu_N(\theta)$
1/5
1/2
β=1
2
10
5
0
20
40
60
80
θ

Fig. A-1

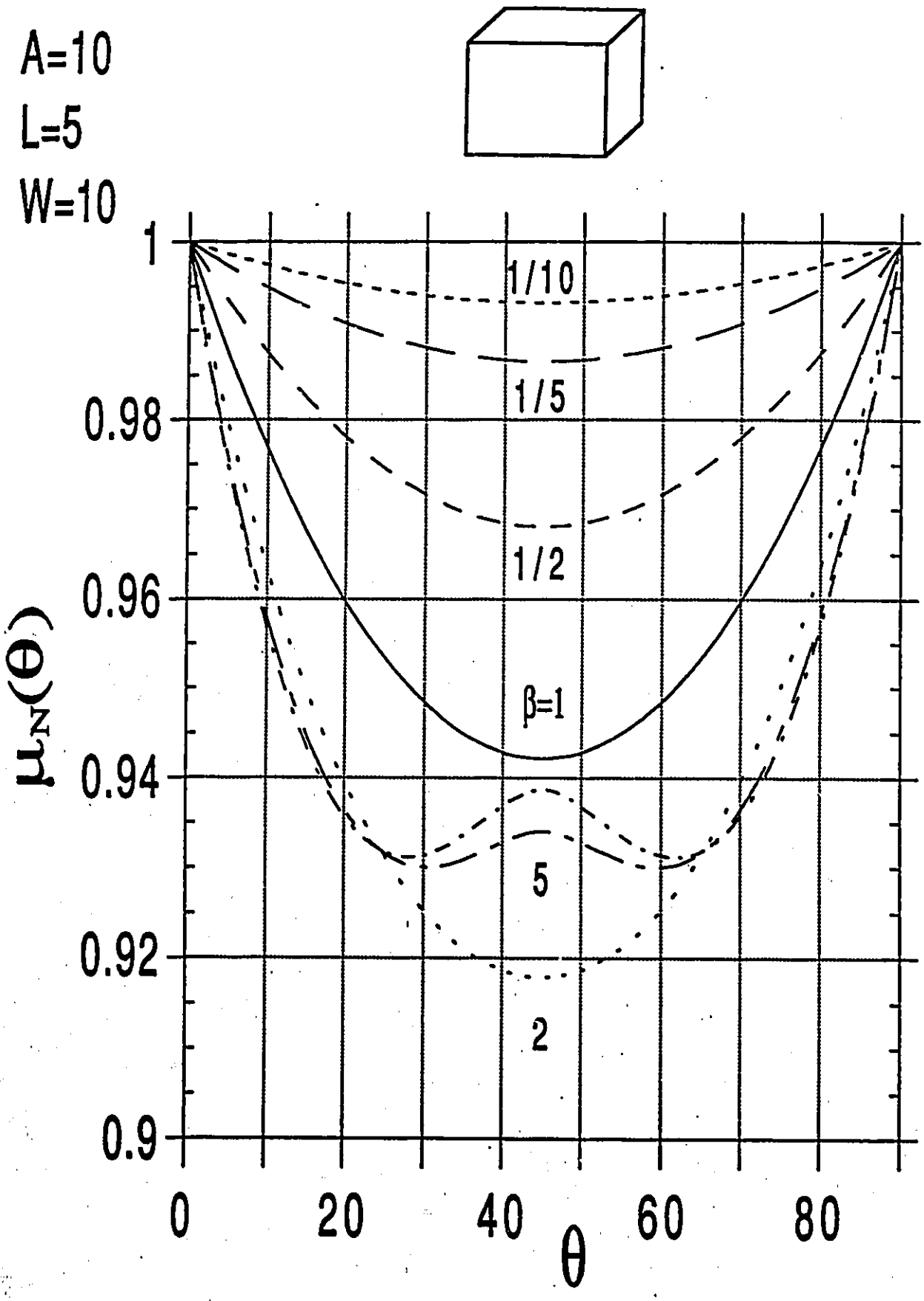
A=10
L=5
W=10
1
0.98
0.96
0.94
0.92
0.9
$\mu_N(\theta)$
1/10
1/5
1/2
β=1
5
2
0
20
40
60
80
θ

Fig. A-2

W=L=A=10

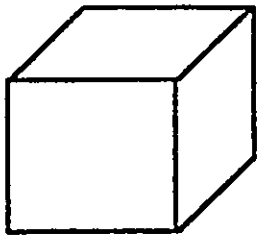

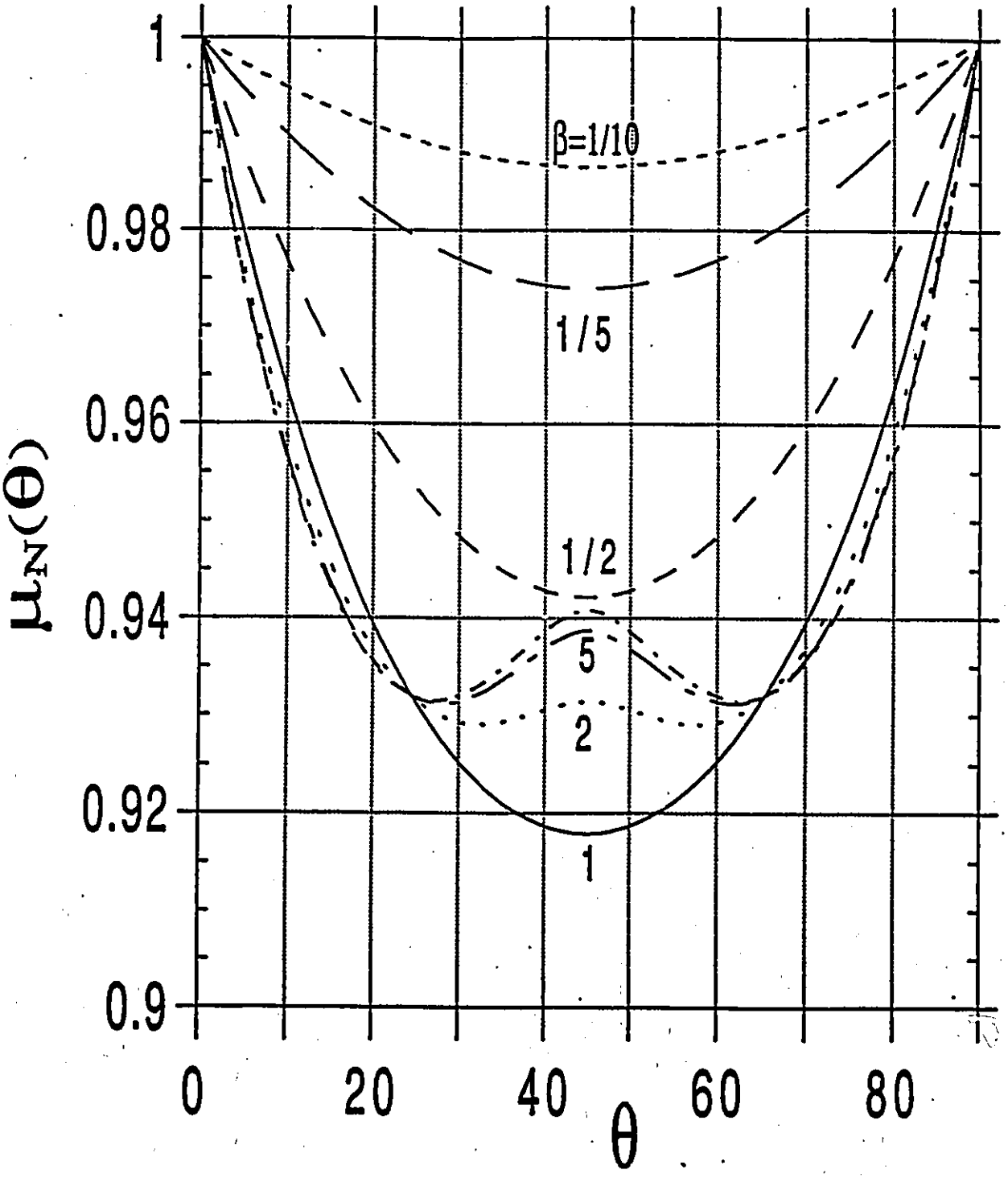

Fig. A-3

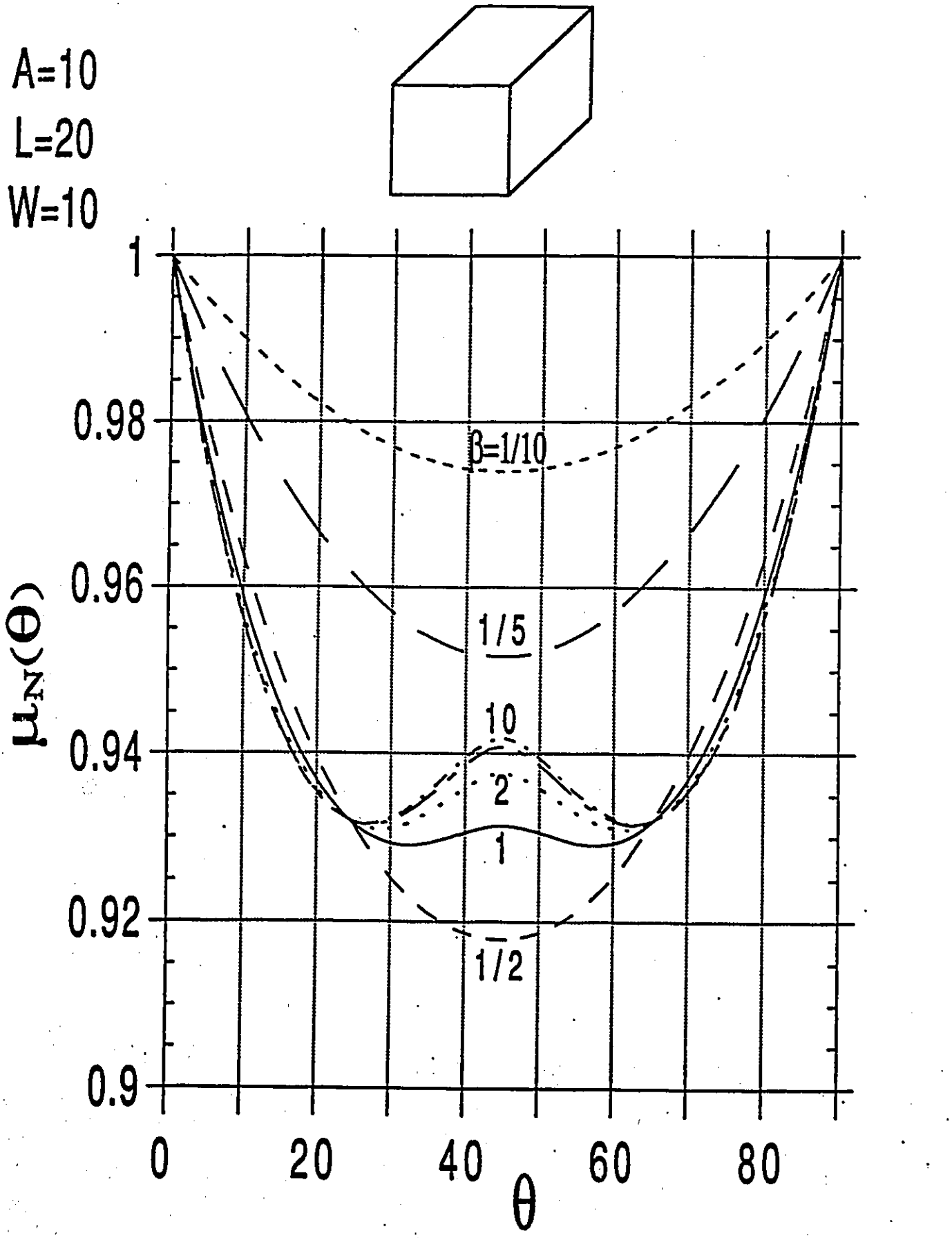
A=10
L=20
W=10
1
0.98
0.96
0.94
0.92
0.9
$\mu_N(\theta)$
β=1/10
1/5
10
2
1
1/2
0
20
40
60
80
θ

Fig. A-4

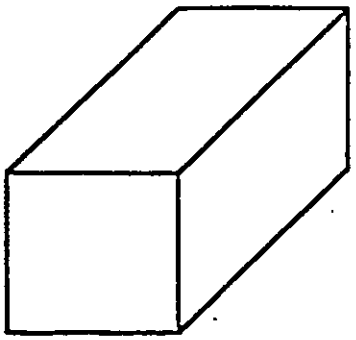

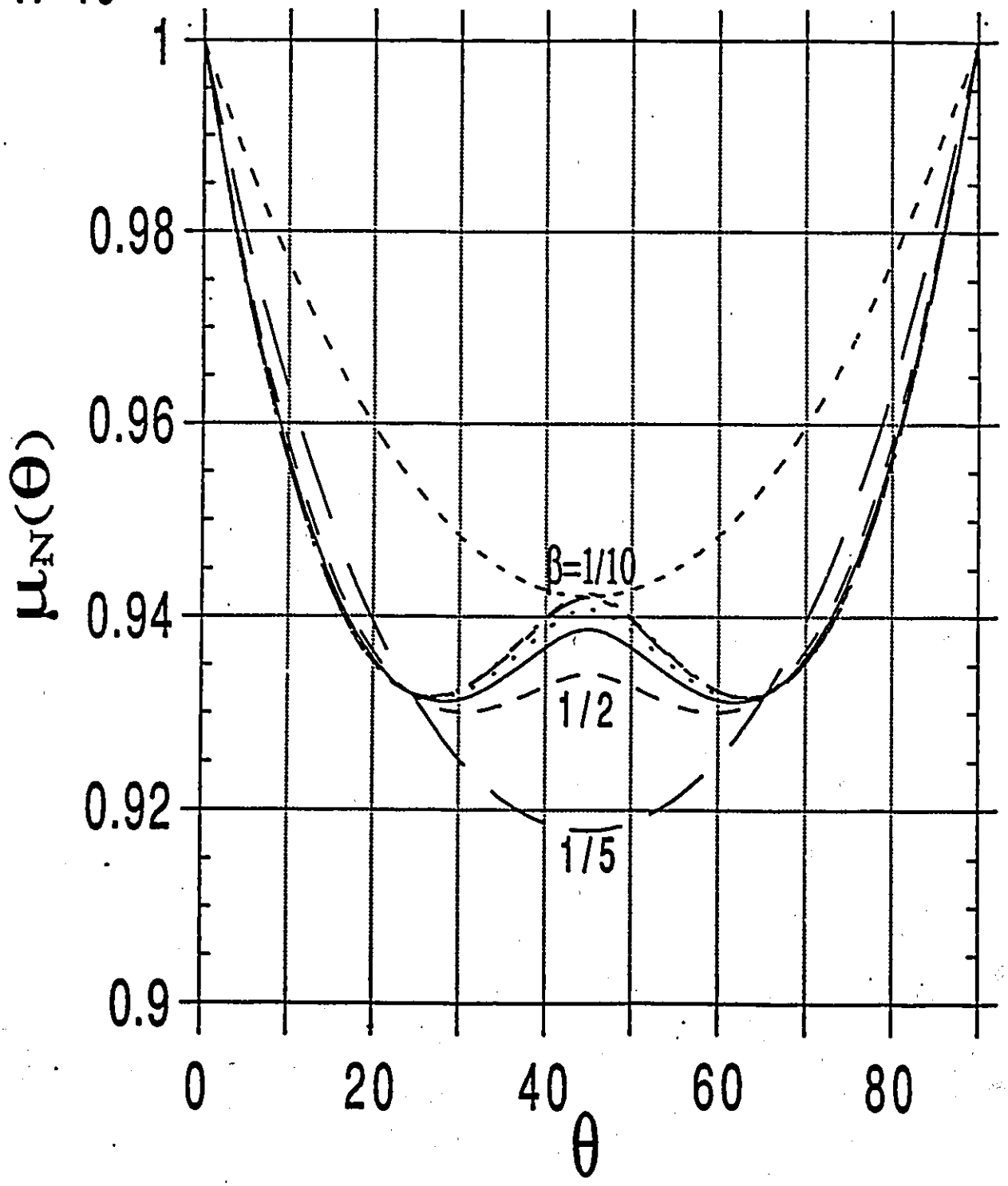
A=10
L=50
W=10
1
0.98
0.96
0.94
0.92
0.9
$\mu_N(\theta)$
β=1/10
1/2
1/5
0
20
40
60
80
θ

Fig. A-5

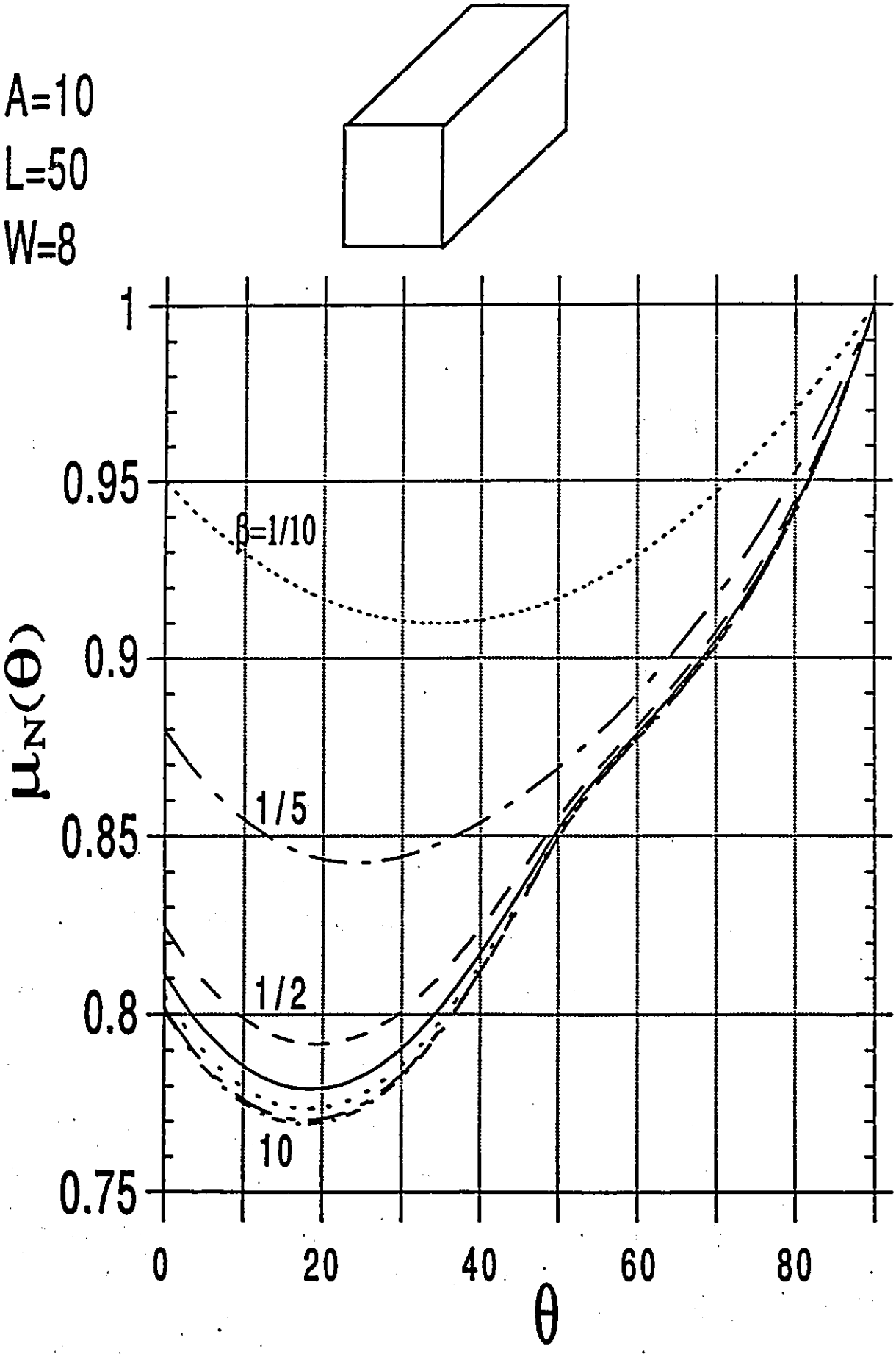
A=10
L=50
W=8
1
0.95
0.9
0.85
0.8
0.75
$\mu_N(\theta)$
β=1/10
1/5
1/2
10
0
20
40
60
80
θ

Fig. A-6

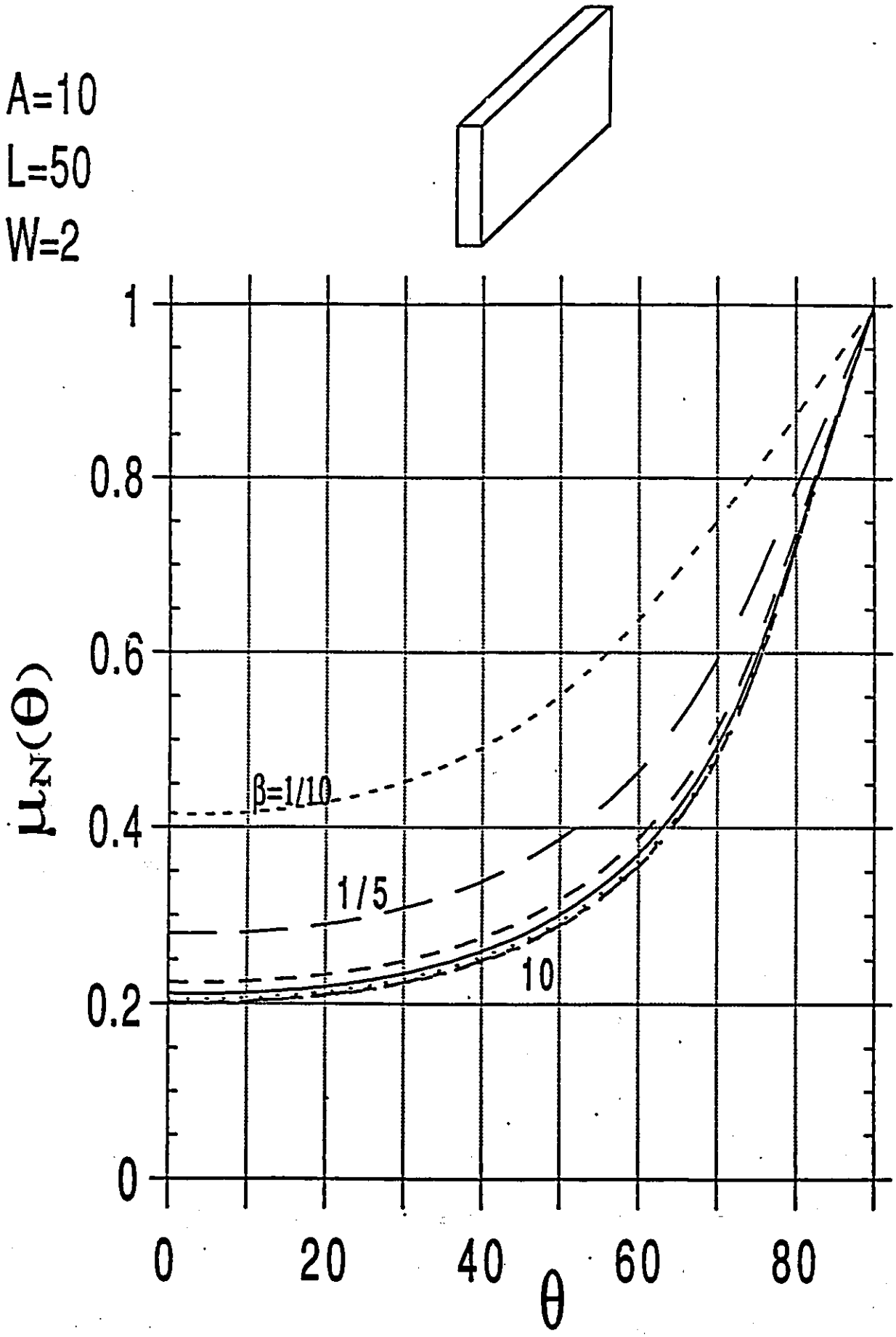

Fig. A-7

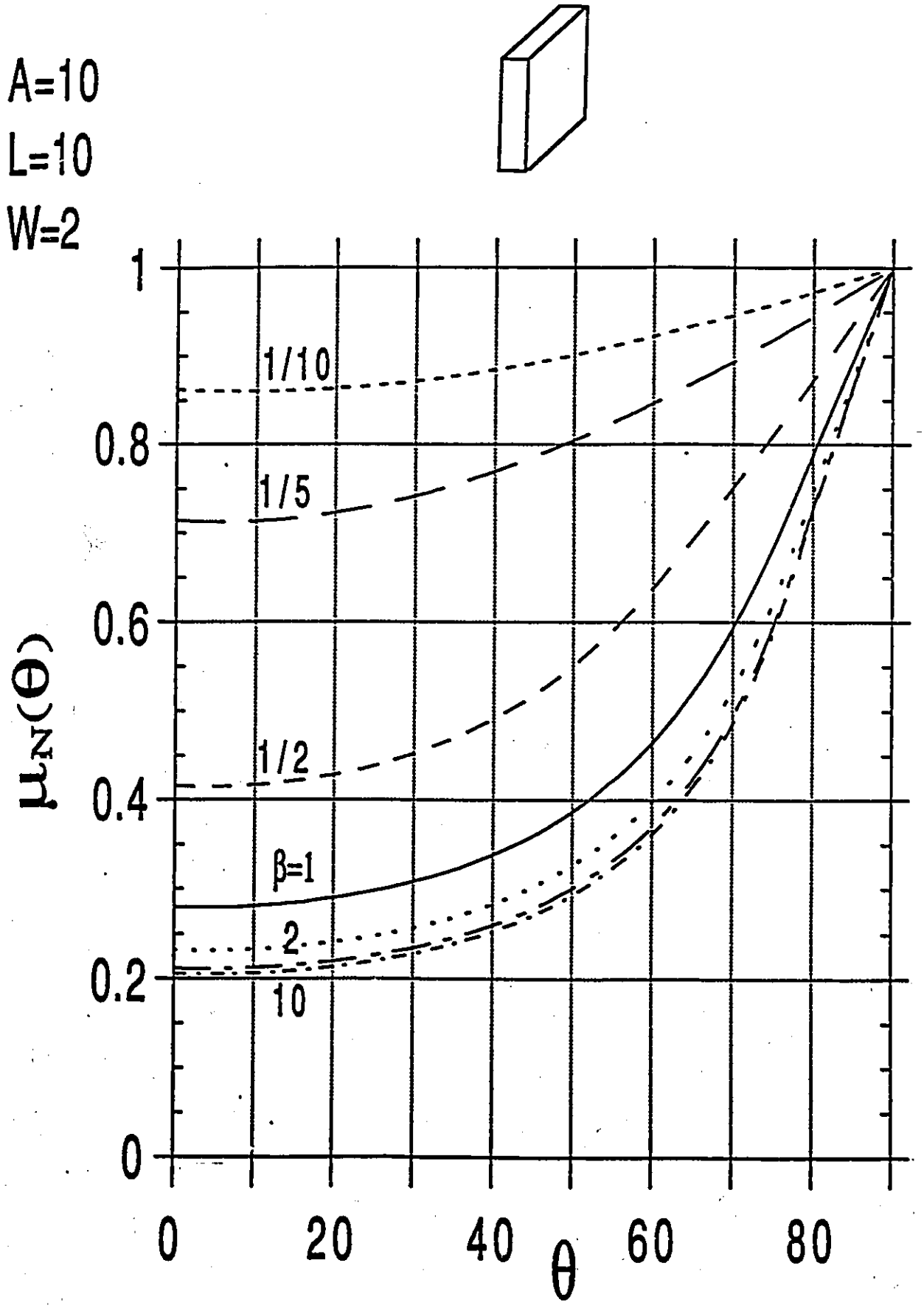

Fig. A-8

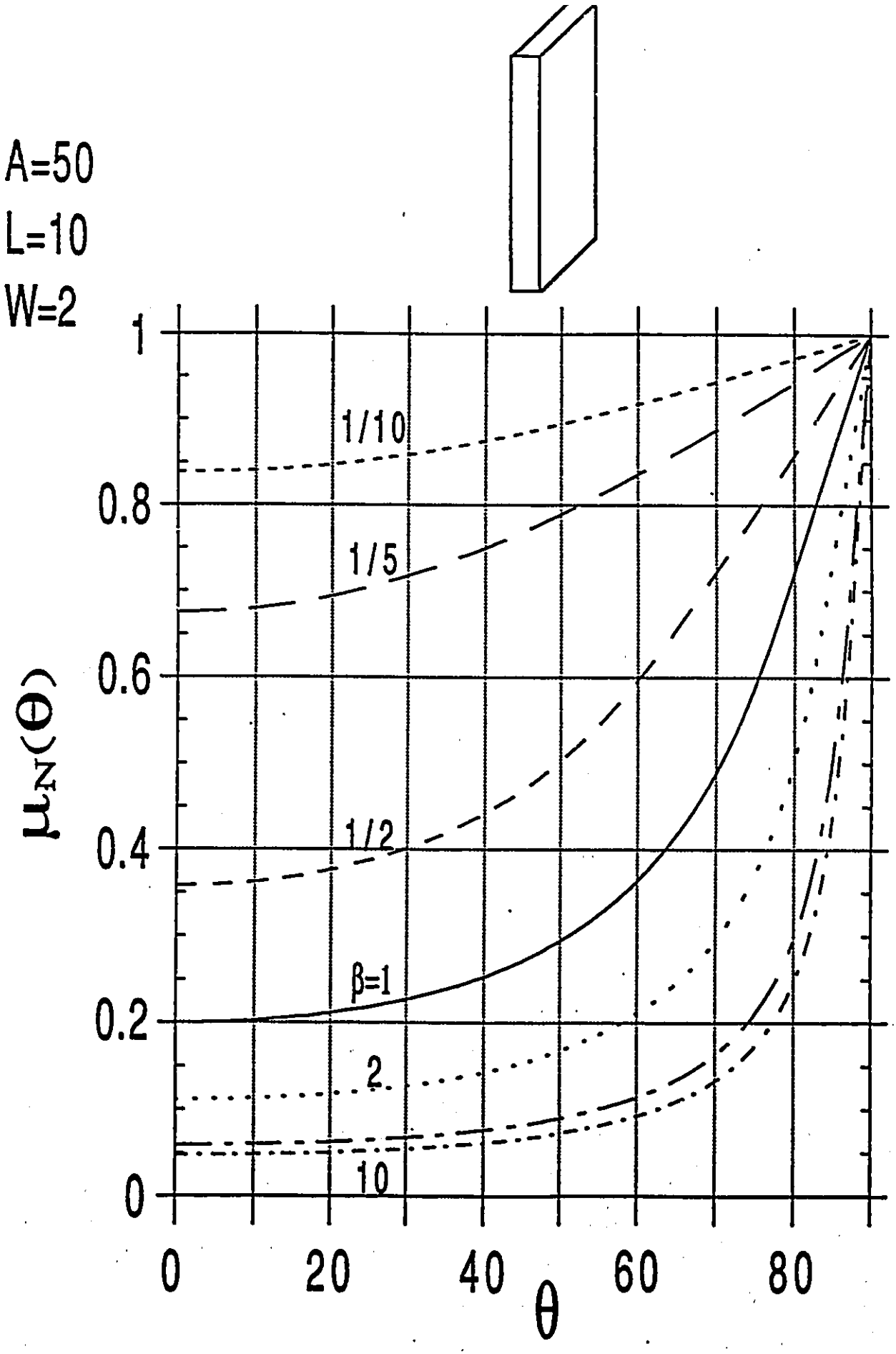

Fig. A-9

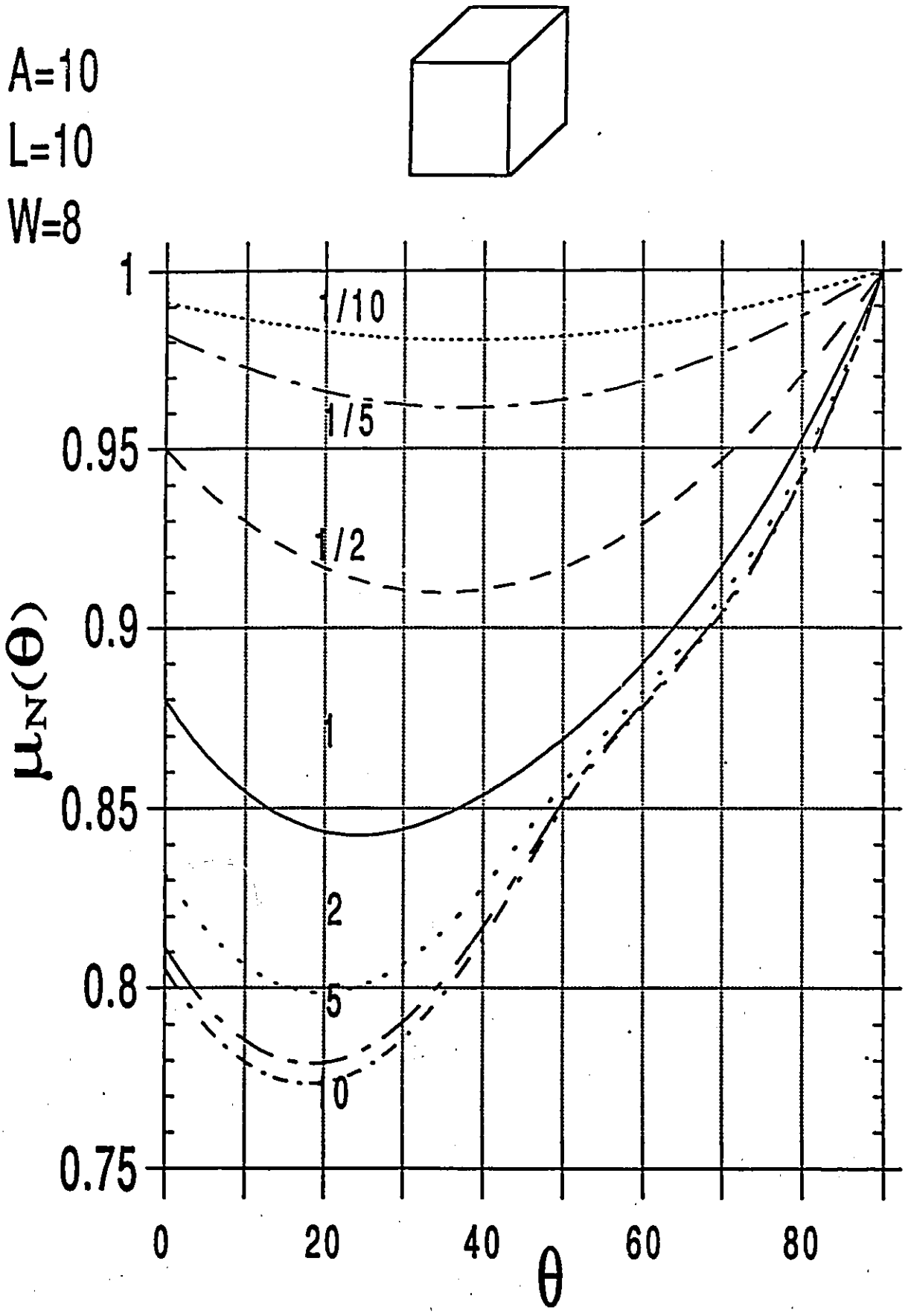
A=10
L=10
W=8
1
0.95
0.9
0.85
0.8
0.75
$\mu_N(\theta)$
1/10
1/5
1/2
1
2
5
0
0
20
40
60
80
θ

Fig. A-10

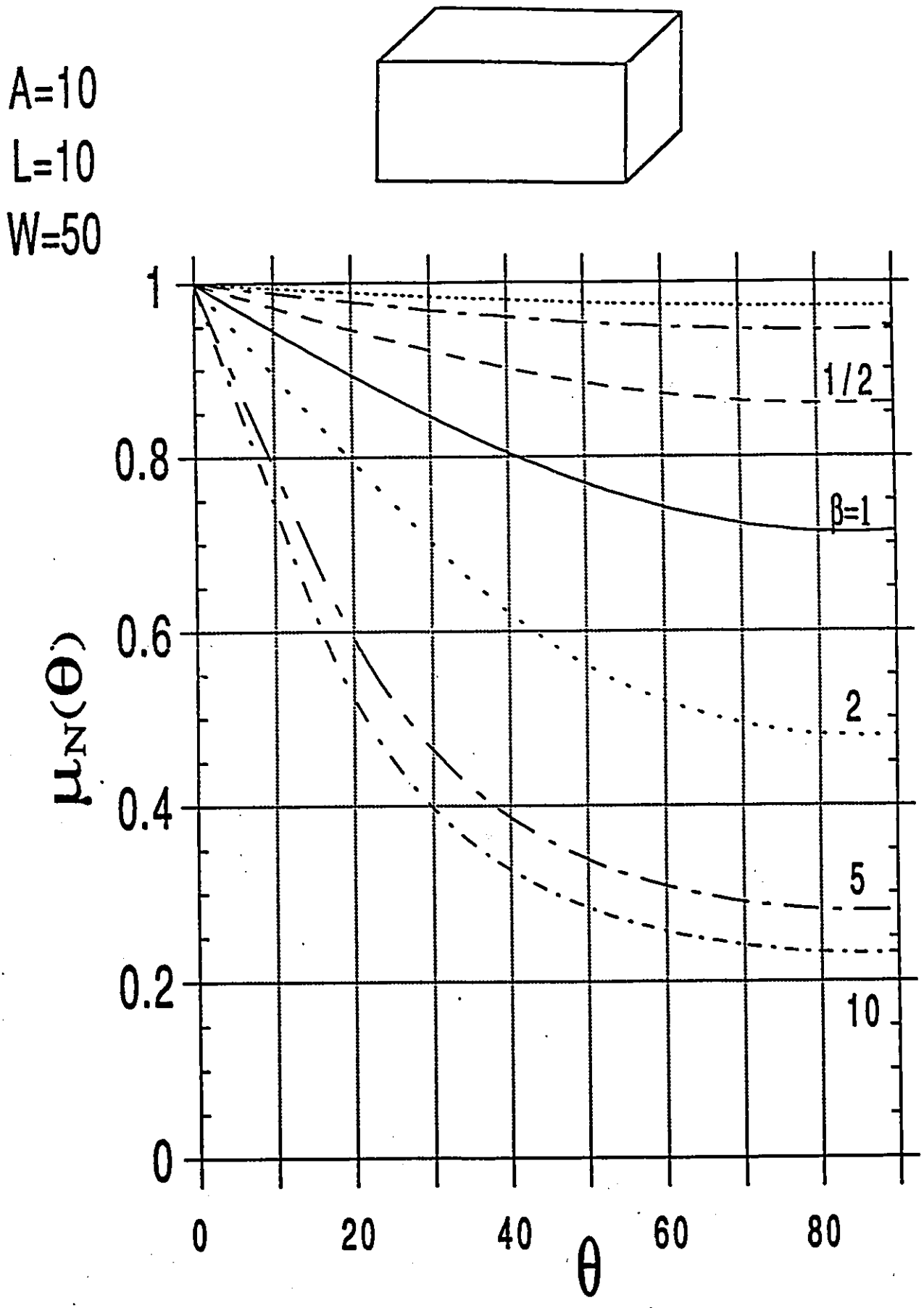

Fig. A-11

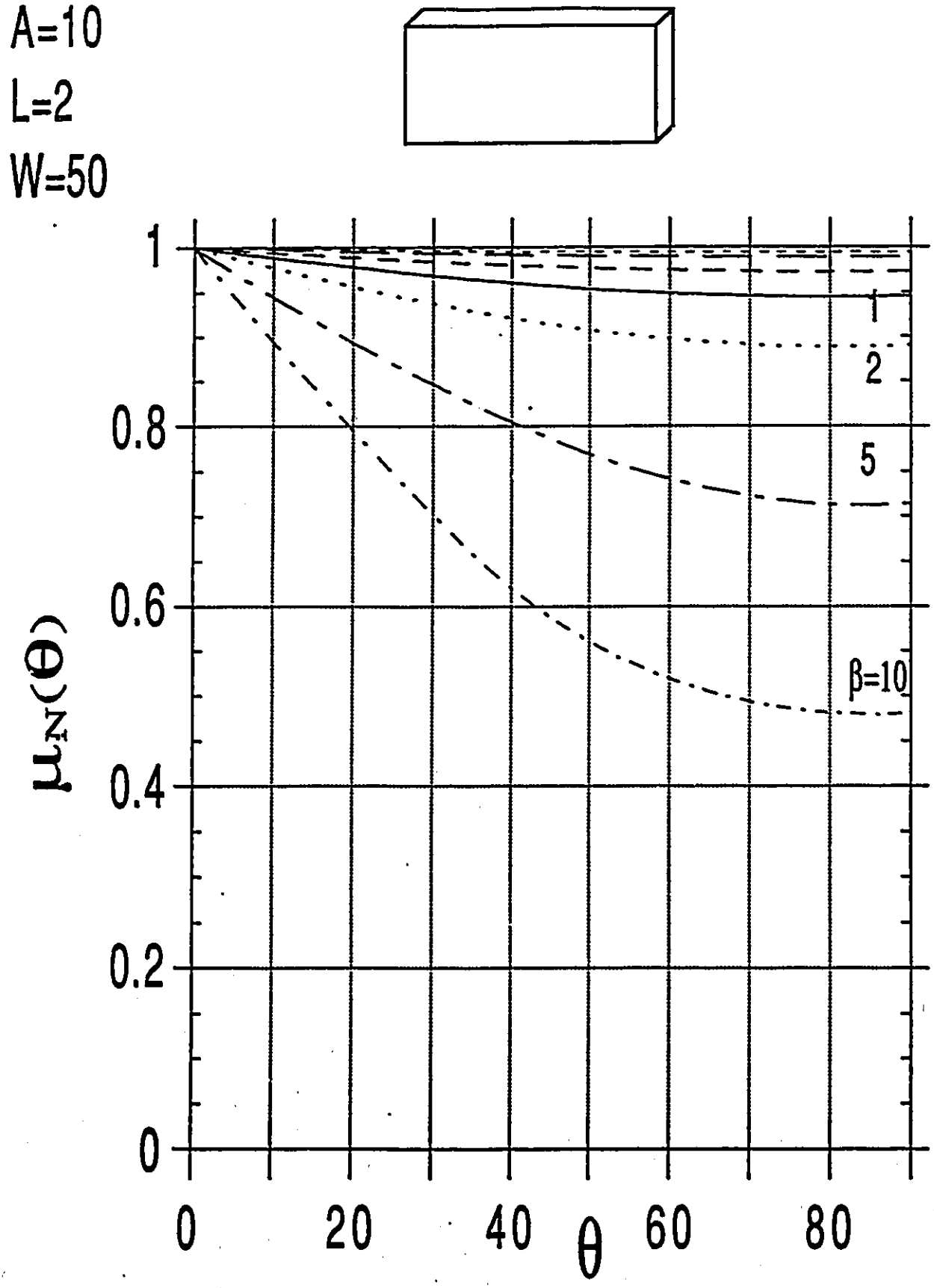

Fig. A-12

APPENDIX B

This appendix is a "travel guide" through the display of families of curves of $\mu_N(\theta)$ vs θ where the anisotropy parameter $\beta(\theta)$ is a function of θ of the general form

$$\beta(\theta) = \frac{j_{cx}(\theta)}{j_{cy}} = \frac{j_c^W \cos^2\theta + j_c^A \sin^2\theta}{j_c^L} = k_1 \cos^2\theta + k_2 \sin^2\theta \qquad \text{(B-1)}$$

(a) Considering the isotropic planes to be vertical and coincide with the yz planes when $\theta = 0$, signifies that $j_c^A = j_c^L = j_{cy}$, hence $k_2 = 1$ and $k_1 = j_c^W/j_c^A = j_c^W/j_c^L = 1/R$. To fix ideas we take,

$$j_c^{ab} = j_c^A = j_c^L = j_{cy}, \text{ and } j_c^c = j_c^W \qquad \text{(B-2)}$$

$$\text{Hence now } R = \frac{j_c^{ab}}{j_c^c} \qquad \text{(B-3)}$$

and eqn B-1 reads

$$\beta(\theta) = \frac{\cos^2\theta}{R} + \sin^2\theta \qquad \text{(B-4)}$$

Although in high T_c materials $j_c^{ab} > j_c^c$, for the sake of completeness we have explored the behavior predicted when $R \gtrless 1$. When $0 < \theta < \pi/2$, the isotropic planes are tilted with respect to the magnetizing field and become horizontal, hence coincide with the xy planes when $\theta = \pi/2$. Here j_c^c is always $\perp$ to the axis of

rotation.

(b) Letting the isotropic planes coincide with the x-y planes when $\theta = 0$ signifies that $j_c^L = j_c^W = j_{cy}$, hence $k_1 = 1$ and $k_2 = j_c^A/j_c^L = j_c^A/j_c^W = 1/R_2$.

Again to fix ideas we take,

$$j_c^{ab} = j_c^L = j_c^W = j_{cy}, \text{ and } j_c^c = j_c^A \tag{B-5}$$

Hence, now,

$$R_2 = \frac{j_c^{ab}}{j_c^c} = R \tag{B-6}$$

and,

$$\beta(\theta) = \cos^2\theta + \frac{\sin^2\theta}{R} \tag{B-7}$$

Therefore, eqns B-4 and B-7 lead to "equivalent" families of curves of $\mu_N(\theta)$ vs θ. In the former the isotropic planes ab are vertical when $\theta = 0$. In the latter the isotropic ab planes are horizontal when $\theta = 0$. In both prescriptions, j_c^c is always $\perp$ to the axis of rotation.

Consequently, the families of curves calculated using eqn B-4 can readily be exploited to yield families of curves using eqn B-7. This is accomplished by rotating the parallelepiped of Figs. B-1 through B-25 by 90° and reversing the θ axis (i.e. 90° becomes 0° and 0° become 90°).

In Figs. B-1 through B-25 we display families of curves of $\mu_N(\theta)$ vs θ calculated using eqn. B-4 with R = 10, 5, 2, 1, 1/2, 1/5 and 1/10. Again the solid lines always exhibit the isotropic

case, $R = \beta = 1$. Also the symbols for the curves and the R values they correspond to is identical to that introduced in the previous set of figures. The values of R are indicated alongside the curves when possible.

Now, however thirteen families of curves, hence 13 figures, are required in order to present the thirteen physically different situations encountered in this exercise since now all 12 sketches of Fig 4 plus the cube need to be addressed. The reader can convince himself that (a) and (i), (b) and (l), (f) and (h), (d) and (j) of Fig. 4 are now no longer equivalent by tracing isotropic planes // to the yz faces of the parallelepipeds when $\theta = 0$ and then rotating the parallelepiped through 90°.

Twelve figures have been added to the "basic" thirteen in order to illustrate more clearly the evolution of the families of curves as the dimensions are modified // and $\perp$ to the axis of rotation.

As a "guide" through this labyrinth of figures we suggest scanning them along the following sequences.

(i) B-1 through B-5, (ii) B-5, B-6, (iii) B-5, B-7, B-8, (iv) B-9, B-4, B-10, (v) B-10 through B-14, (vi) B-10, B-15, B-16, B-17, (vii) B-18, B-19, B-4, B-20, (viii) B-20 through B-23, and (ix) B-20, B-24, B-25.

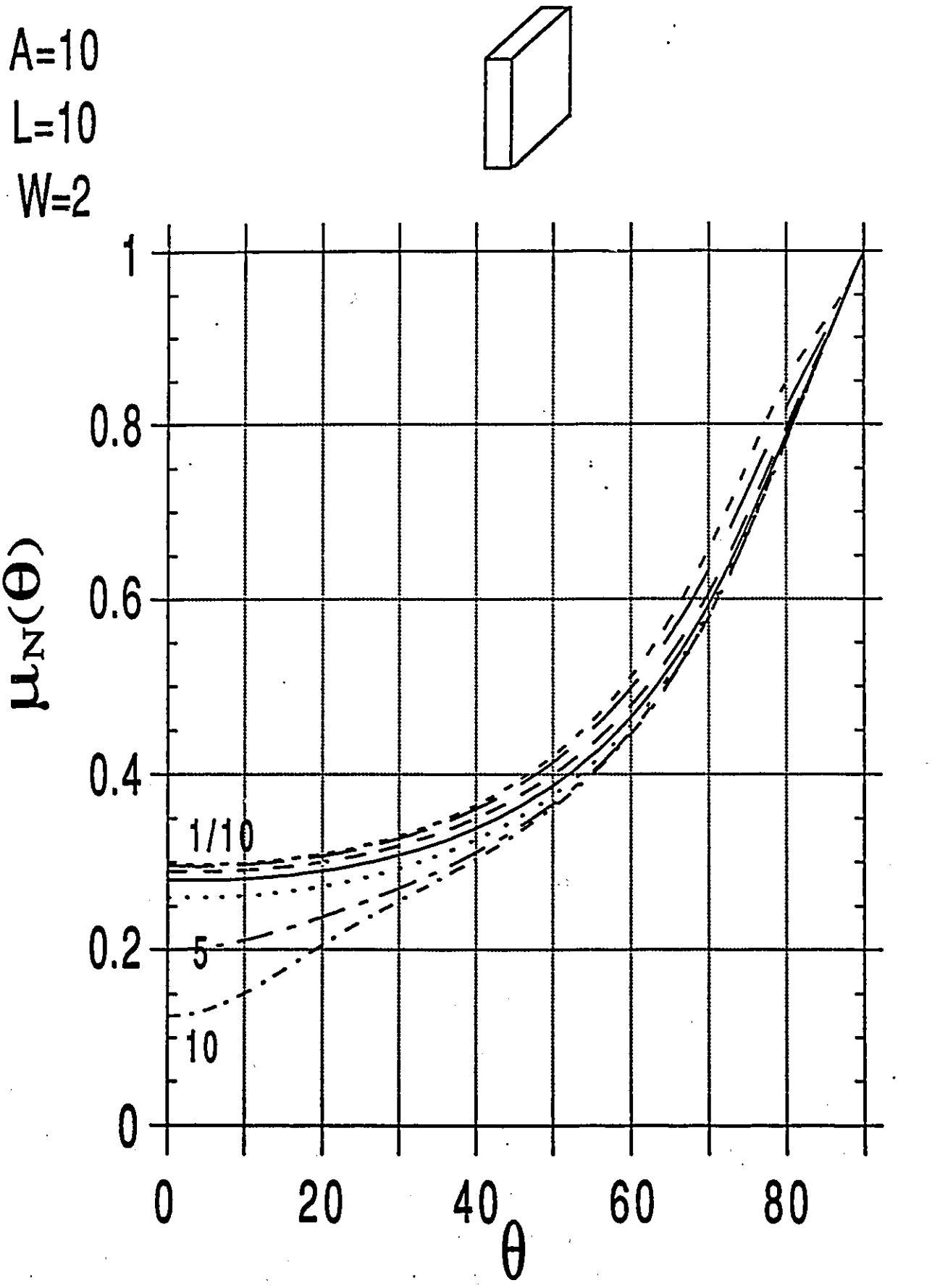

Fig. B-1

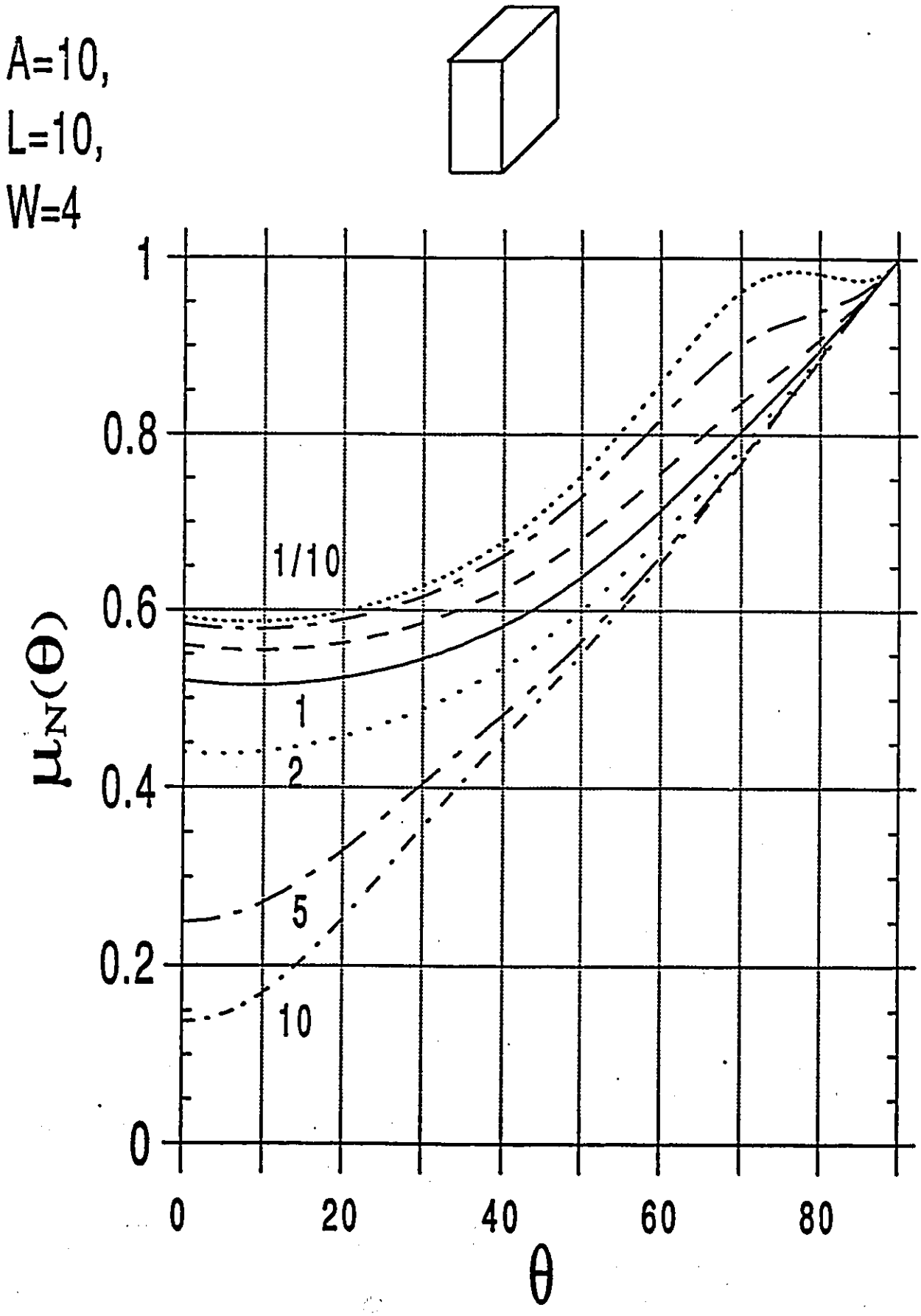

Fig. B-2

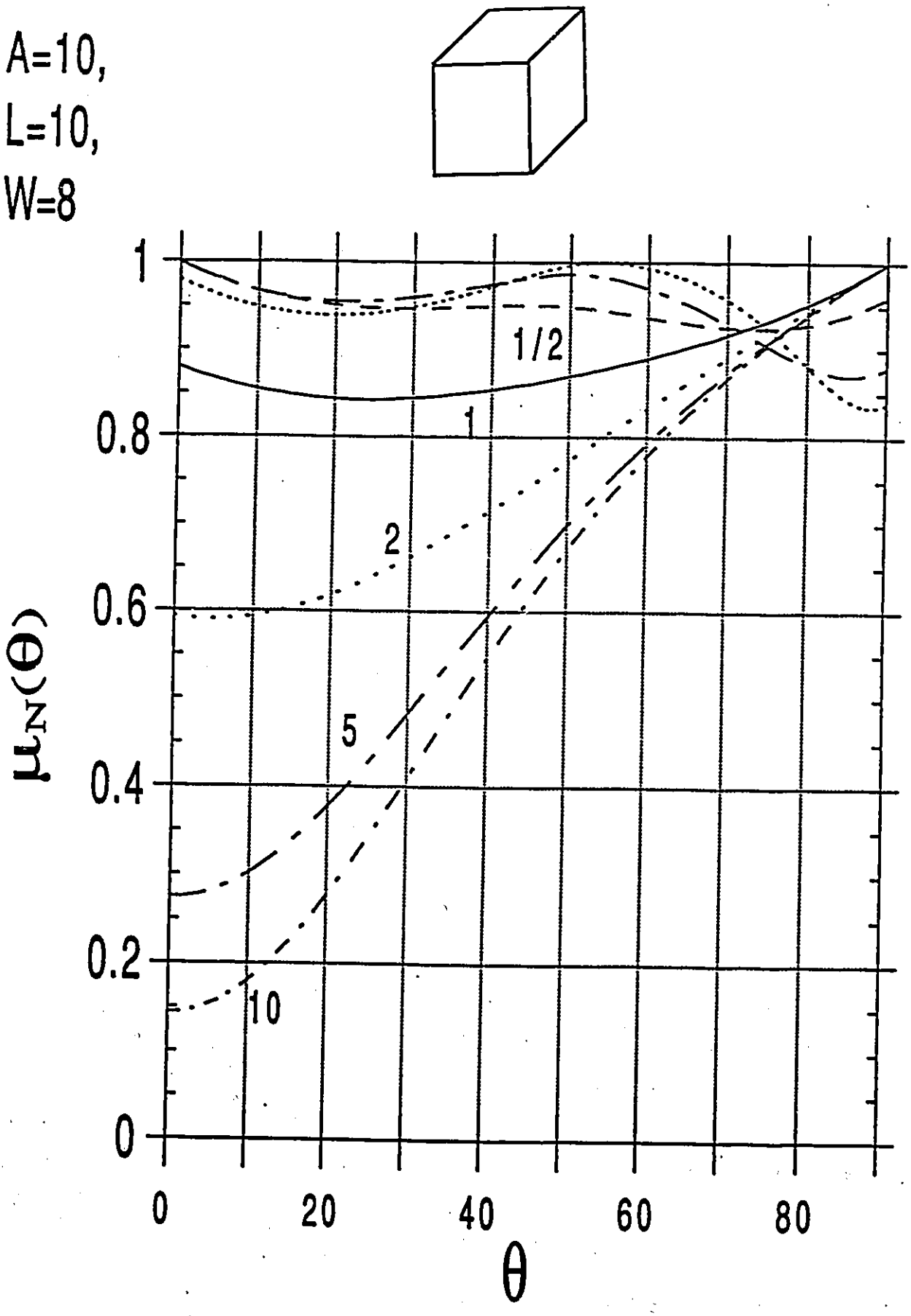

Fig. B-3

A=L=W=10

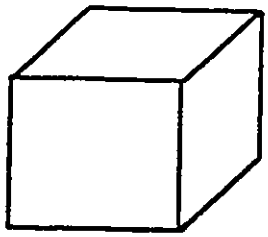

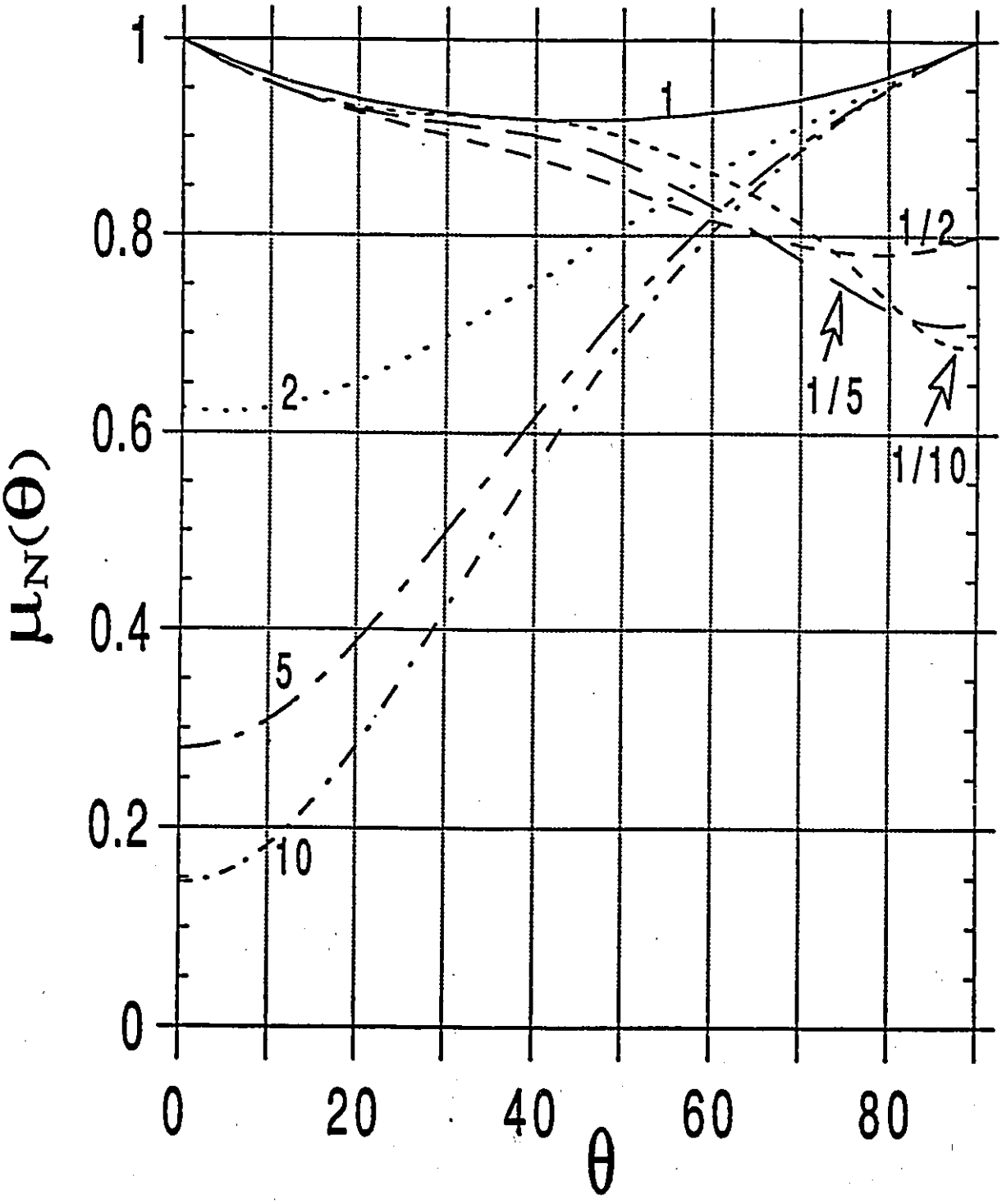

Fig. B-4

A=10

L=10

W=50

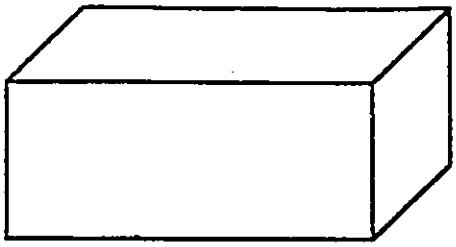

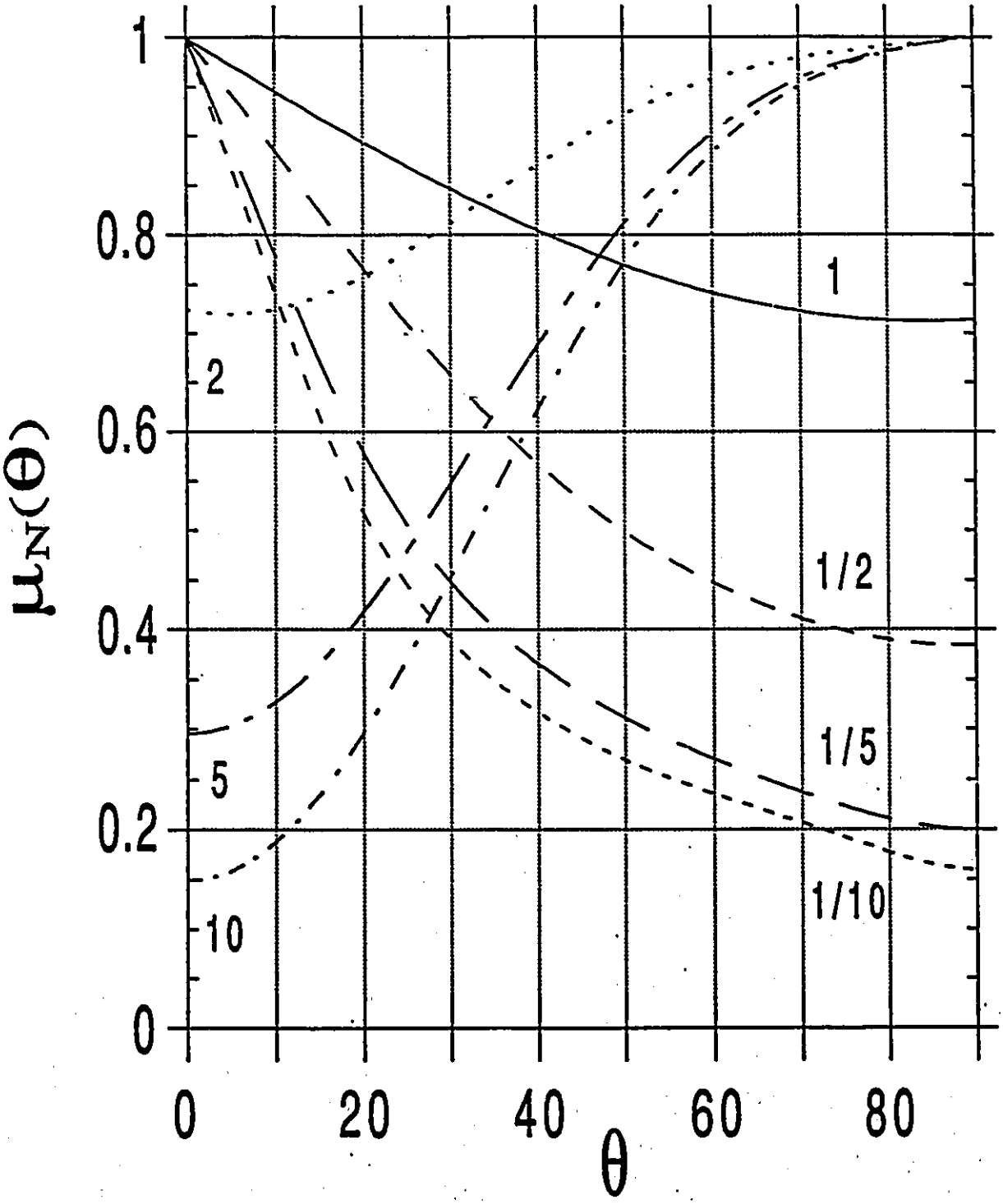

Fig. B-5

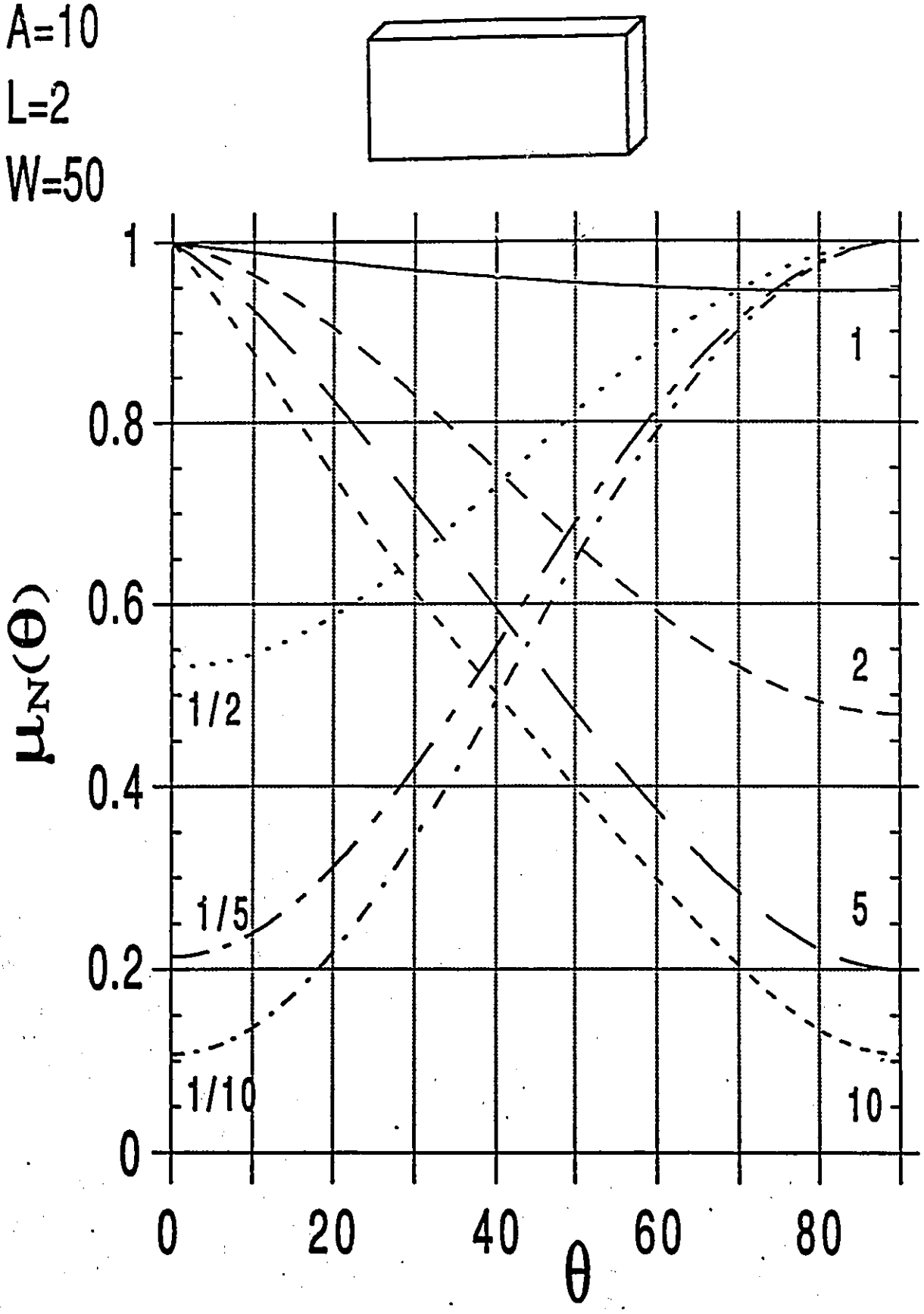

Fig. B-6

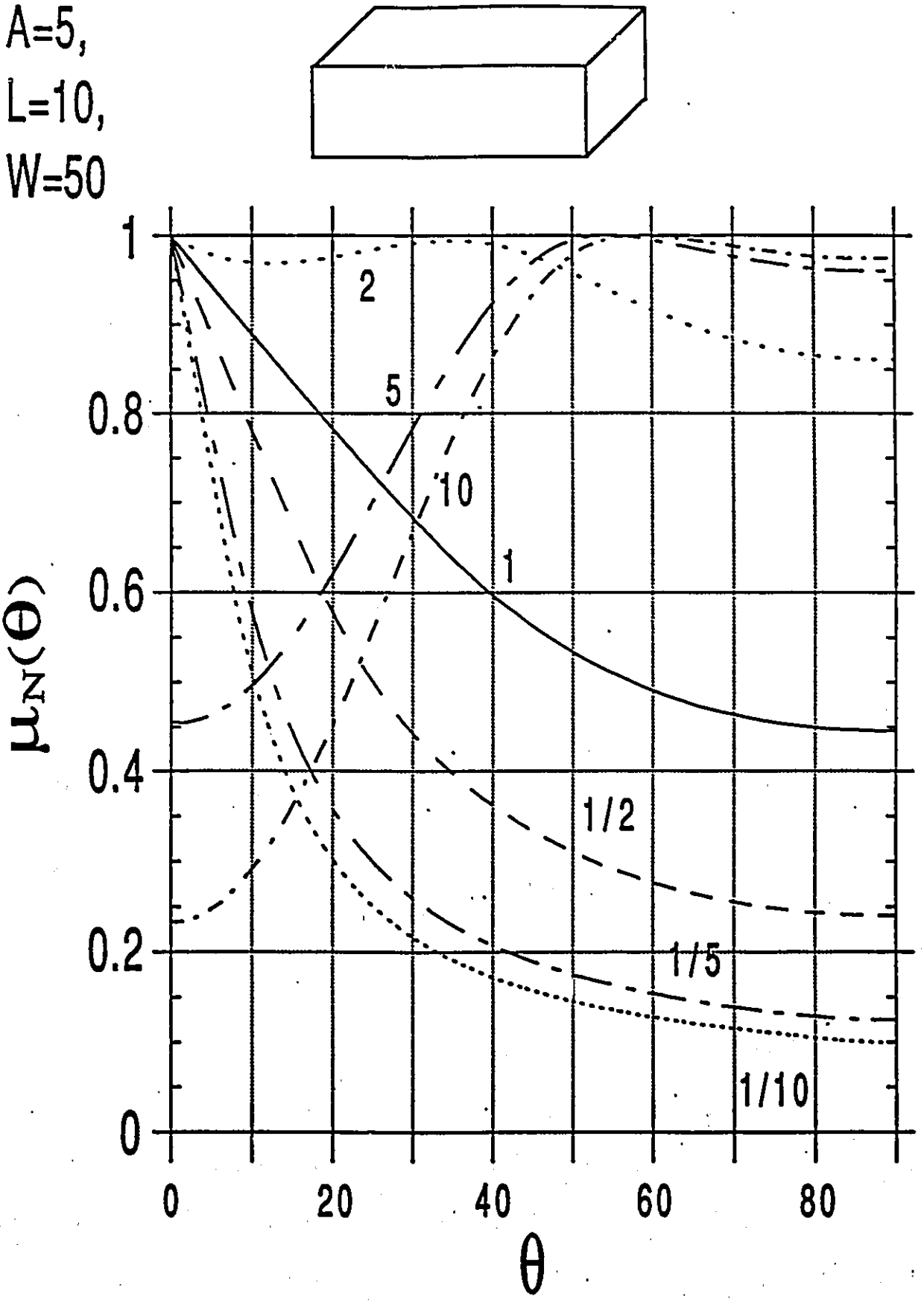

Fig. B-7

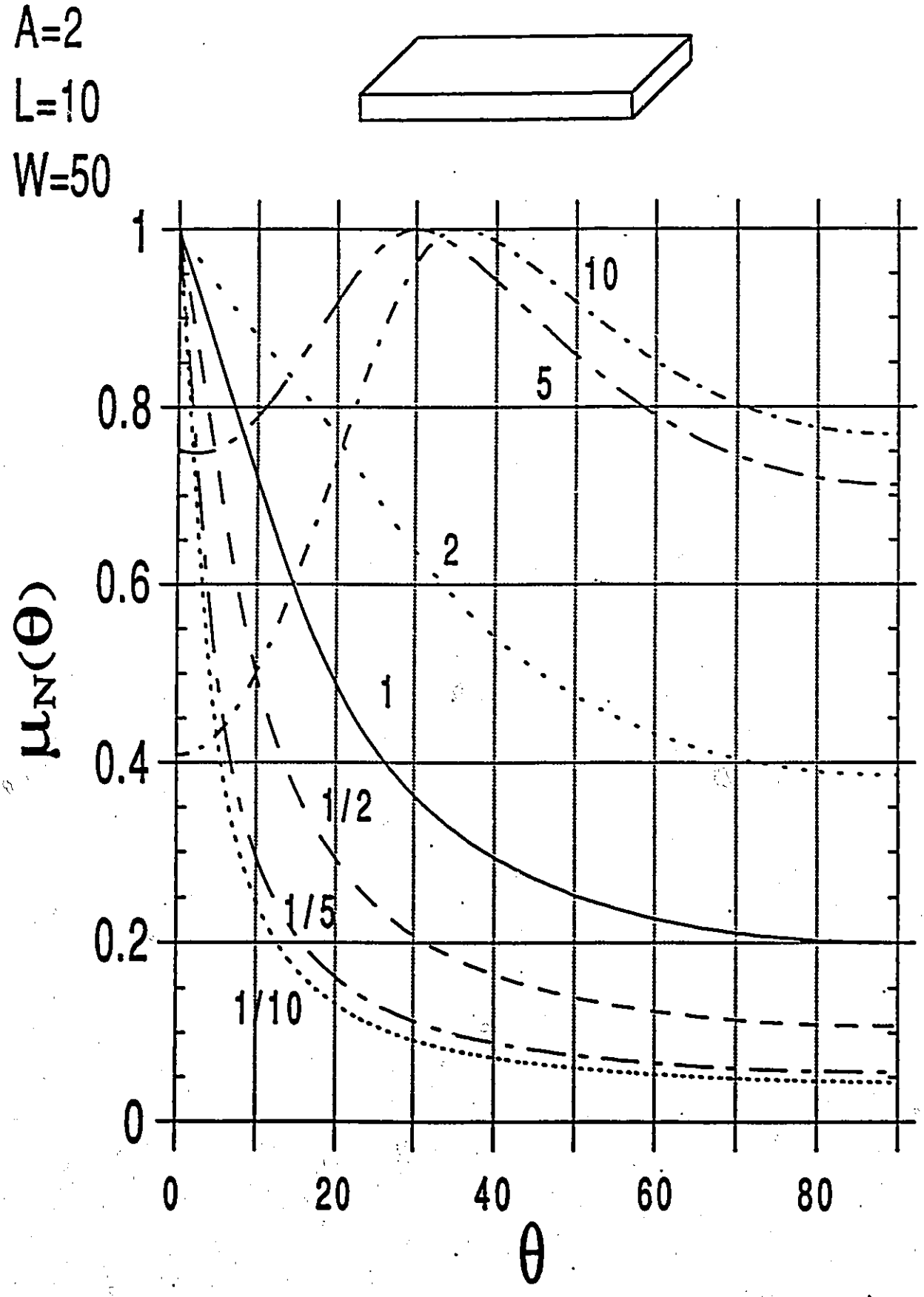
A=2
L=10
W=50
1
0.8
0.6
0.4
0.2
0
$\mu_N(\theta)$
0
20
40
60
80
θ
10
5
2
1
1/2
1/5
1/10

Fig. B-8

A=10

L=2

W=10

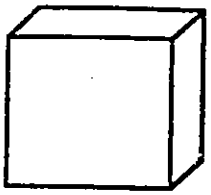

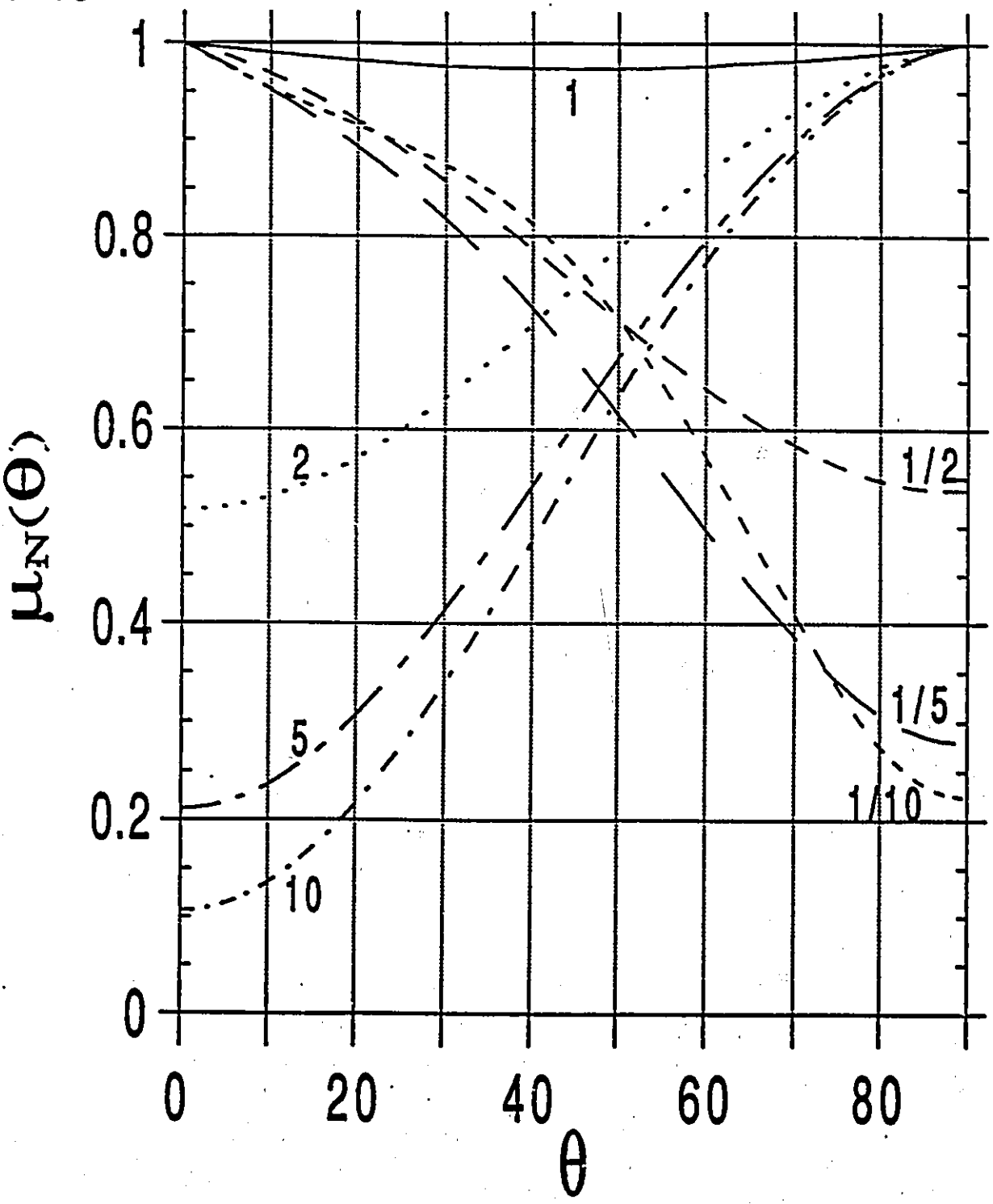

Fig. B-9

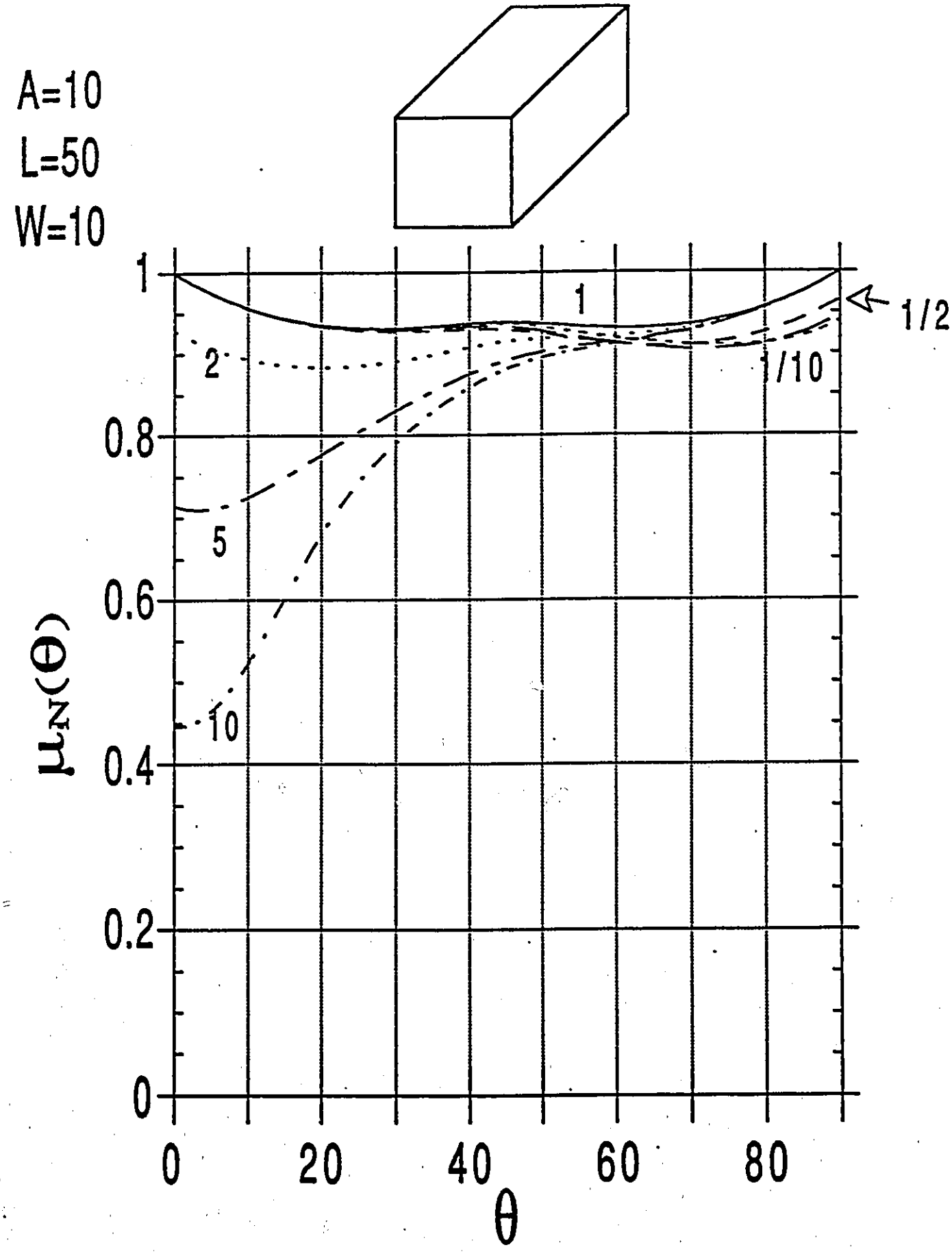

Fig. B-10

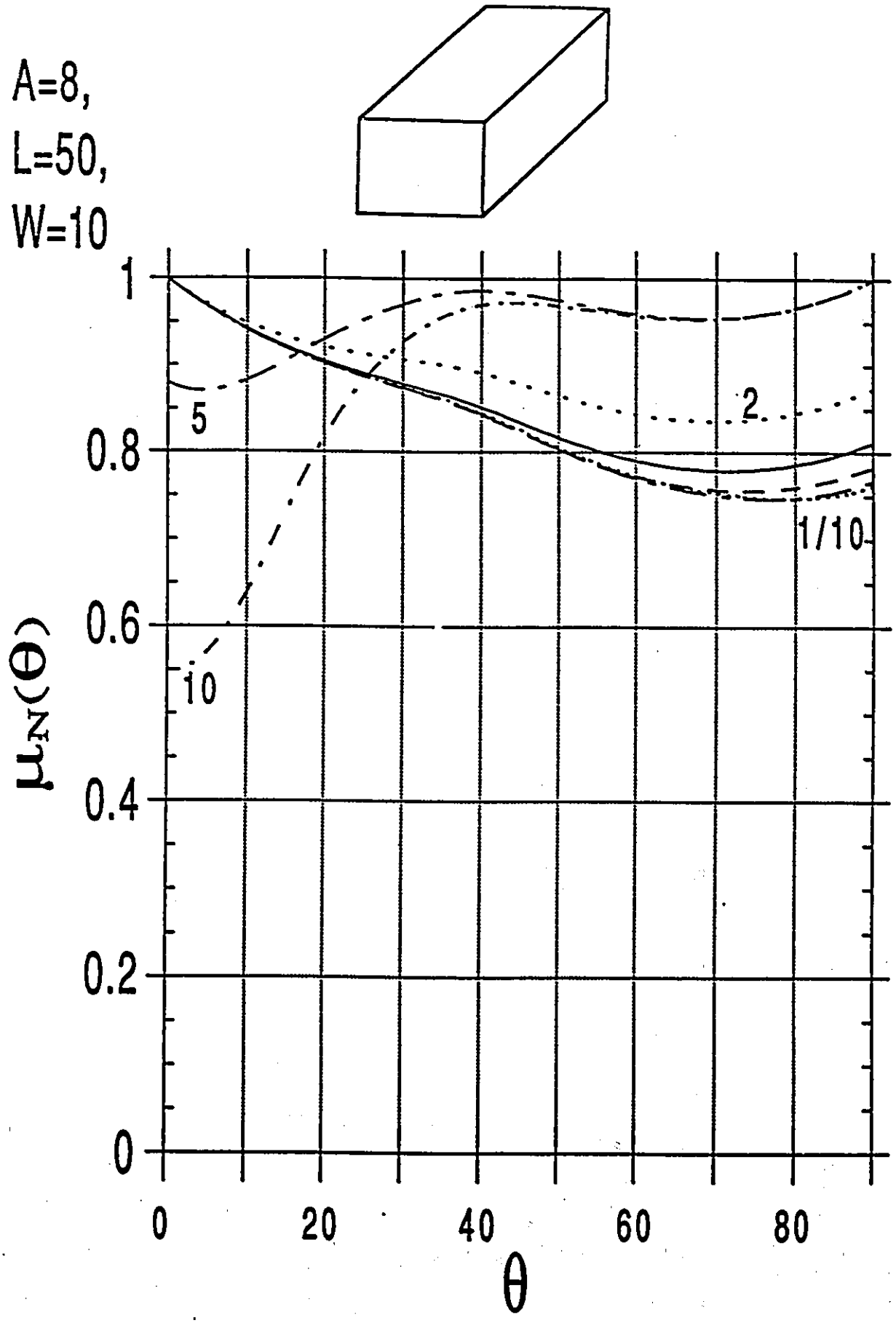

Fig. B-11

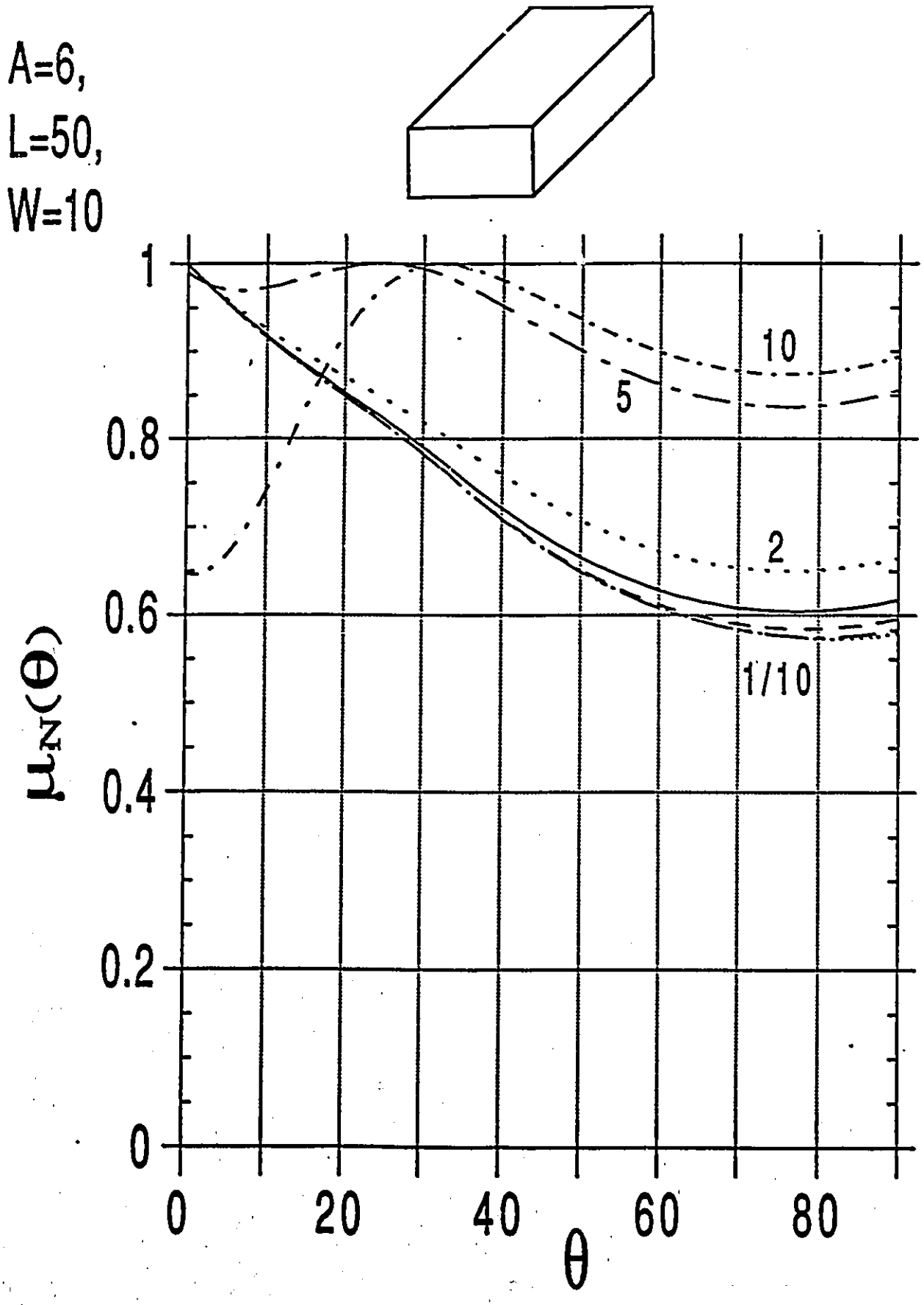

Fig. B-12

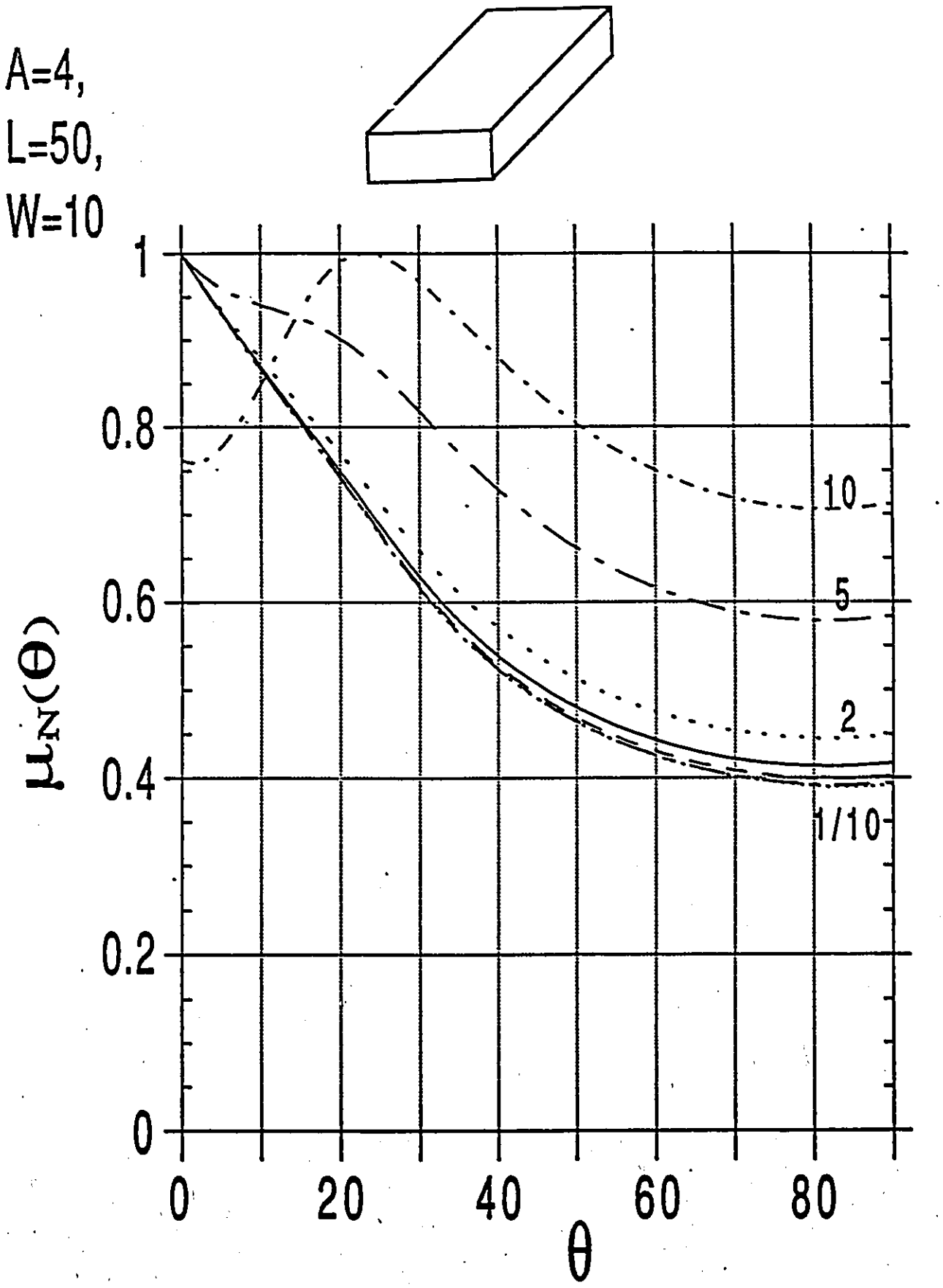

Fig. B-13

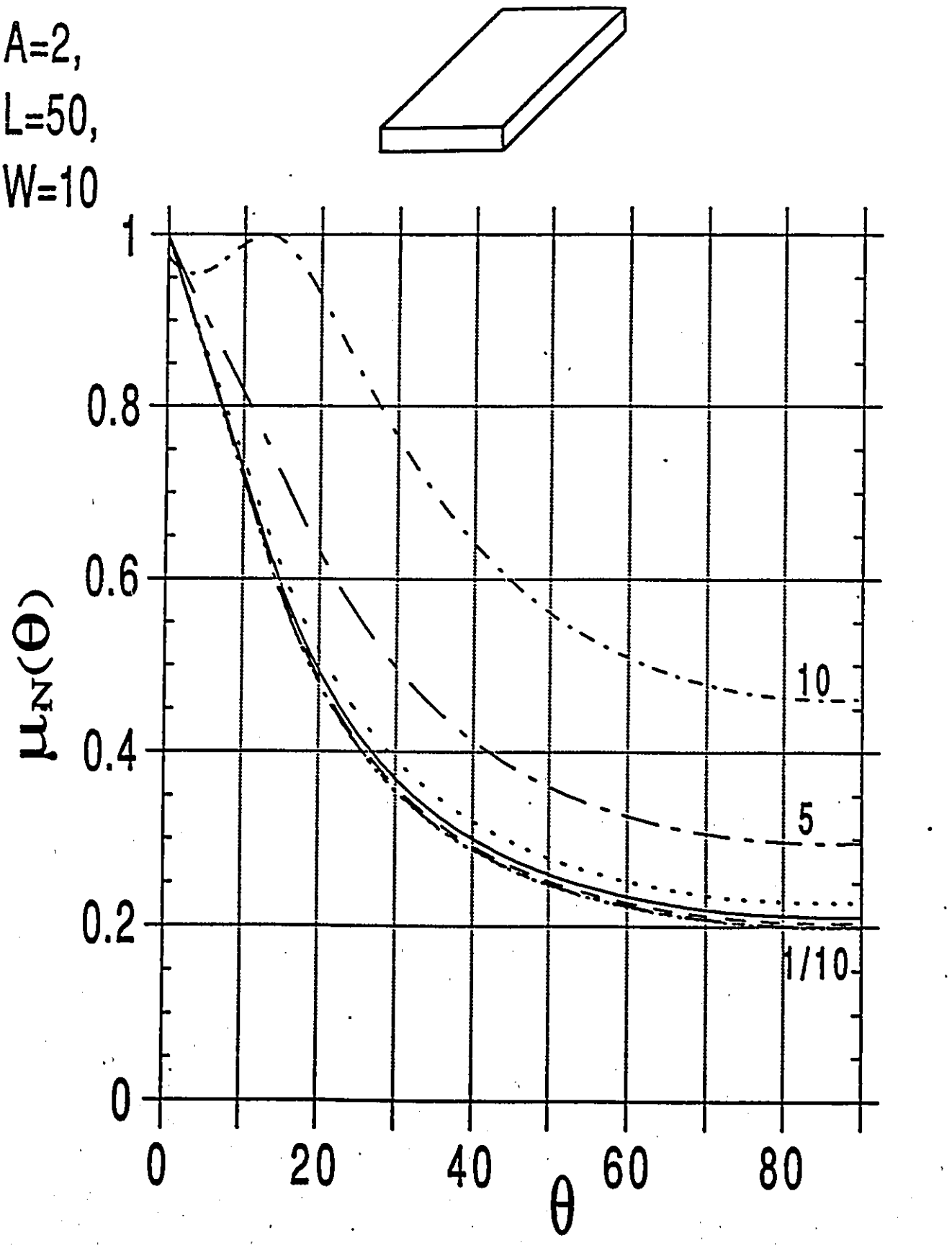

Fig. B-14

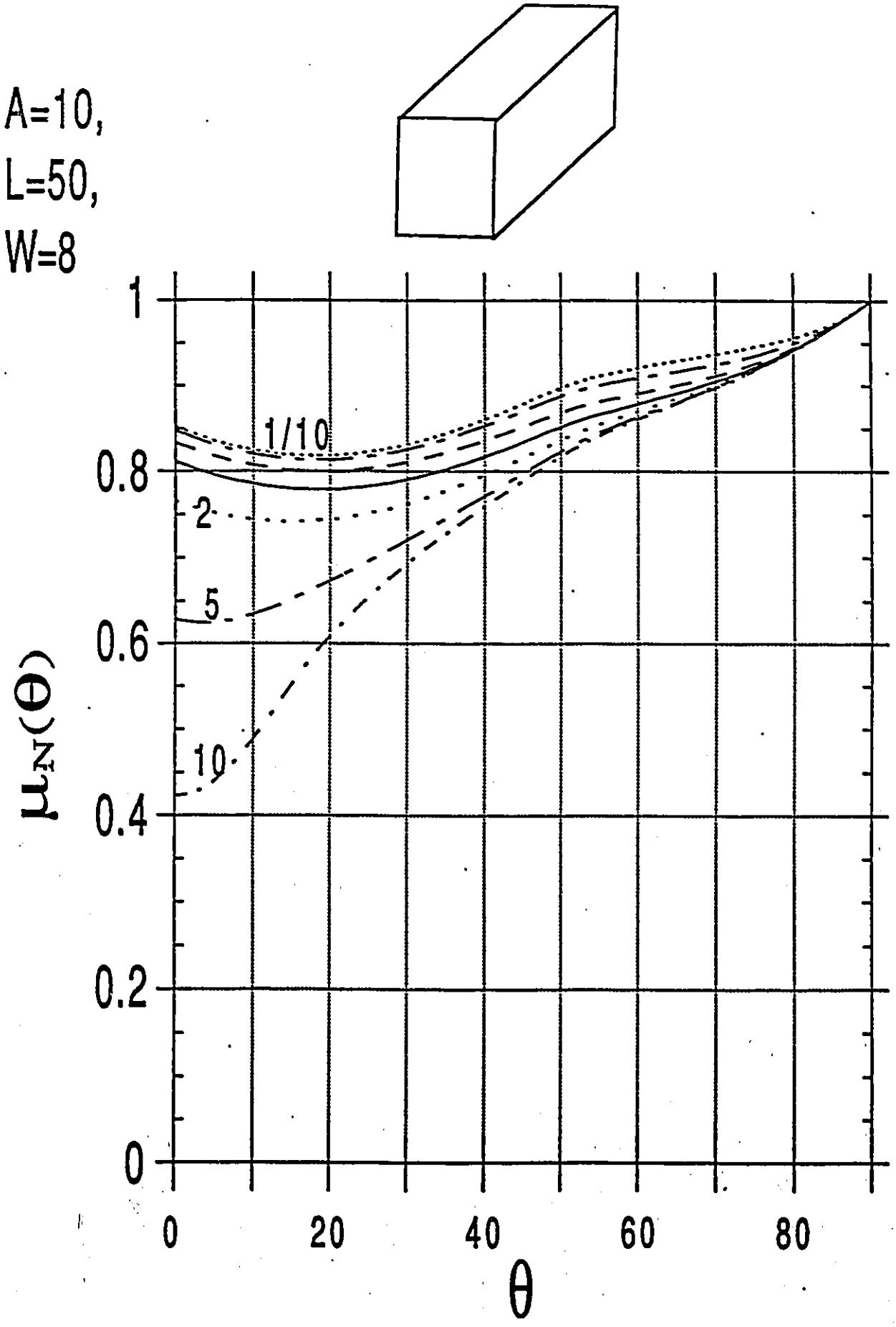

Fig. B-15

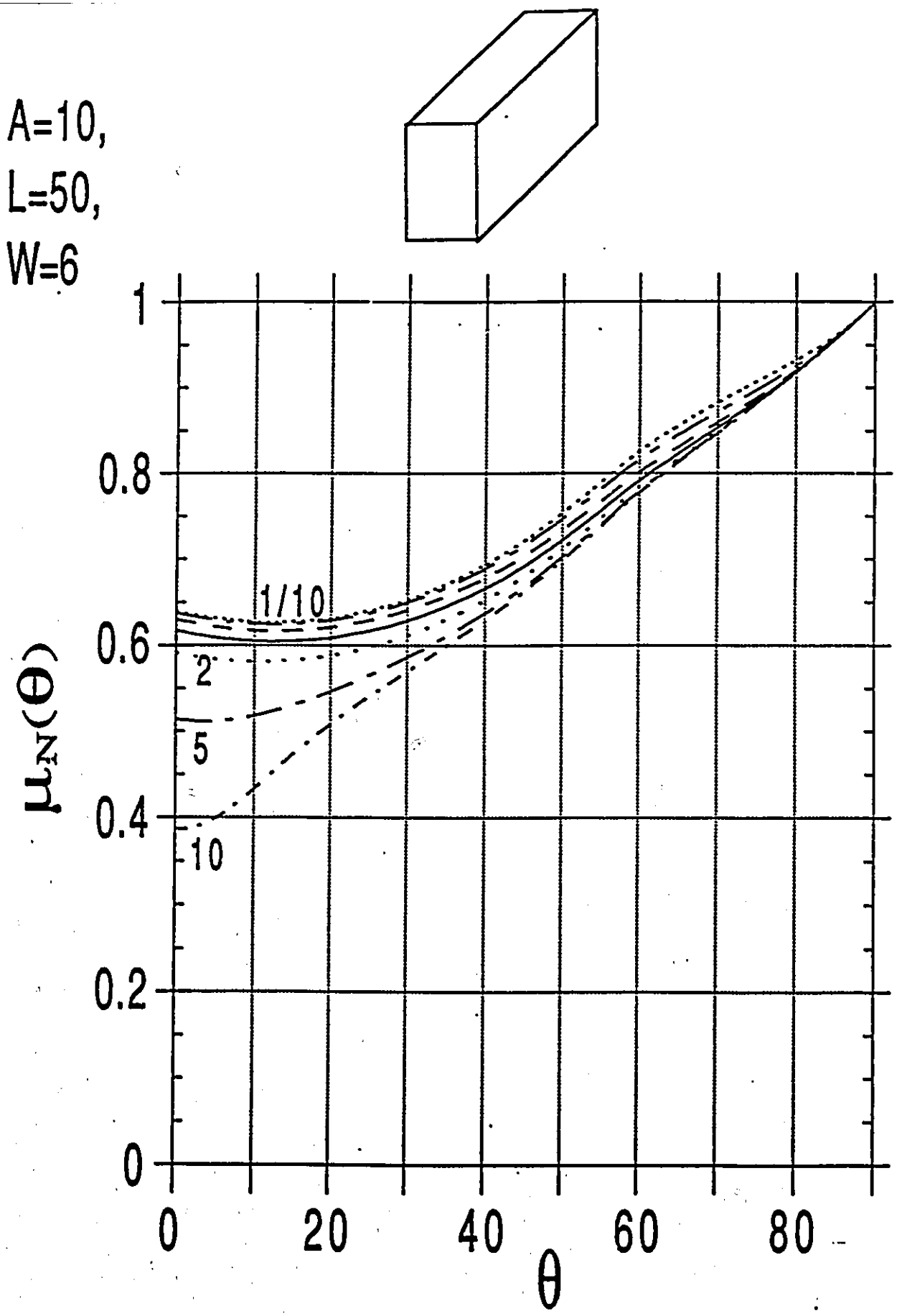

Fig. B-16

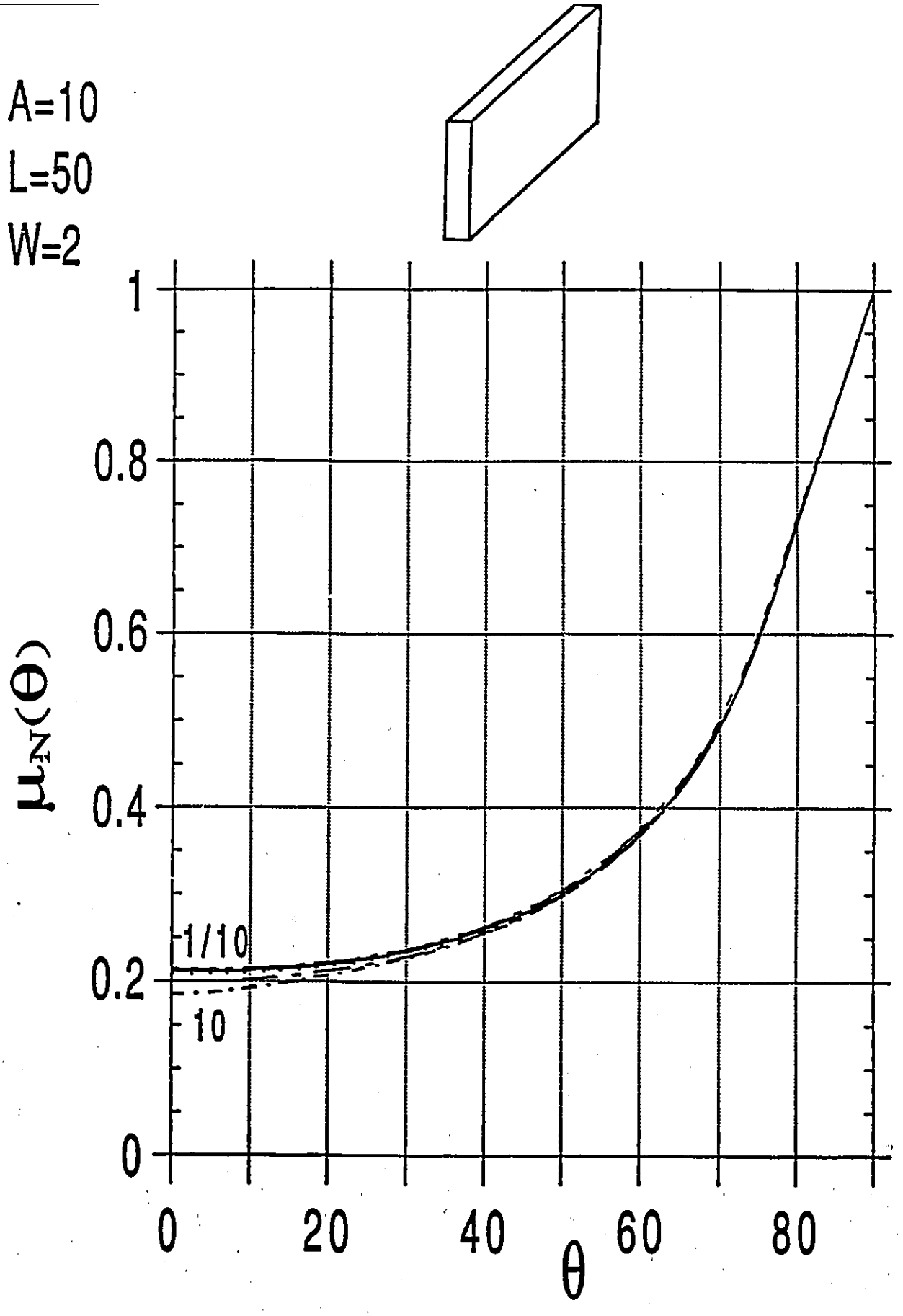

Fig. B-17

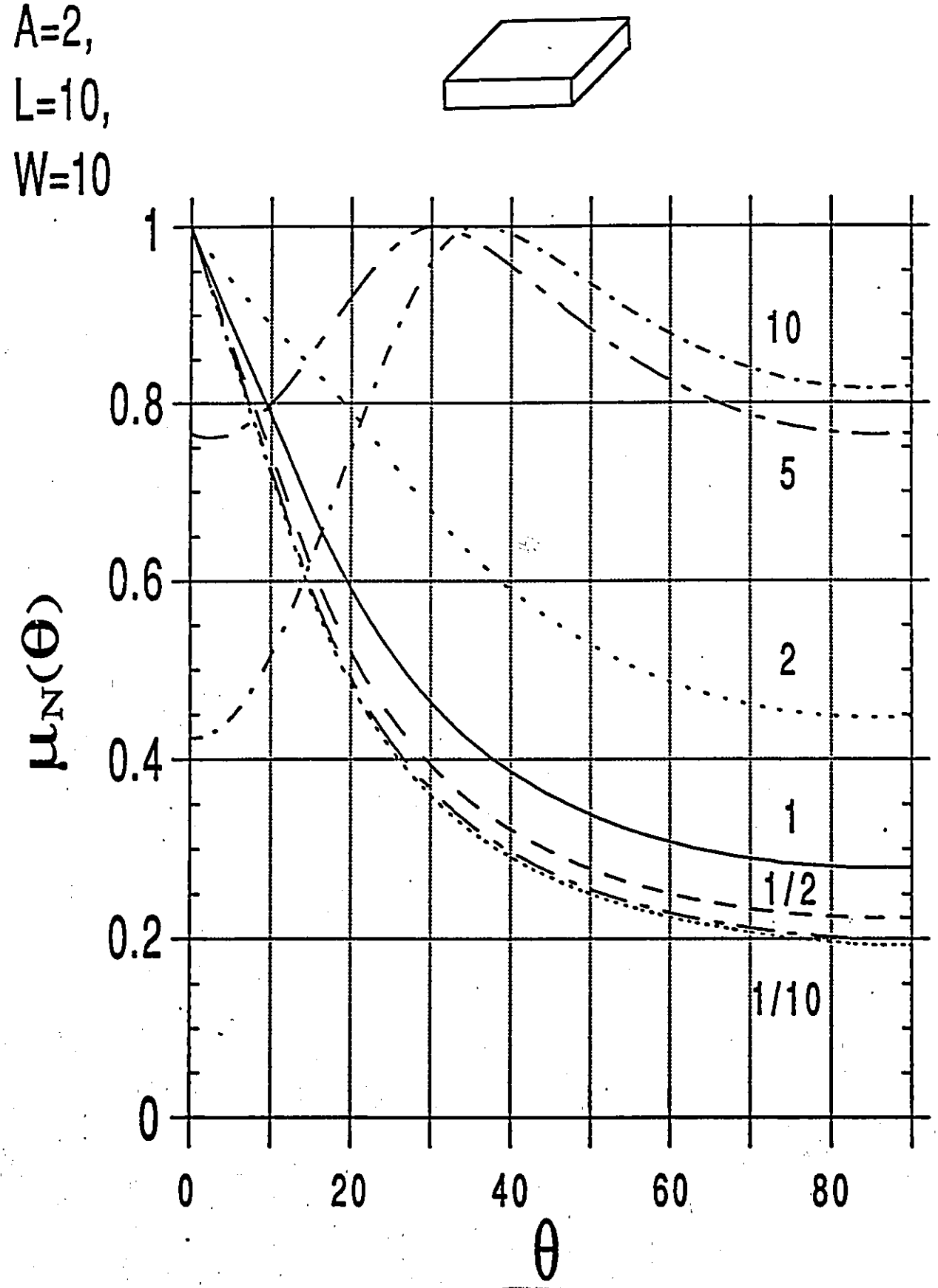
A=2,
L=10,
W=10
1
0.8
0.6
0.4
0.2
0
$\mu_N(\theta)$
0
20
40
60
80
θ
10
5
2
1
1/2
1/10

Fig. B-18

A=5,
L=10,
W=10

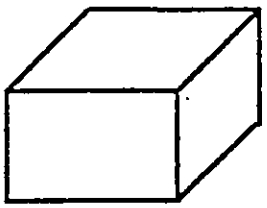

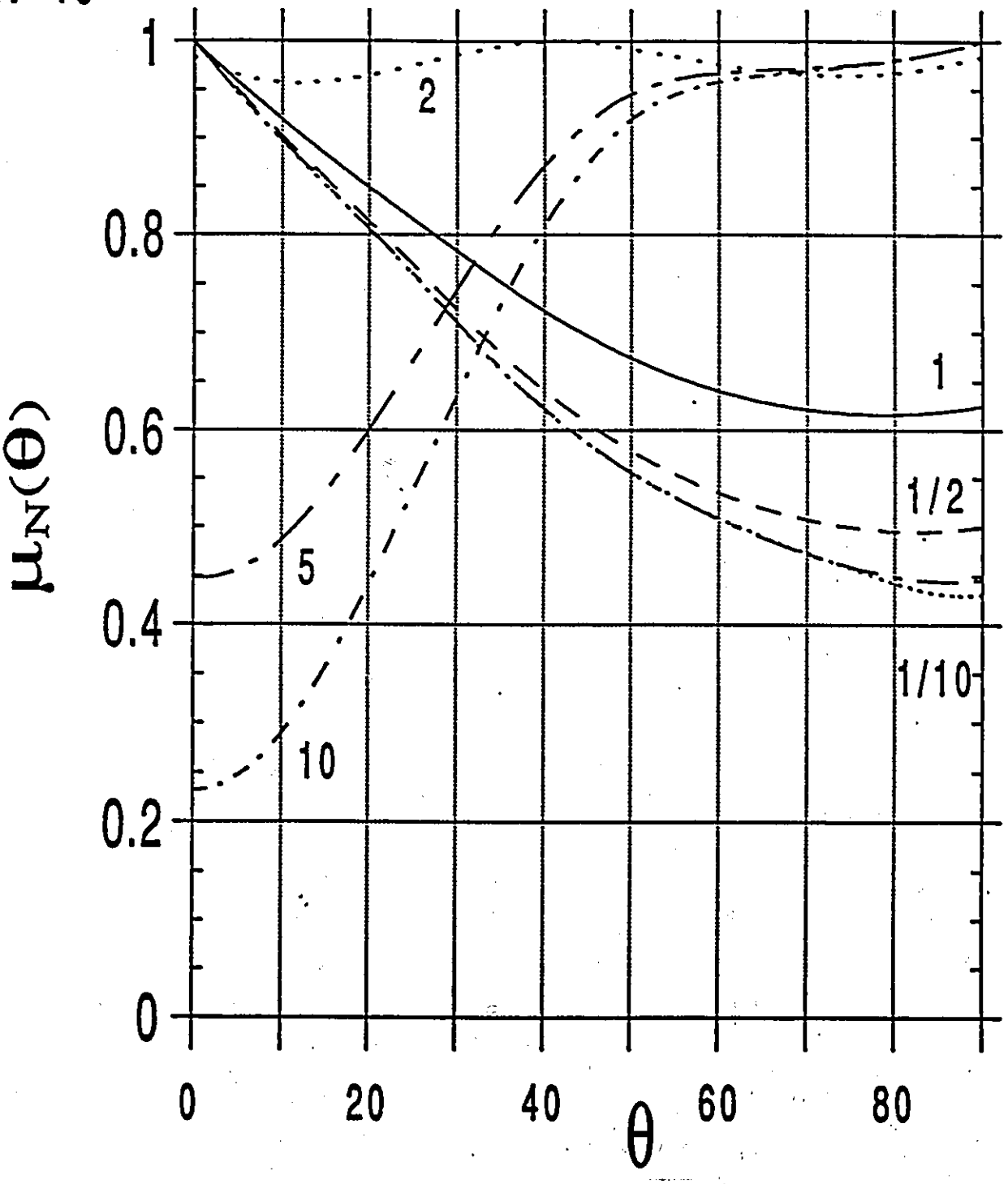

Fig. B-19

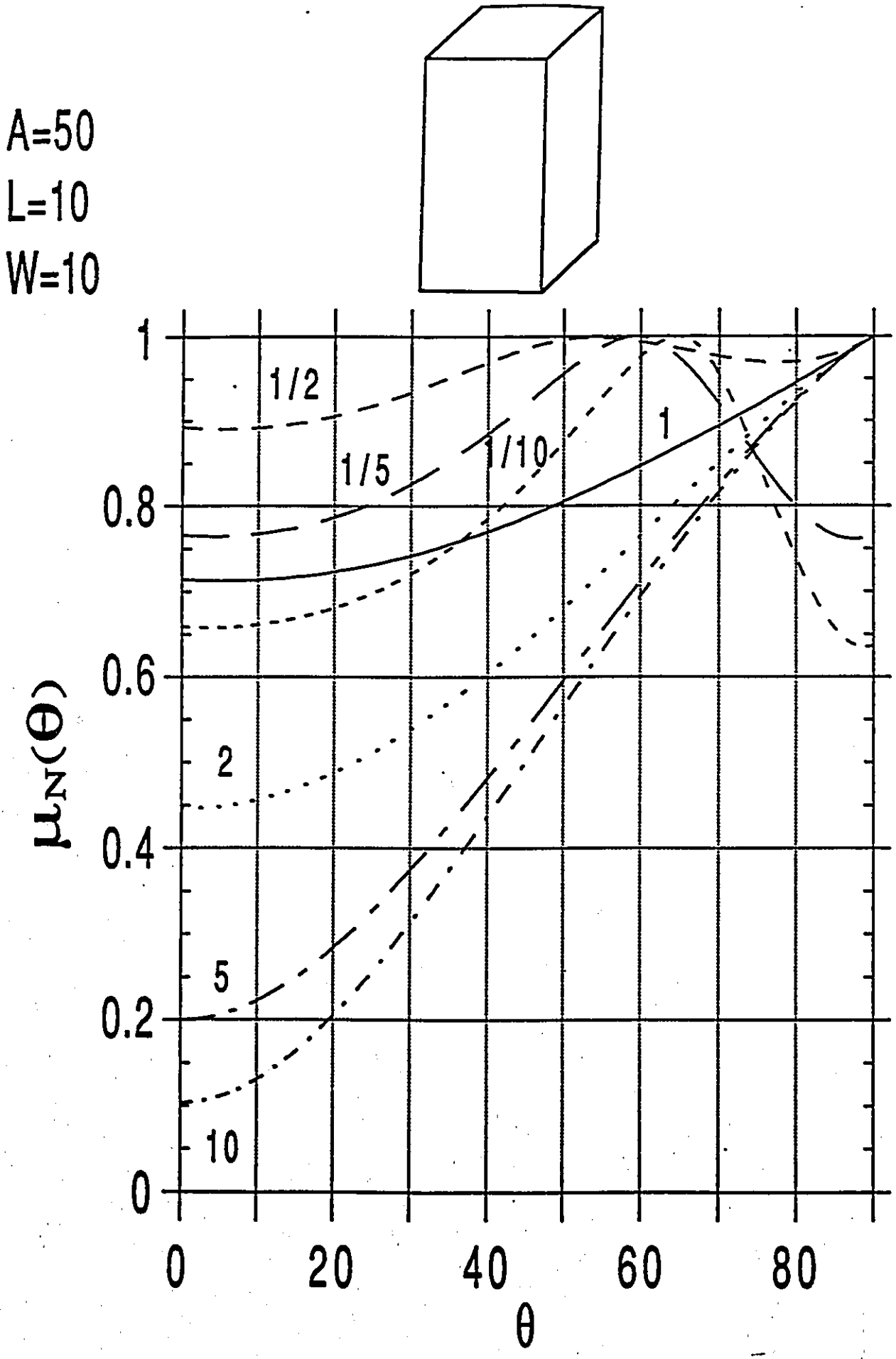

Fig. B-20

A=50,
L=10,
W=8

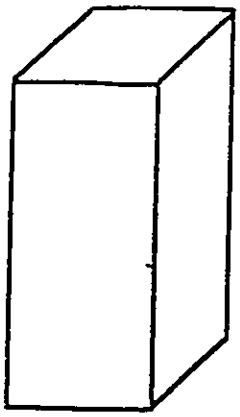

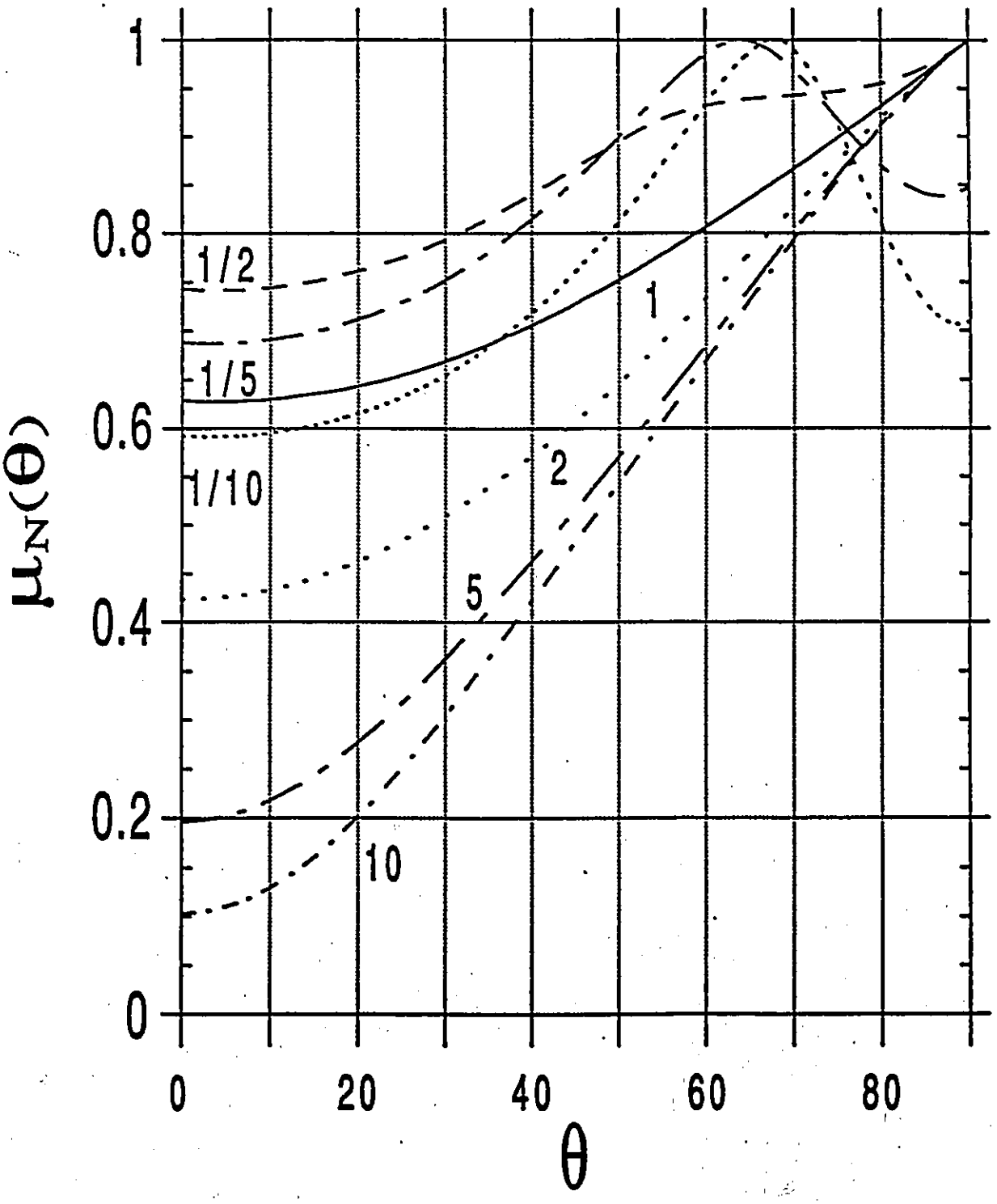

Fig. B-21

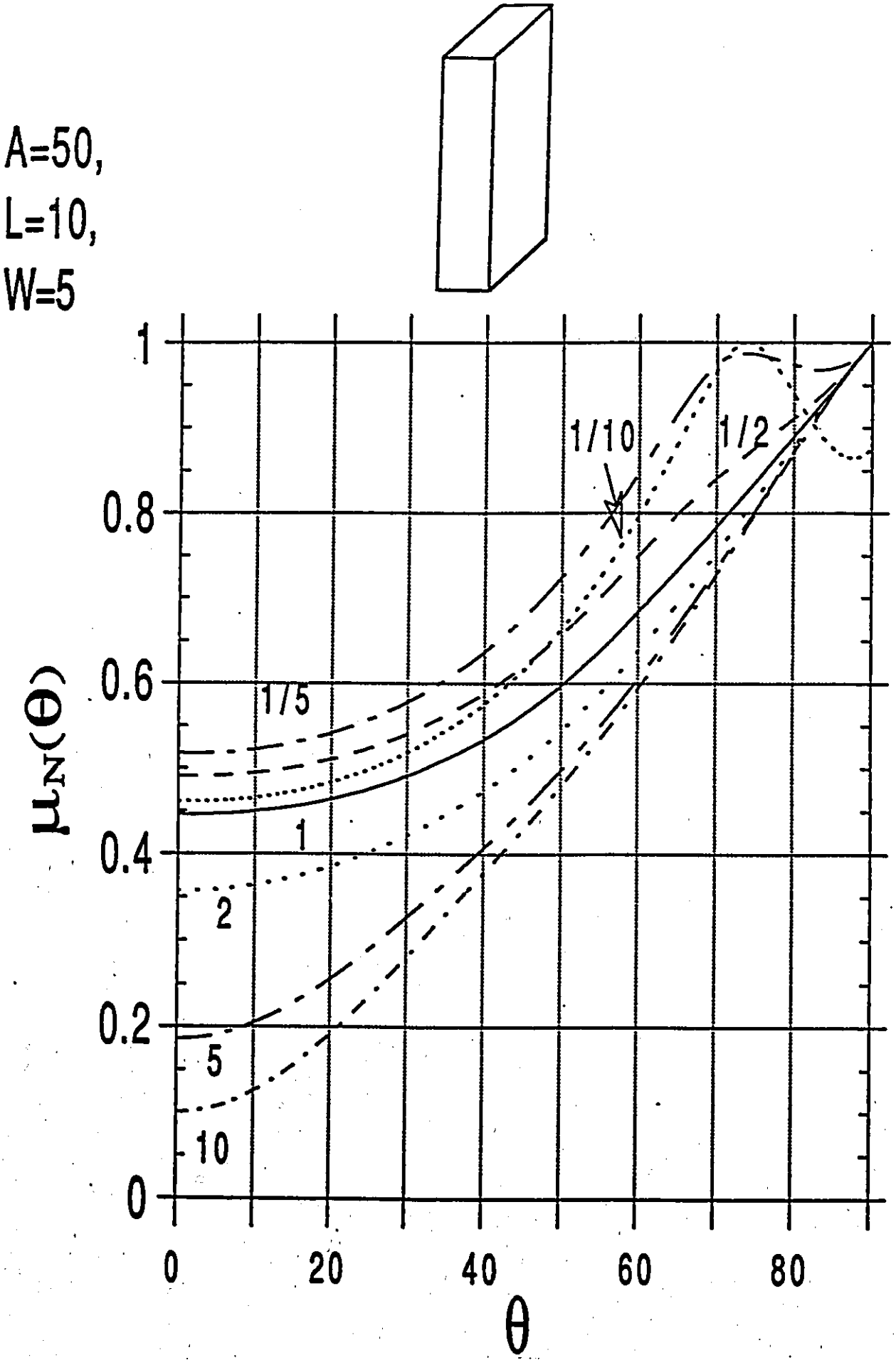

Fig. B-22

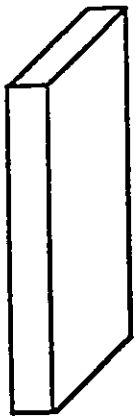

A=50

L=10

W=2

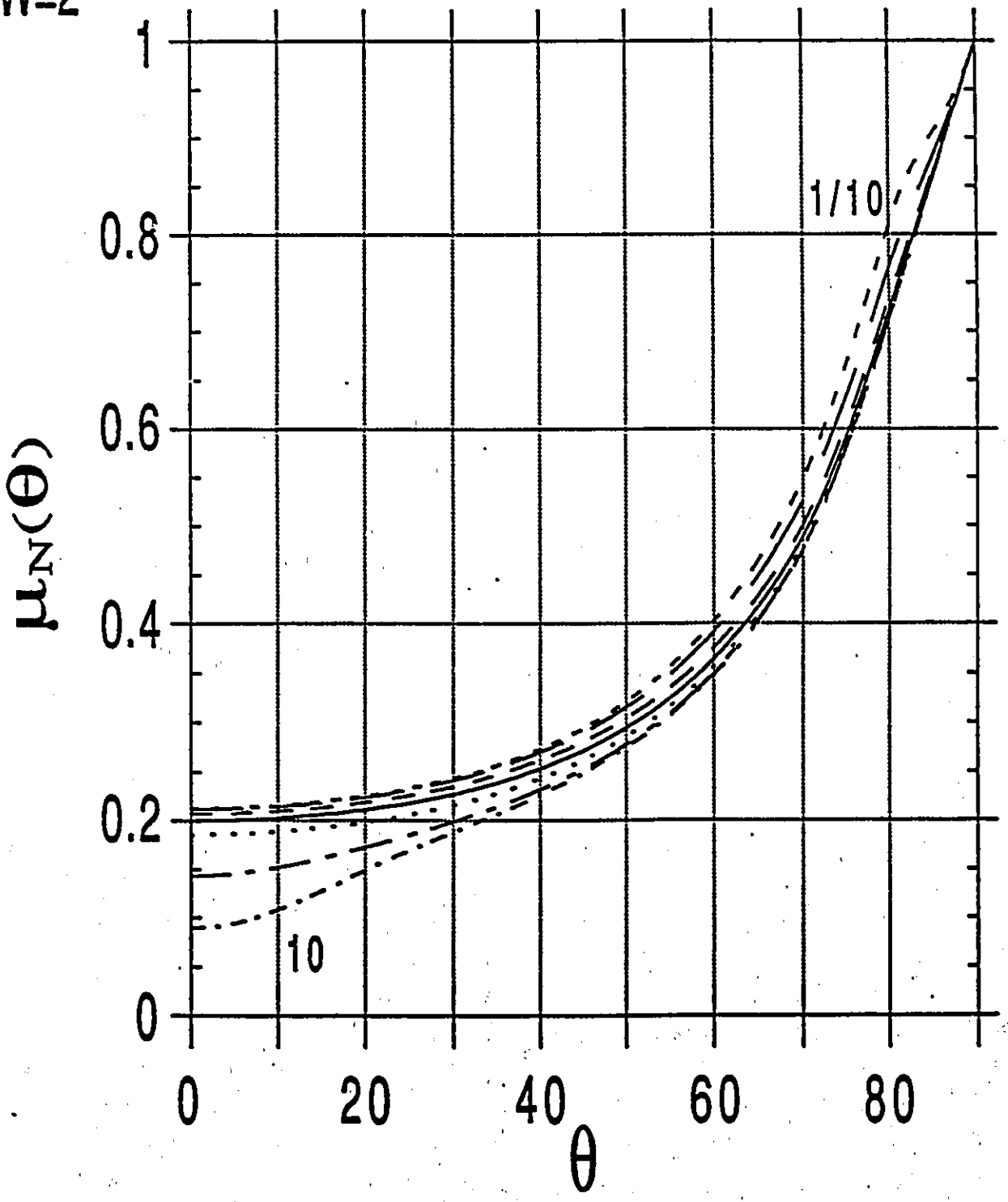

Fig. B-23

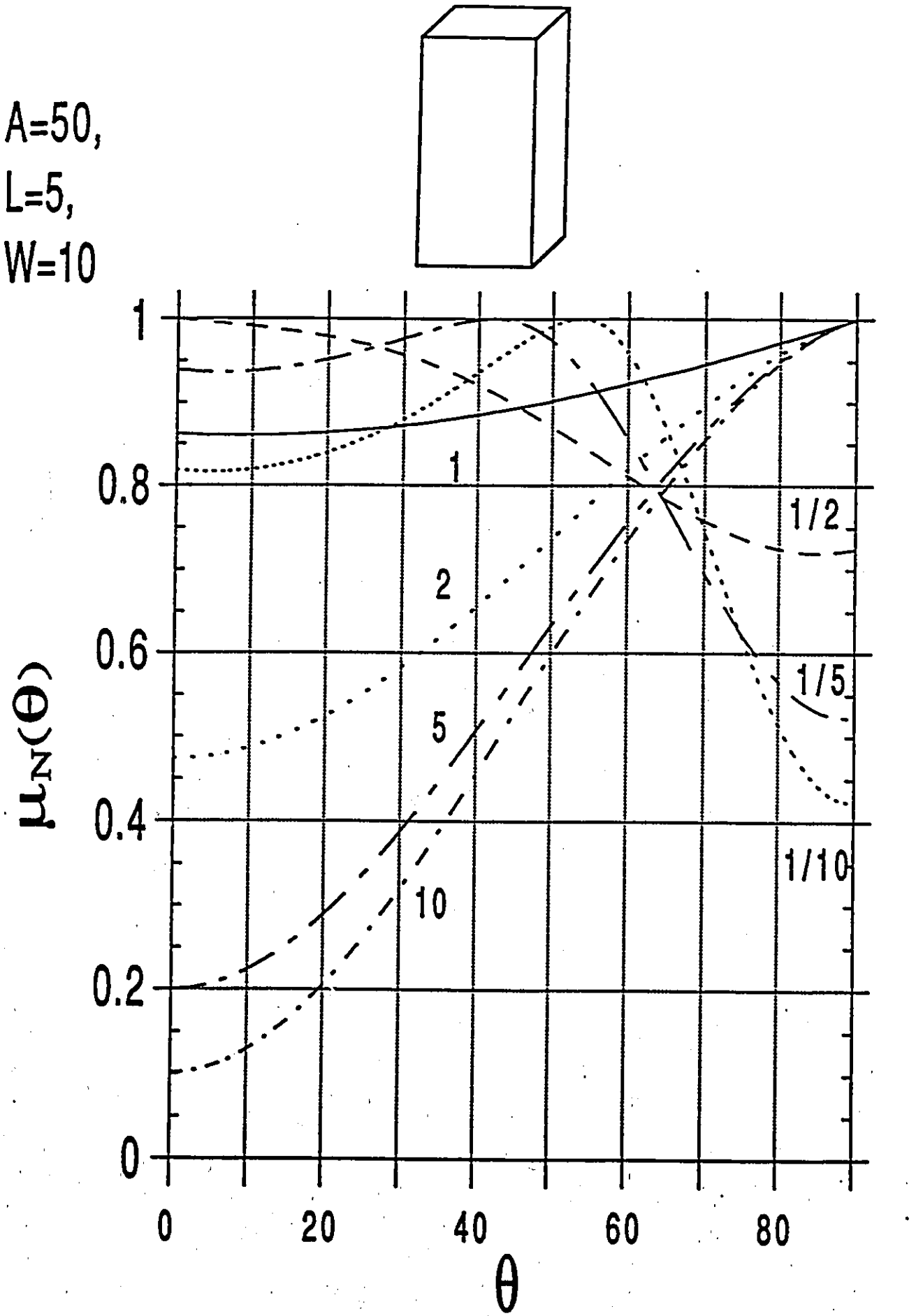
A=50,
L=5,
W=10
1
0.8
0.6
0.4
0.2
0
$\mu_N(\theta)$
0
20
40
60
80
θ
1
2
5
10
1/2
1/5
1/10

Fig. B-24

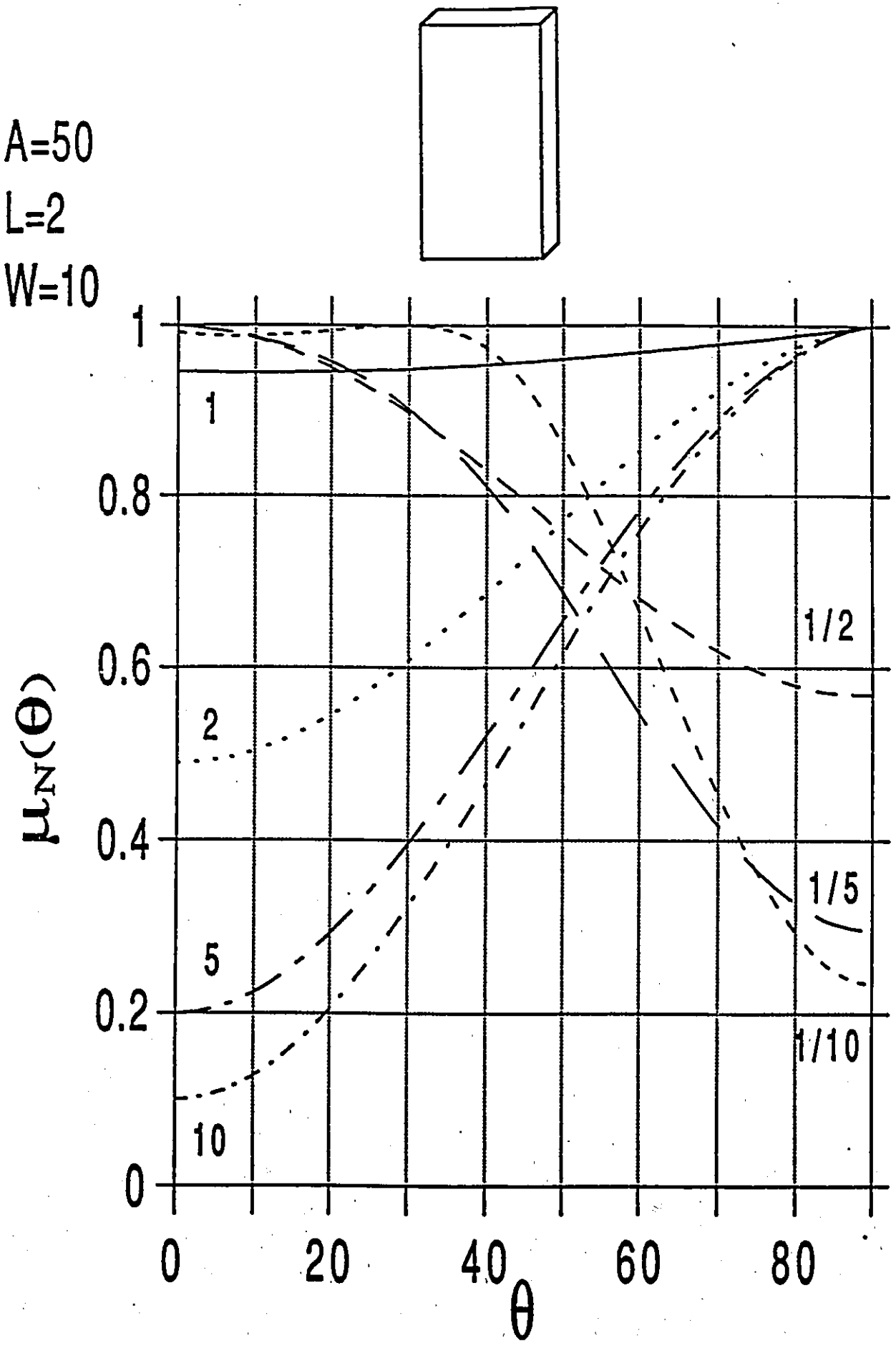
A=50
L=2
W=10
1
0.8
0.6
0.4
0.2
0
$\mu_N(\theta)$
0
20
40
60
80
θ
1
2
5
10
1/2
1/5
1/10

Fig. B-25